INFORMATION TO USERS

This manuscript has been reproduced from the microfilm master. UMI films the text directly from the original or copy submitted. Thus, some thesis and dissertation copies are in typewriter face, while others may be from any type of computer printer.

The quality of this reproduction is dependent upon the quality of the copy submitted. Broken or indistinct print, colored or poor quality illustrations and photographs, print bleedthrough, substandard margins, and improper alignment can adversely affect reproduction.

In the unlikely event that the author did not send UMI a complete manuscript and there are missing pages, these will be noted. Also, if unauthorized copyright material had to be removed, a note will indicate the deletion.

Oversize materials (e.g., maps, drawings, charts) are reproduced by sectioning the original, beginning at the upper left-hand corner and continuing from left to right in equal sections with small overlaps.

Photographs included in the original manuscript have been reproduced xerographically in this copy. Higher quality 6" x 9" black and white photographic prints are available for any photographs or illustrations appearing in this copy for an additional charge. Contact UMI directly to order.

ProQuest Information and Learning
300 North Zeeb Road, Ann Arbor, MI 48106-1346 USA
800-521-0600

Université d'Ottawa · University of Ottawa

MOTION CONTROL OF AN AUTONOMOUS VEHICLE WITH LOSS OF WHEEL-GROUND CONTACT AVOIDANCE USING DYNAMIC MODEL BASED PREDICTIVE CONTROL

A dissertation submitted
at the
Department of Mechanical Engineering
of the
University of Ottawa
in partial fulfilment of the requirements for
a degree of Ph.D.

by

Bumsoo Kim

Ottawa-Carleton Institute for Mechanical and Aerospace Engineering

University of Ottawa

Ottawa, Ontario, Canada, K1N 6N5

August 2000

To my lovely wife Yeonsoon,
and my wonderful sons, Jinseo and Jinhyung

ABSTRACT

Autonomous motion of vehicles requires an operational space control approach which is able to generate and correct the trajectory of the vehicle in order to avoid collisions with unexpected obstacles and takes into account the contact forces between the wheels and the ground such that the slippage and tip-over of the vehicle can be avoided. A dynamic model of the autonomous vehicle is required for such a control approach in order to verify continuously wheel-terrain contact stability. For achieving autonomy, the dynamics based control approach is formulated for a three-wheeled vehicle with front wheel driving and steering. Exact input-output linearization of the vehicle dynamics facilitates the design of the operational space control and permits the enhancement of the autonomy of the vehicle. However, the sufficient smoothness condition for applying feedback linearization has to be continuously observed and this requires the avoidance of actuators torque saturation, wheel-ground longitudinal and lateral slippage and tip-over of the vehicle for motion on horizontal plane as well as inclined surfaces.

In this thesis, first is presented a complete three dimensional kinematic and dynamic model of a three-wheeled autonomous vehicle built in our laboratory. Newtonian dynamics was used for developing the dynamic model of the autonomous vehicle. It continues with the path planning algorithm using the Timoshenko's 4^{th} order differential slender beam equation and the analysis of the two part control scheme. The control scheme contains an external loop for a linear controller, a path planner in operational space, and an inner loop exact input-output linearization controller in curvilinear space(s-δ).

A dynamic model based predictive control is proposed for avoidance of the violation of the smoothness condition for exact linearization, while at the same time conserving path planning results by modifying the input commands.

Acknowledgment

I wish to express my deep appreciation to all those who helped me in completing this research. I would like to express my gratitude to my supervisor, Dr. Dan S. Necsulescu for his time, insight, support, guidance, patience, and sincere attention. I deeply appreciate his sincere enthusiasm in research which will guide me throughout my career.

I am also grateful to my Ph.D. committee members Dr. Liang, Dr. Redekop, Dr. Sasiadek, and Dr. Stiharu for their guidance, reviews, criticisms, and insightful suggestions, throughout the development of this thesis.

Special thanks to my colleagues Rahim Jassemi, Jean de Carufel, Mohammad Eghtesad, Kazuo Kiguchi, Victor Lonmo, and Rob DeAbreu for their technical expertise, guidance, and moral support throughout my research.

Finally, I would like to thank my wife Yeonsoon particularly, whose continuous support and patience throughout my Ph.D. studies have enabled me to produce this thesis. I also would like to thank my children Jinseo and Jinhyung for their patience, understanding, and letting their father work on his thesis.

Most of all, I praise God for making it possible the seemingly impossible.

Table of Contents

List of Figures

Nomenclature

$\mathbf{A}$	the absolute acceleration of the center of mass, O, expressed in X-Y-Z frame
$\mathbf{A}_i$ (i = 1,2,3)	the absolute acceleration of the origins O_i expressed in X-Y-Z frame
A, B, C, D	the coefficients of path planning polynomial
a	curve parameter for path planning algorithm
b	length of the vehicle's wheelbase
c	distance to the robot's centre of mass from the rear axle
CLAMOR	acronym used for the mobile robot which stands for: "Cartesian Linearized Autonomous Mobile Observable Robot"
Den(δ), Num(δ)	a function of steering angle used in the dynamic equations
$\mathbf{F}_{FSAx1}$, $\mathbf{F}_{FSAy1}$, $\mathbf{F}_{FSAz1}$	internal forces in given directions between the vehicle frame and the steering assembly
$\mathbf{F}_{Fx2}$, $\mathbf{F}_{Fy2}$, $\mathbf{F}_{Fz2}$	internal forces in given directions between the vehicle frame and wheel #2
$\mathbf{F}_{Fx3}$, $\mathbf{F}_{Fy3}$, $\mathbf{F}_{Fz3}$	internal forces in given directions between the vehicle frame and wheel #3
$\mathbf{F}_{SAx1}$, $\mathbf{F}_{SAy1}$, $\mathbf{F}_{SAz1}$	internal forces in given directions between the front wheel and the steering assembly
$\mathbf{G}_{xi}$ (i = 1,2,3)	wheel-ground contact forces in the direction of rotation of wheels
$\mathbf{G}_{yi}$ (i = 1,2,3)	wheel-ground contact forces perpendicular to the direction of rotation of wheels
$\mathbf{G}_{zi}$ (i = 1,2,3)	vertical wheel-ground contact forces of the wheels
Grav(δ)	a function of gravitational terms in the dynamic equations

h	the height of the center of mass of the structure from the surface of the inclined plane (equation (3-5))
$\mathbf{I_{SAx1}}$, $\mathbf{I_{SAy1}}$	moment of inertia of the steering assembly about given directions
$\mathbf{I_{x1}}$, $\mathbf{I_{x2}}$, $\mathbf{I_{x3}}$	moment of inertia of a wheel about its direction of motion
$\mathbf{I_{y1}}$, $\mathbf{I_{y2}}$, $\mathbf{I_{y3}}$	moment of inertia of a wheel about its axis of rotation
$\mathbf{J_i}$ (i = 1,2,3)	moment of inertia of the wheels
$\mathbf{J_f}$	moment of inertia of the vehicle frame
$\mathbf{J_{SA}}$	moment of inertia of the steering assembly
K_1, K_2, K_3	gains for the inner loop input-output linearization controller
K_{ext}	external loop proportional control gain
L	distance between the initial and desired position of the vehicle
l	distance between the two rear wheels
$\mathbf{M_{FSAx1}}$, $\mathbf{M_{FSAy1}}$	rotational moments in given directions between the steering assembly and the vehicle frame
$\mathbf{M_{SAx1}}$, $\mathbf{M_{SAy1}}$, $\mathbf{M_{SAz1}}$	rotational moments in given directions between the front wheel and the steering assembly
$\mathbf{M_{xi}}$, $\mathbf{M_{zi}}$ (i = 2,3)	rotational moments in given directions between rear wheels and the vehicle frame
M-Q-P	an inertial frame attached to the surface of Earth
$M = m_f+m_{1t}+m_2+m_3$	the total mass of the vehicle
m_i (i=1,2,3), m_{SA}, m_f	the masses of each wheels, steering assembly, and the vehicle frame, respectively

$m_{1t} = m_1 + m_{SA}$	the combined mass of the front wheel and the steering assembly
N_h	prediction horizon time for MPC
N-Q-R	an inclined inertial frame with respect to M-Q-P inertial frame
O	origin of the X-Y-Z frame
O_{SA}	origin of the steering assembly
O_i (i = 2,3)	origin of two rear wheels
$\mathbf{P}$, $\mathbf{P}_i$ (i = 1,2,3)	absolute position vectors expressed in X-Y-Z frame
Q_i (i = 1~29)	parameters used to simplify the derivation of equations of motion
$\mathbf{R}$, $\mathbf{R}_1$, $\mathbf{R}_2$, $\mathbf{R}_3$	position vectors from the origin of the inertial frame to the origin of the moving frame
$\mathbf{r}_i$ (i = 1,2,3)	relative positions of O_{SA}, O_i (i = 2,3) with respect to O
r_{w1}, r_{w2}, r_{w3}	radius of the wheels
s	arc length along a path
S_a	the distance between the center of mass of the steering assembly and the center point of the front wheel
S_b	the distance between the center of mass of the steering assembly and the linkage point of the steering assembly with the vehicle frame
S_{a+b}	the distance between the center point of the front wheel and linkage point of the steering assembly with the vehicle frame ($S_{a+b} = S_a + S_b$)
S(L)	curvilinear length of the path
S(x)	curvilinear position of the vehicle
u^*	new control variable optimized by MPC

$\mathbf{u}$	
$\mathbf{V}, \mathbf{V}_1, \mathbf{V}_2, \mathbf{V}_3$	velocity vectors of the origins of given frame with respect to inertial frame
X-Y-Z	a moving reference frame attached to the vehicle's center of mass
X_i-Y_i-Z_i (i = 1,2,3)	moving reference frames attached to center or rotation of the three wheels
y(x)	planned path with respect to the vehicle's directional coordinate
$\alpha_1, \alpha_2, \alpha_3$	angular displacements of the wheels
β	the slope of inclined plane
γ	angle between the velocity vector of the vehicle and its longitudinal axis x(t)
γ_i (i = 1 ~ 7)	the weight factors for criterion function
δ	steering angle of the front wheel of the vehicle
θ	orientation angle of the vehicle
θ_i θ_d	initial and desired orientation angle of the vehicle with respect to the inertial frame (N-Q-R), respectively
μ	friction coefficient
ρ	radius of curvature
τ	the transformation matrix defining the rotation of X-Y-Z frame with respect to N-Q-R frame about the vertical axis
τ_d	driving torque of the vehicle
τ_s	steering torque of the vehicle
Φ_k	criterion function in MPC
φ	the angle of the tangent of the path with respect to inertial frame (N-Q-R)
ω_1, ω_δ	angular velocities of front wheel about driving and steering directions

ω_2, ω_3	angular velocities of the rear wheels
ω_θ	angular velocity of the vehicle's frame with respect to the X axis

Generally derivatives will be shown as:

$$\frac{\partial x}{\partial t} = \dot{x} \qquad \frac{\partial^2 x}{\partial t^2} = \ddot{x}$$

The following convention to denote the i^{th} derivative has also been used:

$$\frac{\partial^{(i)}(X)}{\partial t^{(i)}} = X^{(i)}$$

I. INTRODUCTION

1.1 Motivation

A variety of autonomous mobile vehicles were developed in recent years mostly using kinematics based control. At the present time the interest is to further enhance the features for autonomous operation of vehicles in an unknown and open quasi-flat surface. Motion on uneven road conditions imposes complex requirements for the controller of the vehicle, in particular with regard to vehicle dynamics.

For autonomous motion control of unmanned vehicles, an operational space control approach is needed to generate and correct the trajectory of the vehicle in order to avoid collisions with unexpected obstacles and to take into account the contact forces between the wheels and the ground such that the slippage and tip-over of the vehicle can be avoided.

For achieving autonomy, a dynamics based control approach is formulated for a three-wheeled vehicle with front wheel driving and steering. Motion control of the vehicle in operational space is greatly facilitated by the exact input-output feedback linearization of vehicle dynamics. The linearization also permits the development of a real-time collision avoidance scheme using a predictive

control approach thus enhancing autonomy of the vehicle. The sufficient smoothness condition for applying feedback linearization has to be however continuously observed and this requires the avoidance of actuators torque saturation, wheel-ground longitudinal and lateral slippage and tip-over of the vehicle. Also, the smoothness condition has to be observed for motion on the horizontal plane as well as on inclined surfaces.

1.2 Research Goals

There are several areas of research of autonomous mobile vehicles: navigation, path planning, vehicle design and configuration, vision, sensory data acquisition and interpretation, and actuator control for vehicles with complex dynamics, etc.

The areas of research we are concentrating on for autonomous vehicle control are the areas which requires mechanical engineering knowledge, including designing of the vehicle, kinematic and dynamic modeling, path and motion planning, path following and trajectory tracking, posture stabilization and obstacle avoidance issues. This thesis presents first the kinematic and three dimensional dynamic model using Newtonian dynamics of a three wheeled autonomous vehicle for the case of front wheel steering and driving. A three-dimensional dynamic model of the vehicle is strongly recommended instead of using a two-dimensional model for analyzing the effects of the inertia of the vehicle. The thesis continues with the path planning algorithm using Timoshenko's 4^{th} order differential slender beam equation. It is followed by a presentation of the dynamics model based predictive control approach for avoidance of above events by modifying the input commands such that the geometric path planning result is conserved and the smoothness condition for exact linearization is not violated. The approach is presented for the wheel-ground slippage and tip-over

avoidance of the three-wheeled vehicle for inclined plane motion. Experimental tests were performed for verification of the slippage of the wheels through the sensor fusion of the odometers and the accelerometers. And simulation tests presented in the thesis have the purpose to verify the proposed Model Predictive Controller for simple situations in which corrective actions are taken by the controller to avoid smoothness condition violations.

II. LITERATURE REVIEW

The autonomous vehicle can be defined as "the vehicle that is capable of intelligent motion and actions without requiring either a guide to follow or teleoperator control." (Wilfong, G.T. 1990). One of the advantages of the autonomous vehicle is that it can be used to find the trajectory to the target position while avoiding obstacles in a partially unknown environment. There is a variety of potential applications of the autonomous vehicles (industrial, military, scientific, household, and humanitarian) in which an autonomous vehicle will operate in a large and unstructured environment, for example, delivering parts inside a large factory, cleaning an industrial waste site, maintaining a nuclear plant, inspecting and repairing underwater structures, assembling structures in outer space, fire fighting, cleaning windows, aiding handicapped, etc. It is believed that autonomous mobile vehicles will be commonplace in the near future.(McKerrow, P.J., 1991)

Interests in control of autonomous vehicles have been growing rapidly because of the very broad range of their potential applications. The challenge is that these vehicles move intelligently so that they can perform various actions without human intervention. Research on autonomous vehicles began in the late sixties with the pioneering work of Stanford Research Institute. Two versions of

SHAKEY, an autonomous mobile robot, were built in 1968 and 1971. The main purpose of this project was "to study processes for the real-time control of a robot system that interacts with a complex environment" (Nilsson, N.J., 1969) . Indeed, robot vehicles were and still are a very convenient and powerful support for research on artificial intelligence oriented robotics. A second and quite different trend of research began around the same period. It was aimed at solving the problem of robot vehicle locomotion over a rough terrain. Part of this research focused on the design and the study of the kinematics and dynamics of multi-legged robots (McGee, R.B. et al, 1979). However, the research in this field progressed slowly for various reasons, such as the lack of efficient on-board instrumentation (computer, sensors, etc.). Meanwhile the so-called industrial robots (i.e., robot manipulator) become the main body of a fast growing field of robotics.

The present renewal of interest in autonomous vehicles started in the late seventies fostered by powerful on-board signal and data processing capacities offered by microprocessor technology. Today the scientific reasons for using autonomous vehicles as a support for conceptual and experimental work in advanced robotics hold more than ever. Furthermore a number of real-world applications can now be realistically envisioned, some for the near future. These applications range from intervention robots operating in hostile or extremely dangerous environments to day-to-day machines in highly automated factories using flexible manufacturing systems (FMS) technology. Recently a number of robotic missions to Mars have been undertaken. Mars pathfinder and its Sojourner Rover have finished their mission after a spectacular landing and the first use of a roving vehicle on Mars. Balaram, J. (2000), and Cozman, F. (2000) illustrated the limitless possibility of application of mobile robots to the Mars exploration missions. Salichs, M.A. and Moreno, L. (2000) published a survey paper focused on the essential issues on the navigation of mobile robots.

The literature review has been performed in order to serve the focus of this thesis which is on the autonomy feature of robot vehicles based on the kinematics, dynamics modeling and motion control aspects of the autonomous vehicles development.

2.1 Configurations of Wheeled Autonomous Vehicles

Most autonomous vehicles use either wheels, chains or legs to move around. While people and many animals walk on legs, most mobile machines roll on wheels. Wheels are simpler to control, pose fewer stability problems, use less energy per unit distance of motion, and move faster than legs (McKerrow, P.J., 1991). Since the vehicle employed in this research is a wheeled autonomous vehicle, only the publications on wheeled autonomous vehicles are reviewed. However, wheels are only usable on relatively smooth, solid terrain; on soft ground they can slip and get bogged down. In order to scale rough terrain, wheels have to be larger than the obstacles they encounter (McKerrow, P.J., 1991).

The most familiar wheel layout for a vehicle is a four wheel configuration in which the wheels are placed at the corners of a rectangle. Often, the two rear wheels are used for driving and the front two for steering. Alternative arrangements include front wheel drive, four wheel drive, and four wheel steering allowing some limited sideways motion. Most four wheeled vehicles have limited maneuverability because they are unable to move sideways. Also, a wheel suspension system is required to ensure that the wheels are in contact with the ground at all times. When moving in a straight line, all wheels rotate by the same amount, and when turning, the inside wheels rotate slower than the outside wheels to avoid skidding because the contact distance traveled by the inside wheels

is shorter. For an autonomous vehicle to meet these requirements, good mechanical design and independent control of the speed of the drive wheels are needed. Shiller, Z. and Y.R. Gwo, (1991), Sekiguchi, M. et al, (1989), and Crowley J.L., (1989) are some of the major contributors using this four wheel configuration. The vehicle model used in Graettinger, T.J. and Krogh, B.H., (1989) has two wheels, rather than four, but retains approximately the same characteristics as the four-wheeled vehicle as it is mentioned by Ellis, J.R., (1969), Hatwal, H., and Mikulcik, E.C., (1986).

One way to simplify the problems of four-wheeled vehicles is to replace the coupled steering wheels with one wheel and keep the two rear wheels driven. Still the two rear driving wheels must rotate at slightly different speeds for accurate control of turning. Three wheeled vehicles have the advantage that wheel-to-ground contact can be maintained on all wheels without a suspension system. The center of three wheeled vehicle with homogeneous distribution of mass is the center of the triangle defined by the ground contact points of the three wheels. This type of wheel configuration can be found in Steer, B., (1989), Samson, C., (1991), Hemami, A. et al, (1990). In other three wheeled vehicles, two wheels are driven independently and the other is idle caster. In order to steer the vehicle, the wheels should be driven at different speeds. For the robot to follow straight line and curves accurately, motor speeds must be controlled precisely. Giralt, G. et al, (1984), Canudas De Wit, C. and Sordalen, 0.J., (1992), Samson, C., (1990), Saha, S.K. and Angeles, J., (1989), Sordalen, O.J. and Canudas De Wit, C., (1990). Canudas De Wit, C. and Roskam, R., (1991) used the same wheel configuration as above but with the two driving wheels in front. Other variants of the three-wheeled vehicle configuration are found in Nelson, W.L., (1988), Necsulescu, D.S. and Kim, B., (1992, 1998). In one, the single wheel is the drive wheel as well as the steering wheel, enabling the other wheels to idle. Combining driving and steering mechanisms in one wheel results in a more

complex mechanical design. In this research, this tricycle type of three-wheel configuration is used and the kinematics and Newtonian dynamics are analyzed.

Some autonomous vehicles have three wheels controlled by a synchronous drive system (e.g., K2A and Denning mobile robots)found in Cybermation, (1988), Denning mobile robots Inc., (1991). All wheels are used for driving and steering. However, the wheels are coupled with a belt drive or gears, so that they can be steered by the one motor (Holland, J.M., 1989). The body of the robot always maintains a fixed orientation to the external world, and a sensor platform above the body always points in the direction of motion. All wheels are driven by a single motor. Borenstein, J. and Y. Koren, (1989, 1990) uses this type of robot vehicle (K2ARS) for obstacle avoidance control.

The autonomous vehicles described up until now were non-omnidirectional autonomous vehicles, which cannot move sideways. The vehicles mentioned so far have two degrees of freedom and these all have quite a difficult nonholonomic constraint which raised from the kinematic relation between their orientation and velocity. The systems with nonholonomic constraints have some steering control problems which are hard to overcome. In order to minimize the floor space required to turn corners and to eliminate the control problems associated with steering, the vehicle has to be omnidirectional and compact. Some omnidirectional vehicles use special wheels. One is Stanford wheel (Calisle, B., 1983, Campion, G. et al, 1988) which has the rollers perpendicular to the axis of the hub, and the other is Illanator wheel (Muir, P.F., and Newman, C.P., 1987; Feng, D. et al, 1989; Daniel, D.J. et al, 1985) which has rollers 45 degrees to the axis of the hub. Another type of wheel has a hub which is driven, and the rollers are idle. The Stanford wheel system uses three wheels, one at each corner of an equilateral triangle, and aligned such that their axes intersect at the centre of the robot. This arrangement does not need a suspension system, but has less resistance to tipping than

a four-wheel system and if one roller jams the robot is immobilized. Due to the small diameter of the rollers, they have difficulty traversing obstacles lying parallel to their axis of rotation. Each wheel has two modes of motion: a) rotation about the axis of the hub with the rollers remaining still, and b) translation in the direction of the hub axis with the rollers in contact with the floor spinning and the hub fixed. Motion in any other directions involves a combination of hub rotation and roller rotation. An Illanator wheel, as used on the Carnegie-Mellon robot Uranus, can rotate about hub with rollers still, or move at 45 degrees with the hub still and the roller in contact with the ground spinning. Left-handed and right-handed arrangements of the wheel are possible, where left or right is the direction wheel motion with only the rollers spinning. Uranus uses four wheels, two left-handed and two right handed, and requires a suspension system. The wheels are arranged so that the diagonal lines through wheel contact points intersect at the centre of the vehicle. With these wheels, the vehicle can still move forwards or backwards if a roller jams. These vehicles have the ability to achieve decoupled dynamics (in position and orientation) for following paths and avoiding obstacles, but they are more complicated and may need suspension to avoid tipping over. Also the wheels may jam easily. In this research only the non-omnidirectional wheeled vehicles are considered.

2.2 Kinematics and Dynamics Model of the Autonomous Vehicle

The feedback control of an autonomous vehicle can sometimes present subtle and surprising problems particularly due to non-holonomic constraints, i.e. differential constraints which are not integrable (Campion, G. et al, 1990). The position or posture of a vehicle is represented for planar motion by three parameters (x, y, θ) , two for orthogonal translation axes and one for orientation. However, in contrast to robotic manipulators, which are holonomic systems, rolling robots are in

general non-holonomic systems. The non-holonomic constraints in the wheels make kinematic and dynamic analysis more complicated than those of holonomic systems (Saha, S.K. and Angeles, J., 1989). For common tricycle and differential drive vehicle configurations, there are only two degree of freedom for control, that is, steering angle and velocity or the independent velocity of the two wheels of a differential drive vehicle and these vehicles are non-holonomic (Graettinger, T.J. and Krogh, B.H., 1989; Samson, C., 1991; Hemami, A. et al, 1990; Canudas de Wit, C., 1992; Saha, S.K. and Angeles, J.M 1989; Canudas de Wit, C. and Roskam, R., 1991; Necsulescu, D.S. and Kim, B., 1992; Campion, G. et al, 1990; Alexander, J.C. and Maddocks, J.H., 1990; Kanayama, Y. et al, 1990, Barraquand, J. and Latombe, J.C., 1990; and Nakamura, Y. and Hukherjee, R., 1990). Necsulescu and Kim, (1992) examined the nonholonomic constraints on the tricycle model, and Saha and Angeles, (1989) used the concept of orthogonal complement of the matrix of non-holonomic constraints on the differential-drive vehicle configuration for the development of the dynamic equations of motion of the problem. The kinematics and dynamics modeling are essential for the autonomous operation of autonomous vehicles. They are used for the purpose of trajectory planning, simulation, and control.

There is a variety of results in the literature concerning kinematics and dynamics based control for trajectory planning or generation of the autonomous vehicles. A kinematic description of both a tricycle and "turtle" robot architecture for the trajectory planning of an autonomous vehicle was developed for these two architectures and a Gaussian envelope method for modulating the steering angle was proposed by Steer, B., (1989) . A kinematics based piecewise continuous controller, which exponentially stabilizes the robot about the origin for two degrees of freedom autonomous vehicle with non-holonomic constraints, is proposed in Sordalen, 0.J. and Canudas De Wit, C., (1990).

However, the autonomous vehicles in these contributions follow a preplanned trajectory. For an autonomous vehicle given the initial and final goal positions and orientation, it is necessary to generate a path linking the two points. Trajectory generation and obstacle avoidance using virtual force field method based only on kinematics model of the autonomous vehicle is described in Borenstein, J. and Koren, Y., (1989). Kinematics based controller for trajectory generation is also presented in Alexander, J.C. and Maddocks, J.H., 1990; and Kanayama, Y et al, (1990). In order to move fast and accurate, autonomous vehicles need not only a kinematics model but also a dynamics model. Using the kinematics and dynamics models, the goal is to generate a trajectory rather than follow a preplanned trajectory. There are some dynamic based control results presented in the literature. Kinematics and Newtonian dynamics model for the control of a simplified two wheeled vehicle was reported in Graettinger, T.J. and Krogh, B.H., (1989). Saha, S.K. and Angeles, J., (1989) also developed a kinematics and Newtonian dynamics model for a three wheeled vehicle. Shiller, Z and Gwo, Y.R., (1991) did the same work as above for four wheeled vehicles. All these contributions were developed for following a preplanned trajectory, rather than generating one. Canudas De Wit, C. and Roskam, R., (1991) utilized the Lagrangian dynamic model for on line path generation in an obstacle free environment.

Wheeled autonomous vehicles are considered as multiple closed-link chains, with higher pairs of contact points between wheel and surfaces, and with reduced degrees of freedom due to the nonholonomic constraints. The instantaneously coincident coordinates were introduced as the inertial frame coinciding with the vehicle's moving reference frame at each instant of time to simplify the derivation of their matrix equations of multi-body system (Haug, E.J., 1992). In this research, a complete kinematics and Newtonian dynamics model for a tricycle is developed, rather than the two

wheeled equivalent proposed in Graettinger, T.J. and Krogh, B.H., (1989). A set of differential-algebraic equations of motion is developed from Newton-Euler dynamic model using the multi-body dynamics concept (DeSouza, A., and Greg, V.K., 1984; Houston, R.L., 1990; Haug, E.J., 1992).

2.3 Controllability of Non-holonomic Systems

A variety of theoretical and applied control problems have been studied for various classes of nonholonomic control systems. The relative difficulty of the control problem depends not only on the nonholonomic nature of the system but also on the control objective. For some control objectives, classical nonlinear control approaches (e.g., feedback linearization and dynamic inversion, as developed in Isidori, A., (1989)) are effective. Examples of such control objectives include stabilization to a suitably defined manifold that contains the equilibria manifold (Bloch, A. et al, 1992; Campion, G. et al, 1991; Kapitanovsky, A., et al 1993; Mashke, B.M., 1994; Oriolo, G., 1993), stabilization to certain trajectories (Walsh, G.C., 1994), dynamic path following (Sarkar, S., and Montgomery, R., 1992), and output tracking (Getz, N., 1994; Rui, C. and McClamroch, N.H., 1995). Consequently, there are classes of control problems for nonholonomic systems for which standard nonlinear control methods can be applied.

However, many of the most common control objectives, e.g., motion planning and stabilization to an equilibrium state, cannot be solved using the standard nonlinear control methods, and the controllability of these systems does not imply the existence of feedback stabilization. (Bloch and McClamroch, 1989; Samson, C. and Ait-Abderrahim, 1991). Brokett's theorem (Brokett, R.W., 1983) states that the non-holonomic constraints of wheeled autonomous vehicles prevent them from being stabilized at a desired posture with smooth state feedback control. Bloch and McClamroch,

(1989) first demonstrated that smooth feedback cannot stabilize a nonholonomic system to a single equilibrium point. Bloch et al. (1990) also showed that the nonholonomic systems are small-time locally controllable at the origin as in the example of the knife-edge problem. In later publications, the authors explain a general procedure for constructing piecewise analytic state feedback to stabilize the systems about a point (Bloch et al., 1992). Campion et al, (1990) proved that both kinematic and dynamic model of nonholonomic systems satisfy the strong accessibility rank condition, and stated that this property implies controllability (Nijmeijer and Van der Schaft, 1990). Barraquand, J. and Latombe, J., (1990) discussed accessibility, and local weak controllability and showed that for the cases of less than four trailers a nonholonomic vehicle(front wheel drive) is controllable.

There have been several works on the stabilization problems of non-holonomic systems with model uncertainties (Jiang, Z.P. and Pomet, J.B., 1994; Su, C.Y. and Stepanenko, Y., 1994; Hamel, T. and Meizel, D., 1996). Several control strategies have been proposed in the literature for sliding mode control of non-holonomic systems. Chacal, J.A, et al., (1994) proposed a sliding mode control that exploits a property named differential flatness of the kinematics of non-holonomic systems. In Shim, H.S., et al, (1995), a sliding mode control law was proposed in which unicycle-like robots converge to a reference trajectory with bounded errors of position and velocity. The approach was based on dynamic models of non-holonomic mobile robot. Aguilar, L.E., et al., (1997) presented a path-following feedback controller with sliding mode which is robust to localization and curvature estimation errors for a car-like robot. They used a dynamic extension of the usual kinematic model of a car, in the sense that the curvature is considered as a new state variable. Though these results are promising, it is difficult to apply sliding mode control to trajectory tracking problems of non-holonomic mobile robots when the reference trajectory is not given in a closed form. In this case, the

conventional sliding mode that completely decouples state variables is inapplicable because the dimension of the sliding mode is two, which is determined by the number of control input, but that of the output state vector is three. Yang, J.M and Kim, J.H., (1999) proposed a sliding mode controller to realize robust trajectory tracking of the error dynamics of the system with a computed-torque method for feed back linearization of the dynamic equation and showed experimentally the controller asymptotically stabilized to a desired trajectory consisting of three posture variables with two control inputs.

2.4 Path and Motion Planning

There has been a great deal of research on robot motion planning. Motion planning problems are concerned with obtaining open loop controls which steer a nonholonomic control system from an initial state to a final state over a given finite time interval. Maps and diagrams are the tools in motion planning which require the use of classical geometry, topology, algebraic geometry, algebra and computational geometry (Latombe, J.C., 1991). Extending the results of these researches to nonholonomic systems is not simple and direct because a robot may be physically incapable of following a path that changes direction by a large amount at single point, partly due to the degrees of mobility of the robot and partly due to the inability of motors to achieve infinite acceleration (McKerrow, P.J., 1991). These problems of nonholonomic autonomous vehicles made some researchers choose a strategy of considering the paths that satisfy the nonholonomic constraints. This strategy leads to what is called "nonholonomic motion planning". Some examples are the papers in the books edited by Li and Canny, (1993), Murray, Li, and Sastry, (1994), Latombe, (1991). The idea of employing piecewise constant inputs to generate motions in the directions of iterated Lie

brackets has been exploited by Lafferriere, (1991) and Lafferriere and Sussmann, (1993). They proposed a general motion planning algorithm for kinematic models of nonholonomic systems. This strategy uses either an analytical approach as in the papers by Lafferriere and Sussman, (1993) and, Divelbiss, A.W. and Wen, J., (1992) based on Lie Algebra or a differential geometric approach as by (Murray and Sastry, 1990) who extended the work by (Brockett, 1983) of using sinusoids for open loop control of nonholonomic systems. Mukhedee and Anderson, (1993) used Stoke's theorem for the same reason and L. Gurvits, (1992) used the averaging approach. This type of contributions is based on first bringing a given number of coordinates(outputs), using the same number of inputs, to their desired values and then, by using brackets, sinusoidals, closed paths of Stoke's theorem, or using the recursive averaging method, bringing the rest of coordinates to their desired values. These methods that were developed for systems without drift can be extended to power and chained forms but are not yet available to systems with general form of drift (Murray and Sastry, 1991; Sussmann, H., 1991).

Several path planning algorithms are clearly classified by as follows (Kanayama et al, 1988):

- Piece-wise continuous paths,
- Continuous paths,
- Continuous orientation paths,
- Continuous curvature paths, and
- Continuous curvature derivative paths.

The goal is to find smooth paths which satisfy some order of optimality of the curvature of the path. Kanayama and Miyake, (1986) introduced clothoid pairs and proposed the connection of two postures with zero end curvatures. Nelson, (1989) introduced the use of polar polynomials for arc

turns (to replace circle arcs) and Cartesian polynomials (to replace circular arc-arc or arc-line-arc segments for line change maneuvers). The equations have closed forms, unlike the case in former proposals. Kanayama and Hartman, (1989) use the squares of path curvature and path curvature derivative as two cost functions to find circular arcs and the set of cubic spirals as the answers of path planning problem of symmetric postures. The idea presented in this research is that in order to have a good dead reckoning (position sensing using odometry), the path has to be of continuous curvature. The dynamics of the vehicle achieves continuity of the curvature and its derivative by using the steering angle (or its derivatives) as the input to the system. Their open loop approach does not explicitly address other parameters that may affect the dynamics of the vehicle when traveling along the path.

2.5 Path Following and Trajectory Tracking

Although path planning is generally assumed to be an open-loop control scheme, there are approaches using closed-loop controllers under various names. For example Kanayama et al, (1988) proposed a method called "locomotion control" which works as a flexible interface between path planner and motor-wheel system. To differentiate between current and reference postures (positions and orientations), they chose v and ω (propulsion and angular velocities) as inputs and used a PID controller to make e_x, e_y and e_θ, (errors in Cartesian positions and orientation) go to zero. Even if the stability issue of their controller was not clear, they applied it on their autonomous vehicle Yambico-11. Nelson and Cox, (1989) proposed a "path control" which separates the path-errors (between measured and reference states) into tangential and normal and the velocity errors into two heading and speed errors. These four values are used in compensating for differences between steering angles

and driving angular velocities of the reference and actual systems. The controller has no proof for stability, but it was tested on the autonomous vehicle Blanche. Hemami et al, (1990) use linear equations for slip angles and side forces from vehicle dynamics models and assume the steering angle as the only input to upgrade the linear proportional controller of previous works into a nonlinear one. There is no study of stability of the controller and again, it was tested in simulation (using position and orientation errors). Later, Hemami et al, (1992) used a time varying linearized version of the dynamic model of their system and applied optimal control theory to design a controller for " path tracking". Their cost function contained a quadratic function of position and orientation errors and steering angle. Kanayama, Kimura, Miyazaki and Naguchi, (1990) analyzed the stability of their proposed controller for tracking using the Lyapunov direct method. They assumed heading and angular velocities of the vehicle as the inputs and a simple Cartesian kinematic set of equations for stable tracking. They also noticed that tracking a virtual vehicle makes the reference posture time-variable and the system by definition becomes non-autonomous, a fact that usually is ignored in the literature.

One of the most quoted papers in control of autonomous vehicles is a paper by Graettiger and Krogh, (1989) in which they suggest time rescaling for traveling along the path in order to satisfy torque constraints and other constraints for vehicles. Many contributions focused on path following as opposed to trajectory tracking because time assignment changes can be made. Dahl and Neilson, (1989, 1990) applied this idea using the "s" path parameter which changes on-line the nominal trajectory. Canudas De Wit, C. and Roskam, R., (1991) modified the feedback law presented by Dahl and Neilson, but, in both contributions the heading and angular velocities were the inputs rather than actual torques.

Canudas De Wit and Sordalen, (1992) extended their work on stabilization to path following problem. They proved that if the desired path is composed of a sequence of straight lines and circle segments and there are two vectors of desired velocities and maximum deviations at connecting points between each two consecutive segments (velocities could be negative or zero), then a feedback law guaranties following that path. The kinematics of their system was the simple case of a system without drift.

Having steering angle(or its derivatives) as the main state of the control law causes some error in positioning of the system. Shin et al, (1991) suggest a feedforward component in the control system to compensate for that error if the steering dynamics is modeled exactly by a first order system. They also used a fifth-order equation of the path parameter "s" as the error along the path to re-plan the path at each control cycle. After converting the new path into steering angle, this constitutes the feedback part of their controller . Samson, C., (1992) uses "s", "y" (normal to the path from the current point to the desired one) and θ(orientation) as the states and not the usual Cartesian coordinates. By applying Lyapunov direct method, he shows that with one input, it is possible to make y and θ follow their desired values. The advantage of this approach is that it leaves the other input (heading velocity) to control the third variable(s), but the system equations used were kinematics based and correspond to a simple vehicle.

2.6 Feedback Linearization

Feedback linearization is a powerful technique to force a dynamic system to behave linearly. It consists in extending the plant by a nonlinear feedback that compensates its nonlinearity, so that the dynamics of the new composed system is linear (Isidori, A., 1989). Almost every physical system

is fundamentally nonlinear. A linear system approach is often used for the design of a controller based on the linear approximation of the system about a desirable operating point. Under reasonable conditions, the linear controller can be used to stabilize and regulate the system about the operating point. Robust methods were developed to enlarge the region where such linear controllers can effectively control the nonlinear system.

For many of these systems, when the goal is to have this ability and maneuverability to track a rich set of output trajectories, one common approach is to linearize the system about the reference trajectory to obtain a linear time-varying system. This system is valid in a very small neighbourhood of the desired trajectory and a time-varying compensator has to be designed. For a nonholonomic system in general and a vehicle with ideal rolling condition in particular, one of the goals is trajectory tracking or path following. The linear approximation is, however, valid for only for a small region and not for a long trajectory or path. For these systems linear approximation results in a non-square matrix and the system becomes uncontrollable (Samson, C. and Ait-Abderrahim, 1990).

The alternative approach is to use nonlinear control theory and in particular input-output linearization using state feedback. This method is useful for tracking and stabilization of nonlinear systems with stable internal dynamics(Slotine, 1991; and Isidori, 1989). Examples of applying this method to vehicles and autonomous vehicles are given in Necsulescu et al, (1994) and d'Andrea-Novel et al, (1992). Yun and Ymamoto, (1993), for dynamic model of a two rear wheels driven autonomous vehicle, used feedback linearization and showed that its internal dynamics is stable if the vehicle keeps moving forward. Deng and Brady, (1993) developed a controller for trajectory tracking of a dynamic model of a tricycle with front wheel steering and driving. Sarkar et al, (1994) did the same thing for path following of a vehicle with two driving wheels.

2.7 Model Predictive Control

Model Predictive Control (MPC) is probably the most important approach to the advanced control of complex interacting industrial processes. Uniquely amongst modern theories, MPC can handle real-time state and actuator constraints in a natural way, enabling plants to operate more closely to their ultimate profitable margins. The richness of the field (there being wide ranges of choice in model structures, prediction horizons and optimization criteria) allows a control designer to tailor MPC for one's application, whether it be a high-speed machine tool, a patient in the operating room, or a large-scale industrial process (Clarke, D., 1994). MPC formulation integrates optimal control, stochastic control, control of processes with dead time, multi-variable control, and future references when available. The MPC research literature is by now large, but review articles have appeared at regular intervals. The three MPC papers presented at the Chemical Process Control (CPC) V conference in 1996 are an excellent starting point (Lee, J.H. and Cooley, B. (1997); Mayne, D.Q. (1997); Qin, S.J. and Badgwell, T.A. (1997)). Qin and Badgwell presented comparisons of industrial MPC algorithms that practitioners may find particularly useful. Kwon provided a very extensive list of references (Kwon, W.H., 1994). Allgöwer and coworkers have presented a recent mini course covering the area (Allgöwer, F., et al, 1999). Finally, Rowlings, J.B. provided a reasonably accessible and self-contained tutorial exposition on MPC (Rowlings, J.B., 2000).

The concept of predictive control was introduced in the late seventies simultaneously by the development and application of heuristic approaches: IDCOM (Identification/Command) by Richalet, (1978), and DMC (Dynamic Matrix Control) by Cutler and Ramaker, (1980). Self-tuning and adaptive control researchers, disappointed by instabilities of their early-generation algorithms, discovered the robustness of adaptive MPC in the development of methods such as GPC (Generalized

Predictive Control) (Clarke et al, 1987, 1989). MPC is not a specific control strategy but more of a very ample range of control methods developed around certain common ideas. These design methods lead to linear controllers which have practically the same structure and present adequate degrees of freedom. The ideas appearing in greater or lesser degree in all the predictive control family are basically (Camacho, E. and Bordons, C., 1995):

- Explicit use of a model to predict the process output at future time instants (horizon).
- Calculation of a control sequence minimizing a certain objective function.
- Receding strategy, so that at each instant the horizon is displaced towards the future, which involves the application of the first control signal of the sequence calculated at each step.

The various MPC algorithms only differ amongst themselves in the model used to represent the process the type of noise assumed and the cost function to be minimized.

There are many applications of predictive control used successfully at the present time. Applications in the cement industry, drying towers and in robot arms, are described in Clarke, (1988), whilst developments for distillation columns, PVC plants, steam generators or servos are presented in Richalet, J., (1978, 1993). The good performance of these applications shows the capacity of the MPC to achieve highly efficient control systems able to operate during long periods of time with hardly any intervention.

Predictive controllers can be (and have been) derived for and applied to multi-input, multi-output (MIMO) processes. Extending predictive controllers for SISO processes to MIMO processes is straightforward (Kinnaert, M., 1989). In contrast to LQ and pole-placement controllers, predictive controllers can be derived for nonlinear processes. A nonlinear model of the process is then used explicitly to design the controller (Soeterboek et al, 1991).

Predictive control is an open methodology. That is, within the framework of predictive control there are many ways to design a predictive controller. As a result, over ten different predictive controllers, each with different properties, have been proposed in the literature over the last decade. Some well-known predictive controllers are GPC (Generalized Predictive Control; Clarke et al, 1987), DMC (Dynamic Matrix Control; Cutler and Ramaker, 1980), EPSAC (Extended Prediction Self-Adaptive Control; De Keyser and Van Cauwenberghe, 1985), PFC (Predictive Functional Control; Richalet et al, 1987), EHAC (Extended Horizon Adaptive Control, Ydstie, 1984) and UPC (Unified Predictive Control, Soeterboek, 1990).

In this thesis, a combined control approach of a feedback linearization and of a Model Predictive Controller is proposed for motion control of the autonomous vehicle . The embedded feedback linearization allows to restate the predictive problem as a linear one, while the MPC can be designed either to improve performance or to avoid reaching input bounds, which are known to be a possible cause of instability for standard feedback linearization.

An MPC algorithm for the control of sheet and film processes has been developed which directly addresses actuator limitations and model uncertainties. The MPC algorithm proved to be implemented in real time and robust for model uncertainties (VanAntwerp, J.G., and Braatz, R. D., 2000). Katende, E., and Jutan, A., (2000) developed a nonlinear generalized predictive control (NLGPC) algorithm for the temperature control for a batch reactor system and compared the algorithm with a self-tuning PID controller (Katende, E., and Jutan, A., 1993), the generalized minimum variance (GMV) controller (Clarke and Gawthrope, 1975), and the well-known generalized predictive control (GPC) algorithm (Clarke et al, 1987) . They proved the controllers listed above are robust and perform reasonably well under noisy conditions and changing system parameters and

also the NLGPC showed distinctive advantages over the other controllers on their performances.

There are a few attempts of applying model predictive controller for mobile robot navigation in real time. Gomez-Ortega, J. and Camacho, E. F., (1994, 1996) had implemented an MPC combined with a neural-network for a mobile robot navigation. And Gomez-Ortega, J. et al, (1997) replaced the neural-network algorithm with a fuzzy logic controller while maintaining the same MPC utilizing a nonlinear kinematic model of the vehicle. Both designs had to be trained from a set of training patterns, and allowed the application of a real time predictive control strategy for mobile robot navigation with unforseen obstacles. Recently Ramirez,D. R., et al , (1999) used a stochastic algorithms called GA (Genetic Algorithm) with an MPC for the same application. They achieved good solutions in real time experimentally by applying GAs to the online optimization in the MPC problem, but they only used the kinematic model of the vehicle.

III. MODELLING OF AN AUTONOMOUS VEHICLE MOVING ON AN INCLINED SURFACE

3.1 Kinematic model of the vehicle

In order to facilitate the development of the dynamic model and the control law, multiple reference frames should be chosen for wheeled vehicles. Two inertial frames and four moving reference frames are chosen for a wheeled vehicle with rigid body structure and wheels moving on an inclined plane which has a slope β (Fig. 3.1). One inertial frame, M-Q-P, has the plane M-Q placed on the horizontal ground surface, while the second inertial frame, N-Q-R, contains the inclined plane N-Q of the motion of the vehicle. The two inertial frames have a common axis Q and the angle between M-Q and N-Q planes is β. One moving reference frame X-Y-Z is attached to the vehicle structure (X-axis along the vehicle, Y-axis parallel to the rear axle, and Z-axis perpendicular to X-Y plane originated at O in the vehicle's centre of mass). Three other moving frames, X_i-Y_i-Z_i (i=1,2,3), with origins O_i, are attached to the three wheels, with Z_i parallel to Z (Fig. 3.2).

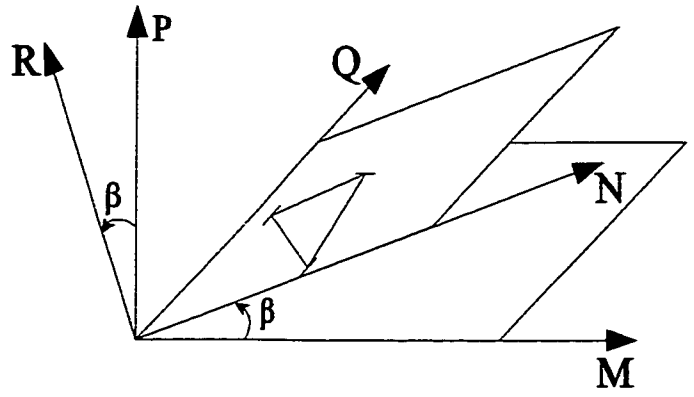

Figure 3.1 Inertial frame transformation

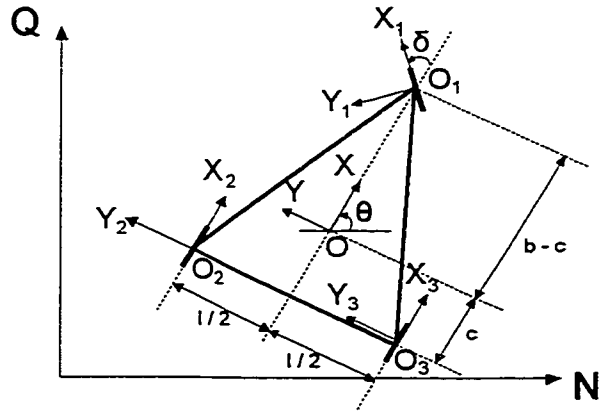

Figure 3.2 The moving reference frames for the lateral motion of the autonomous vehicle.

The coordinate transformation gives the position(N,Q,R) in N-Q-R plane of a point defined by the position(X,Y,Z) in X-Y-Z plane where the θ is the orientation angle between N and X axis of the two inertial frames, N-Q-R and X-Y-Z.

$$\begin{bmatrix} X \\ Y \\ Z \end{bmatrix} = \begin{bmatrix} \cos\delta & -\sin\delta & 0 \\ \sin\delta & \cos\delta & 0 \\ 0 & 0 & 1 \end{bmatrix} \begin{bmatrix} X_1 \\ Y_1 \\ Z_1 \end{bmatrix}, \qquad \begin{bmatrix} N \\ Q \\ R \end{bmatrix} = \begin{bmatrix} \cos\theta & -\sin\theta & 0 \\ \sin\theta & \cos\theta & 0 \\ 0 & 0 & 1 \end{bmatrix} \begin{bmatrix} X \\ Y \\ Z \end{bmatrix} = \tau \begin{bmatrix} X \\ Y \\ Z \end{bmatrix} \tag{3-1}$$

$$\begin{bmatrix} M \\ Q \\ P \end{bmatrix} = \begin{bmatrix} \cos\beta & 0 & -\sin\beta \\ 0 & 1 & 0 \\ \sin\beta & 0 & \cos\beta \end{bmatrix} \begin{bmatrix} N \\ Q \\ R \end{bmatrix} \tag{3-2}$$

For determining the moving reference frame's position and orientation with regard to the inertial frame, the (algebraic) vectors for absolute positions of the origins $\mathbf{R}$, $\mathbf{R}_i$ (i=1,2,3) and the orientation angles θ of X, X_2, X_3 and $\theta+\delta$ of the X_1 axis with regard to N are defined.

For inclined plane motion analysis only N-Q and X-Y components are needed, i.e., 8 components for the 4 position vectors. These components are, however, dependent, given that for the case of assuming the vehicle structure a rigid body, the following holonomic constraints result, (Fig. 3.3)

$$\boldsymbol{R}_i = \boldsymbol{R} + \tau \boldsymbol{r}_i \qquad (i = 1,2,3) \tag{3-3}$$

where $\mathbf{r}_i$ are relative positions of the origins O_{sa} (origin of the steering assembly) for the front wheel and O_i (i=2,3) for the rear wheels with regard to X-Y-Z frame origin, O. (Fig. 3.3 and 3.5).

$$
\begin{aligned}
\boldsymbol{r}_1 &= [b-c \quad 0 \quad r_{w1}+s_{a+b}-h]^T \\
\boldsymbol{r}_2 &= [-c \quad \frac{l}{2} \quad r_{w2}-h]^T \\
\boldsymbol{r}_3 &= [-c \quad -\frac{l}{2} \quad r_{w3}-h]^T
\end{aligned}
\tag{3-4}
$$

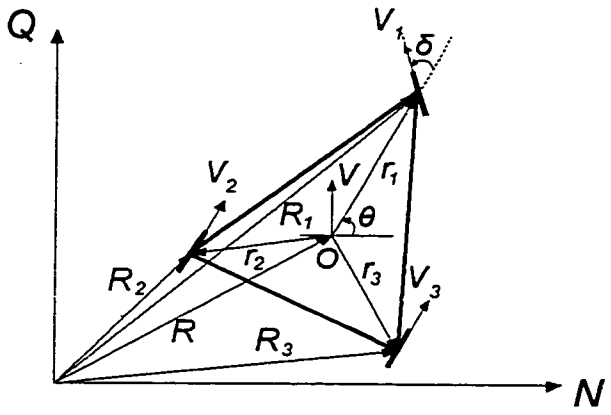

Figure 3.3 Velocity diagram for no slip conditions

h is defined as the height of the centre of mass of the structure from the surface of the inclined plane,

$$
h = \frac{b-c}{2b}(r_{w2}+r_{w3}) + \frac{c}{b}(r_{w1}+s_{a+b}) \tag{3-5}
$$

where, $\mathbf{r}_{wi}$ are the radii of each wheels (i=1,2,3)

$\mathbf{s}_{a+b}$ is the distance between the center point of the front wheel and linkage point of the steering assembly with the robot frame ($\mathbf{s}_{a+b}=\mathbf{s}_a+\mathbf{s}_b$)

$\boldsymbol{\tau}$ is the transformation matrix defining the rotation of X-Y-Z with regard to N-Q-R about the vertical axis

$$\tau = \begin{bmatrix} \cos\theta & -\sin\theta & 0 \\ \sin\theta & \cos\theta & 0 \\ 0 & 0 & 1 \end{bmatrix} \tag{3-6}$$

Equation(3-3) represents 6 scalar holonomic constraints.

Given that the transformation matrix has the property

$$\tau^T = \tau^{-1} \tag{3-7}$$

eq. (3-3) can be expressed with regard to the X-Y-Z frame as

$$P_i = P + r_i \tag{3-8}$$

where the absolute position vectors $\mathbf{P}_i$ and $\mathbf{P}$, expressed in X-Y-Z frame, are denoted as

$$P_i = \tau^T R_i = [x_i \quad y_i \quad z_i]^T \tag{3-9}$$

$$P = \tau^T R = [x \quad y \quad z]^T \tag{3-10}$$

Absolute velocities of the origins O_i expressed in N-Q-R frame are obtained by differentiation of Eq. (3-3). For $\dot{\mathbf{r}}_i = 0$ (from rigid body assumption),

$$\dot{R}_i = \dot{R} + \dot{\tau} r_i \qquad i = 1,2,3 \tag{3-11}$$

Absolute velocities $\mathbf{V}$ and $\mathbf{V}_i$ (i=1,2,3) expressed in X-Y-Z frame

$$V = [V_x \quad V_y \quad V_z]^T \tag{3-12}$$

$$V_i = [V_{xi} \quad V_{yi} \quad V_{zi}]^T \tag{3-13}$$

can be obtained from R_i and R as follows

$$V_i = \tau^T \dot{R}_i \qquad i = 1,2,3 \tag{3-14}$$

$$V = \tau^T \dot{R} \tag{3-15}$$

Equation (3-11), using eq. (3-14) and (3-15), becomes

$$V_i = V + \tau^T \dot{\tau} r_i \qquad i = 1,2,3 \tag{3-16}$$

The time derivative of eq. (3-10) gives

$$\dot{P} = \dot{\tau}^T R + \tau^T \dot{R} \tag{3-17}$$

Using eq. (3-7),(3-10), and (3-15), eq. (3-17) becomes

$$\dot{P} = \dot{\tau}^T \tau P + V \tag{3-18}$$

The time derivative of $\tau^T \tau = I$ gives

$$\dot{\tau}^T \tau = -\tau^T \dot{\tau} \tag{3-19}$$

such that eq. (3-18) becomes

$$V = \dot{P} + \tau^T \dot{\tau} P \tag{3-20}$$

From eq. (3-6), the following result is obtained

$$\boldsymbol{\tau}^T\dot{\boldsymbol{\tau}} = \begin{bmatrix} 0 & -\dot{\theta} & 0 \\ \dot{\theta} & 0 & 0 \\ 0 & 0 & 0 \end{bmatrix} \tag{3-21}$$

In explicit form, equation (3-16) becomes

$$\boldsymbol{V}_1 = \begin{bmatrix} V_{x1} \\ V_{y1} \\ V_{z1} \end{bmatrix} = \begin{bmatrix} V_x \\ V_y \\ V_z \end{bmatrix} + \begin{bmatrix} 0 & -\dot{\theta} & 0 \\ \dot{\theta} & 0 & 0 \\ 0 & 0 & 0 \end{bmatrix} \begin{bmatrix} b-c \\ 0 \\ r_{w1}+s_a-h \end{bmatrix} = \begin{bmatrix} V_x \\ V_y+(b-c)\dot{\theta} \\ V_z \end{bmatrix} \tag{3-22}$$

$$\boldsymbol{V}_2 = \begin{bmatrix} V_{x2} \\ V_{y2} \\ V_{z2} \end{bmatrix} = \begin{bmatrix} V_x-(l/2)\dot{\theta} \\ V_y-c\dot{\theta} \\ V_z \end{bmatrix} \tag{3-23}$$

$$\boldsymbol{V}_3 = \begin{bmatrix} V_{x3} \\ V_{y3} \\ V_{z3} \end{bmatrix} = \begin{bmatrix} V_x + (l/2)\dot{\theta} \\ V_y - c\dot{\theta} \\ V_z \end{bmatrix} \tag{3-24}$$

Absolute accelerations of the origins O_i of X_i-Y_i-Z_i frames (i=1,2,3) expressed in X-Y-Z frame are obtained by derivation from eq. (3-14)

$$\dot{\boldsymbol{V}}_i = \boldsymbol{\tau}^T\ddot{\boldsymbol{R}}_i + \dot{\boldsymbol{\tau}}^T\dot{\boldsymbol{R}}_i \qquad i=1,2,3 \tag{3-25}$$

Denoting the absolute acceleration of O expressed in X-Y-Z frame

$$\boldsymbol{A}_i = \begin{bmatrix} A_{xi} & A_{yi} & A_{zi} \end{bmatrix}^T \qquad i=1,2,3 \tag{3-26}$$

it is given by

$$\boldsymbol{A}_i = \boldsymbol{\tau}^T\ddot{\boldsymbol{R}}_i \qquad i=1,2,3 \tag{3-27}$$

Taking into account eq. (3-14) and (3-27), eq. (3-25) becomes

$$\dot{V}_i = A_i + \dot{\tau}^T \tau V_i \qquad i=1,2,3 \tag{3-28}$$

or, using eq. (3-19),

$$A_i = \dot{V}_i + \tau^T \dot{\tau} V_i \qquad i=1,2,3 \tag{3-29}$$

Following the same procedure, the relationships between the absolute velocity $\mathbf{V}$ and the absolute acceleration $\mathbf{A}$ of the center of mass $\mathbf{O}$ expressed in X-Y-Z frame as

$$A = \tau^T \ddot{R} = [A_x \quad A_y \quad A_z]^T \tag{3-30}$$

it results from time derivative of eq. (3-15) as

$$A = \dot{V} + \tau^T \dot{\tau} V \tag{3-31}$$

For obtaining the relationships between $\mathbf{A}_i$ and $\mathbf{A}$, the derivative of eq. (3-11) is used

$$\ddot{R}_i = \ddot{R} + \ddot{\tau} r_i \tag{3-32}$$

Pre-multiplying eq. (3-32) by τ^T, and using (3-27) and (3-30), the following equation is obtained

$$A_i = A + \tau^T \ddot{\tau} r_i \tag{3-33}$$

Given eq. (3-6), $\tau^T \ddot{\tau}$ results as

$$\tau^T \ddot{\tau} = \begin{bmatrix} -\dot{\theta}^2 & -\ddot{\theta} & 0 \\ \ddot{\theta} & -\dot{\theta}^2 & 0 \\ 0 & 0 & 0 \end{bmatrix} \tag{3-34}$$

In explicit form, eq. (3-33) becomes

$$\boldsymbol{A}_1 = \begin{bmatrix} A_{x1} \\ A_{y1} \\ A_{z1} \end{bmatrix} = \begin{bmatrix} A_x \\ A_y \\ A_z \end{bmatrix} + \begin{bmatrix} -\dot{\theta}^2 & -\ddot{\theta} & 0 \\ \ddot{\theta} & -\dot{\theta}^2 & 0 \\ 0 & 0 & 0 \end{bmatrix} \begin{bmatrix} b-c \\ 0 \\ r_{w1}+s_a-h \end{bmatrix} = \begin{bmatrix} A_x-(b-c)\dot{\theta}^2 \\ A_y+(b-c)\ddot{\theta} \\ A_z \end{bmatrix} \tag{3-35}$$

$$\boldsymbol{A}_2 = \begin{bmatrix} A_{x2} \\ A_{y2} \\ A_{z2} \end{bmatrix} = \begin{bmatrix} A_x + c\dot{\theta}^2 - (l/2)\ddot{\theta} \\ A_y - c\ddot{\theta} - (l/2)\dot{\theta}^2 \\ A_z \end{bmatrix} \tag{3-36}$$

$$\boldsymbol{A}_3 = \begin{bmatrix} A_{x3} \\ A_{y3} \\ A_{z3} \end{bmatrix} = \begin{bmatrix} A_x + c\dot{\theta}^2 + (l/2)\ddot{\theta} \\ A_y - c\ddot{\theta} + (l/2)\dot{\theta}^2 \\ A_z \end{bmatrix} \tag{3-37}$$

The constraints for velocities, eqs. (3-22) ~ (3-24), and for accelerations, eqs. (3-35) ~ (3-37), were obtained from the holonomic constraint, eq. (3-3). The assumptions with regard to the contact between the wheels and the ground impose further constraints. In the case of assuming ideal rolling, i.e. no loss of contact and no side-way slip for the wheels, the wheel angular speeds $\dot{\alpha}_i$(i=1,2,3) about their axes Y_i and the absolute speeds $\mathbf{V}_i$ of the origins O_i expressed in X-Y frame are linked by the following differential constraints (Fig. 3.3),

$$V_1 = \begin{bmatrix} V_{x1} \\ V_{y1} \\ V_{z1} \end{bmatrix} = \begin{bmatrix} r_{w1}\dot{\alpha}_1 \cos\delta \\ r_{w1}\dot{\alpha}_1 \sin\delta \\ 0 \end{bmatrix} \tag{3-38}$$

$$V_2 = \begin{bmatrix} V_{x2} \\ V_{y2} \\ V_{z2} \end{bmatrix} = \begin{bmatrix} r_{w2}\dot{\alpha}_2 \\ 0 \\ 0 \end{bmatrix} \tag{3-39}$$

$$V_3 = \begin{bmatrix} V_{x3} \\ V_{y3} \\ V_{z3} \end{bmatrix} = \begin{bmatrix} r_{w3}\dot{\alpha}_3 \\ 0 \\ 0 \end{bmatrix} \tag{3-40}$$

where r_{wi} (i=1,2,3) are the radii of the wheels and δ is the front wheel steering angle.

The nine differential scalar constraints given by eqs. (3-38) ~ (3-40) are reduced to eight independent constraints if it is taken into account that eqs. (3-23) and (3-24) give

$$V_{y2} = V_{y3} \tag{3-41}$$

such that $V_{y2} = 0$ in eq. (3-39) implies in this case $V_{y3} = 0$, which makes redundant second equation of (3-40). Also from eqs.(3-22) to (3-24), $V_{z1} = V_{z2} = V_{z3}$ such that out of 9 eqs.(3-38), (3-39), and (3-40) three equations are dependent, i.e. only six independent constraints remain, three equations from eq.(3-38), first two from eq.(3-39), and first one of eq.(3-40).

Eq. (3-38) contains one non-holonomic constraint

$$\frac{V_{y1}}{V_{x1}} = \tan\delta \tag{3-42}$$

while the other differential constraints are integrable. The dynamic model contains, however, reaction forces between the wheels and the ground which are associated with these differential constraints and for this reason all differential constraints are retained .

The 17 coordinates used for determining the motion of the vehicle structure ($x,y,z,x_1, y_1,z_1, x_2,y_2,z_2, x_3,y_3,z_3, \theta$) and the wheels ($x_1, y_1,z_1, x_2, y_2,z_2, x_3, y_3,z_3, \alpha_1, \alpha_2, \alpha_3, \delta$) are subject to 9 scalar holonomic constraints given by eq. (3-3) and 6 independent differential constraints out of the 9 constraints given by eqs. (3-38) ~ (3-40). Consequently, the vehicle has only two degrees of freedom, however, due to retaining the 5 independent differential constraints, only 9 of the coordinates will be eliminated. The 9 scalar holonomic constraints given by eq. (3-3) will be used to eliminate the 9 coordinates x_i,y_i,z_i (i=1,2,3) out of 17 coordinates such that the equations will be written with regard to the retained 8 coordinates $x,y,z,\theta,\alpha_1,\alpha_2,\alpha_3, \delta$.

The constraints for accelerations can be obtained from eqs. (3-29) and (3-38) ~ (3-40)

$$\boldsymbol{A}_1 = \begin{bmatrix} A_{x1} \\ A_{y1} \\ A_{z1} \end{bmatrix} = \dot{\boldsymbol{V}}_1 + \begin{bmatrix} 0 & -\dot{\theta} & 0 \\ \dot{\theta} & 0 & 0 \\ 0 & 0 & 0 \end{bmatrix} \boldsymbol{V}_1 = \begin{bmatrix} r_{w1}\ddot{\alpha}_1\cos\delta - r_{w1}\dot{\alpha}_1\dot{\delta}\sin\delta - r_{w1}\dot{\alpha}_1\dot{\theta}\sin\delta \\ r_{w1}\ddot{\alpha}_1\sin\delta + r_{w1}\dot{\alpha}_1\dot{\delta}\cos\delta + r_{w1}\dot{\alpha}_1\dot{\theta}\cos\delta \\ 0 \end{bmatrix} \tag{3-43}$$

$$\boldsymbol{A}_2 = \begin{bmatrix} A_{x2} \\ A_{y2} \\ A_{z2} \end{bmatrix} = \begin{bmatrix} r_{w2}\ddot{\alpha}_2 \\ r_{w2}\dot{\theta}\dot{\alpha}_2 \\ 0 \end{bmatrix} \tag{3-44}$$

$$\boldsymbol{A}_3 = \begin{bmatrix} A_{x3} \\ A_{y3} \\ A_{z3} \end{bmatrix} = \begin{bmatrix} r_{w3}\ddot{\alpha}_3 \\ r_{w3}\dot{\theta}\dot{\alpha}_3 \\ 0 \end{bmatrix} \tag{3-45}$$

The elimination of V_{xi}, V_{yi}, V_{zi} from the differential constraints for velocities, eqs. (3-38) ~ (3-40), is obtained using the derivative of the holonomic constraint (3-3) in the form given in eqs. (3-22) ~ (3-24), such that the following 5 independent scalar differential constraints result for the retained 8 coordinates, $x,y,z,\theta,\alpha_1,\alpha_2,\alpha_3, \delta$.

$$V_x = r_{w1}\dot{\alpha}_1 \cos\delta \tag{3-46}$$

$$V_y + (b-c)\dot{\theta} = r_{w1}\dot{\alpha}_1 \sin\delta \tag{3-47}$$

$$V_x - (l/2)\dot{\theta} = r_{w2}\dot{\alpha}_2 \tag{3-48}$$

$$V_y - c\dot{\theta} = 0 \tag{3-49}$$

$$V_x - (l/2)\dot{\theta} = r_{w3}\dot{\alpha}_3 \tag{3-50}$$

plus the trivial constraint, $V_z = 0$ due to the assumption of no loss of wheel-ground contact .

The non-holonomic constraint in terms of V_x, V_y and δ results from eqs. (3-46), (3-47) and (3-49),

$$\tan\delta = \frac{bV_y}{cV_x} \tag{3-51}$$

Similarly, the elimination of A_{xi}, A_{yi}, A_{zi} from the constraints for accelerations, eqs. (3-43) ~

(3-45) is obtained using eqs. (3-35) ~ (3-37) resulting in the following 6 differential constraints in scalar form

$$r_{w1}\ddot{\alpha}_1 \cos\delta - r_{w1}\dot{\alpha}_1(\dot{\delta}+\dot{\theta})\sin\delta = A_x - (b-c)\dot{\theta}^2 \tag{3-52}$$

$$r_{w1}\ddot{\alpha}_1 \sin\delta + r_{w1}\dot{\alpha}_1(\dot{\delta}+\dot{\theta})\cos\delta = A_y + (b-c)\ddot{\theta} \tag{3-53}$$

$$r_{w2}\ddot{\alpha}_2 = A_x + c\dot{\theta}^2 - (l/2)\ddot{\theta} \tag{3-54}$$

$$r_{w2}\dot{\theta}\dot{\alpha}_2 = A_y - c\ddot{\theta} - (l/2)\dot{\theta}^2 \tag{3-55}$$

$$r_{w3}\ddot{\alpha}_3 = A_x + c\dot{\theta}^2 + (l/2)\ddot{\theta} \tag{3-56}$$

$$r_{w3}\dot{\theta}\dot{\alpha}_3 = A_y - c\ddot{\theta} + (l/2)\dot{\theta}^2 \tag{3-57}$$

plus the trivial constraint $A_z = 0$.

Only five independent constraints result out of the six given by eqs. (3-52) ~ (3-57). This can be proved as follows:

Eq. (3-56) can be obtained by eliminating $A_y - c\ddot{\theta}$ between eqs. (3-55) and (3-57), taking the derivative of the resulting equation and using eq. (3-54). The equations (3-52) ~ (3-56) will be used as independent differential constraints for the dynamic model of the vehicle.

For the purpose of controlling the system and developing the dynamic model, all the velocities need to be expressed as functions of ω_1, ω_δ and δ. By using equations (3-46) ~ (3-50) the following 5 independent equations result:

$$\omega_\theta = 1/b\, r_1 \omega_1 \sin(\delta) \tag{3-58}$$

$$\omega_2 = 1/r_2(\cos(\delta) - l/(2b)\sin(\delta))r_1\omega_1 \tag{3-59}$$

$$\omega_3 = 1/r_3(\cos(\delta) + l/(2b)\sin(\delta))r_1\omega_1 \tag{3-60}$$

$$V_x = r_1\omega_1\cos(\delta) \tag{3-61}$$

$$V_y = r_1\omega_1 c/b\ \sin(\delta) \tag{3-62}$$

For the same purpose as with the velocities, the absolute accelerations of the origin o_i (i=1,2,3) in X-Y-Z frame need to be expressed as functions of A_x, A_y (directional accelerations of the centre of mass of the vehicle with respect to the vehicle moving reference frame), and the angular velocities ω_θ, ω_2. Equation (3-55) gives,

$$\dot{\omega}_\theta = (A_y - \frac{l}{2}\omega_\theta^2 - r_2\omega_\theta\omega_2)/c \tag{3-63}$$

Using this expression in equations (3-35) ~ (3-37), we get:

$$A_{xl} = A_x - (b-c)\omega_\theta^2 \tag{3-64}$$

$$A_{yl} = \frac{b}{c}A_y - l\frac{(b-c)}{2c}\omega_\theta^2 - r_2\frac{l}{2c}\omega_\theta\omega_2 \tag{3-65}$$

$$A_{x2} = A_x - \frac{l}{2c}A_y + (c + \frac{l^2}{4c})\omega_\theta^2 + r_2\frac{l}{2c}\omega_\theta\omega_2 \tag{3-66}$$

$$A_{y2} = r_2\omega_\theta\omega_2 \tag{3-67}$$

$$A_{x3}=A_x+\frac{l}{2c}A_y+(c-\frac{l^2}{4c})\omega_\theta^2-r_2\frac{l}{2c}\omega_\theta\omega_2 \tag{3-68}$$

$$A_{y3}=l\omega_\theta^2+r_2\omega_\theta\omega_2 \tag{3-69}$$

3.2 The 3-D Newtonian dynamic model of the autonomous vehicle for Inclined Plane Motion

A Newtonian dynamic model of the vehicle is obtained using free body diagrams for the rigid vehicle frame (Fig. 3.4), steering assembly (Fig. 3.5), and for each of the 3 wheels (Fig. 3.6 and Fig. 3.7). The derivation of Newton Euler equations of motion uses absolute acceleration expressed in X-Y-Z frame.

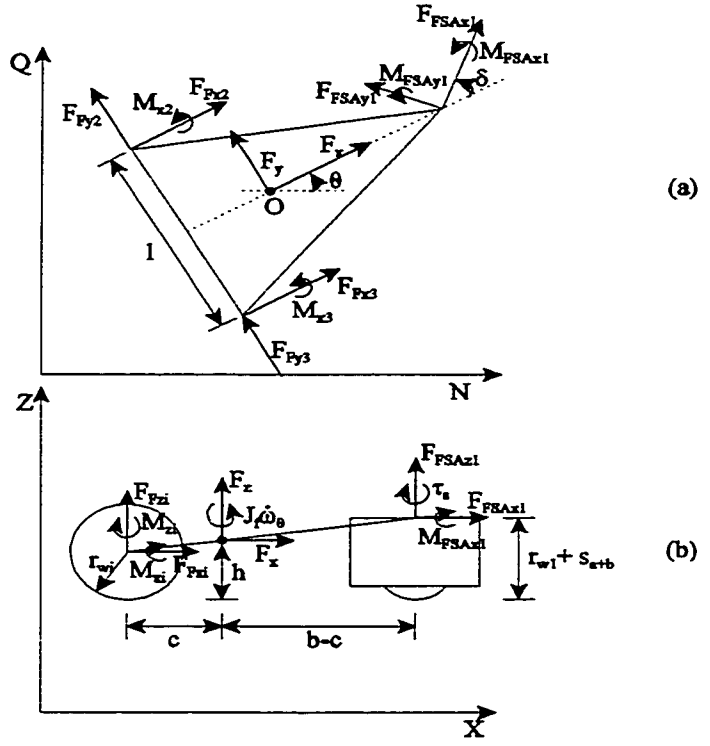

Figure 3.4 Free body diagram for the vehicle frame: (a) top view and, (b) side view

For the rigid vehicle frame, six equations of motion are obtained for the three dimensional translation and the rotation about axes X, Y, Z (Fig. 3.4).

$$m_f A_x = F_{FSAxl}\cos\delta - F_{FSAyl}\sin\delta + F_{Fx2} + F_{Fx3} - m_f g \sin\beta\cos\theta \qquad (3\text{-}70)$$

$$m_f A_y = F_{FSAx1}\sin\delta + F_{FSAy1}\cos\delta + F_{Fy2} + F_{Fy3} + m_f g\sin\beta\sin\theta \tag{3-71}$$

$$m_f A_z = F_{FSAz1} + F_{Fz2} + F_{Fz3} - m_f g\cos\beta \tag{3-72}$$

$$J_f\dot{\omega}_\theta = (b-c)(F_{FSAx1}\sin\delta + F_{FSAy1}\cos\delta) - \frac{l}{2}F_{Fx2} + \frac{l}{2}F_{Fx3} - c(F_{Fy2}+F_{Fy3}) - M_{z2} - M_{z3} - \tau_s \tag{3-73}$$

$$\begin{aligned} 0 = {} & (h - s_{a+b} - r_{w1})(F_{FSAx1}\sin\delta + F_{FSAy1}\cos\delta) + \frac{l}{2}F_{Fz2} - (r_{w2}-h)F_{Fy2} \\ & - \frac{l}{2}F_{Fz3} - (r_{w3}-h)F_{Fy3} - M_{x2} - M_{x3} - (M_{SAx1}\cos\delta - M_{SAy1}\sin\delta) \end{aligned} \tag{3-74}$$

$$\begin{aligned} 0 = {} & -(b-c)F_{Fz1} - (h - s_{a+b} - r_{w1})(F_{FSAx1}\cos\delta - F_{FSAy1}\sin\delta) + cF_{Fz2} \\ & + (r_{w2}-h)F_{Fx2} + cF_{Fz3} + (r_{w3}-h)F_{Fx3} - (M_{SAx1}\sin\delta + M_{SAy1}\cos\delta) \end{aligned} \tag{3-75}$$

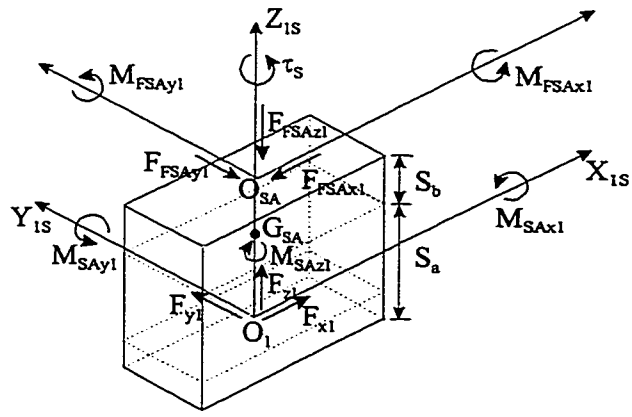

Figure 3.5 Free body diagram for the steering assembly

For the steering assembly, six equations of motion are obtained for the translation and for the

rotation about X_1 Y_1 Z_1 axes (Fig. 3.5).

$$m_{SA}A_{xl} = [F_{SAxl} - F_{FSAxl} - m_{SA}g\sin\beta\cos(\theta+\delta)]\cos\delta - [F_{SAyl} - F_{FSAyl} + m_{SA}g\sin\beta\sin(\theta+\delta)]\sin\delta \quad (3\text{-}76)$$

$$m_{SA}A_{yl} = [F_{SAxl} - F_{FSAxl} - m_{SA}g\sin\beta\cos(\theta+\delta)]\sin\delta + [F_{SAyl} - F_{FSAyl} + m_{SA}g\sin\beta\sin(\theta+\delta)]\cos\delta \quad (3\text{-}77)$$

$$m_f A_z = F_{SAzl} - F_{FSAzl} - m_{SA}g\cos\beta \quad (3\text{-}78)$$

$$-I_{SAxl}(\omega_\theta+\omega_\delta)\omega_1 = s_b F_{FSAyl} + s_d F_{SAyl} + M_{FSAxl} - M_{SAxl} \quad (3\text{-}79)$$

$$I_{SAyl}\dot{\omega}_1 = -s_b F_{FSAxl} - s_d F_{SAxl} + M_{FSAyl} - M_{SAyl} \quad (3\text{-}80)$$

$$J_{SA}(\dot{\omega}_\theta+\dot{\omega}_\delta) = \tau_s - M_{SAzl} \quad (3\text{-}81)$$

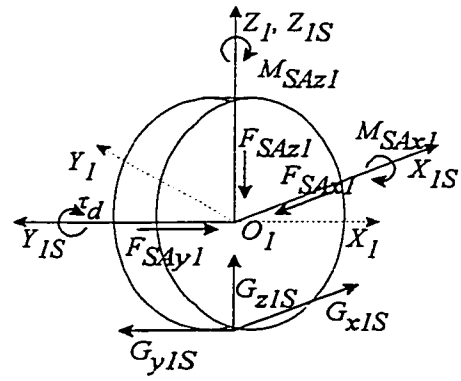

Figure 3.6 Free body diagram for the front driving and steering wheel.

For the front wheel, six equations of motion are obtained for the translation and for the

rotation about X_1 Y_1 Z_1 axes (Fig. 3.6).

$$\begin{aligned} m_1 A_{xl} = &[G_{xl} - F_{SAxl} - m_1 g \sin\beta \cos(\theta+\delta)]\cos\delta \\ &-[G_{yl} - F_{SAyl} + m_1 g \sin\beta \sin(\theta+\delta)]\sin\delta \end{aligned} \tag{3-82}$$

$$\begin{aligned} m_1 A_{yl} = &[G_{xl} - F_{SAxl} - m_1 g \sin\beta \cos(\theta+\delta)]\sin\delta \\ &+[G_{yl} - F_{SAyl} + m_1 g \sin\beta \sin(\theta+\delta)]\cos\delta \end{aligned} \tag{3-83}$$

$$m_1 A_{zl} = G_{zl} - F_{SAzl} - m_1 g \cos\beta \tag{3-84}$$

$$-I_{xl}(\omega_\theta + \omega_\delta)\omega_1 = r_{wl} G_{yl} + M_{SAxl} \tag{3-85}$$

$$I_{yl}\dot{\omega}_1 = \tau_d - r_{wl} G_{xl} \tag{3-86}$$

$$J_1(\dot{\omega}_\theta + \dot{\omega}_\delta) = M_{SAzl} \tag{3-87}$$

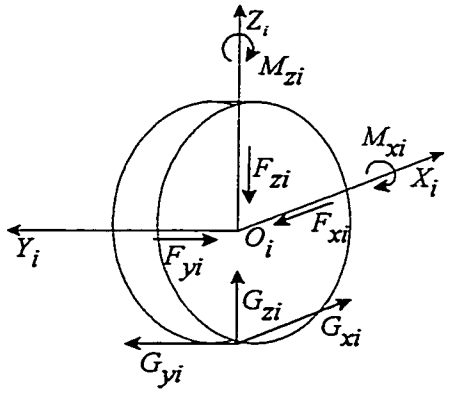

Figure 3.7 Free body diagram for the two rear wheels

For each of the two rear wheels, six equations of motion are obtained for the translation and for the rotation about X_i Y_i Z_i axes (i = 2,3) (Fig. 3.7).

$$m_i A_{xi} = G_{xi} - F_{Fxi} - m_i g \sin\beta \cos\theta \tag{3-88}$$

$$m_i A_{yi} = G_{yi} - F_{Fyi} + m_i g \sin\beta \sin\theta \tag{3-89}$$

$$0 = G_{zi} - F_{Fzi} - m_i g \cos\beta \tag{3-90}$$

$$-I_{xi} \omega_\theta \omega_i = r_{wi} G_{yi} + M_{xi} \tag{3-91}$$

$$I_{yi} \dot{\omega}_i = -r_{wi} G_{xi} \tag{3-92}$$

$$J_i \dot{\omega}_i = M_{zi} \tag{3-93}$$

The equations are linear in internal forces F_{FSAx1}, F_{FSAy1}, F_{FSAz1}, F_{SAx1}, F_{SAy1}, F_{SAz1}, F_{Fxi}, F_{Fyi}, F_{Fzi} (i=2,3), and internal moments M_{FSAx1}, M_{FSAy1}, M_{FSAz1}, M_{SAx1}, M_{SAy1}, M_{SAz1}, M_{xi}, M_{yi}, M_{zi} (i=2,3). These internal forces and moments are not needed for the control of the vehicle and are eliminated from the equations of motion (3-70) ~ (3-93) using the constraints (3-63) ~ (3-69) of the associated absolute accelerations A_{xi}, A_{yi}, A_{zi} (i=1,2,3) leading to the following ten equations of motion. The detailed procedures of elimination of the internal forces and moments are described in Appendix A.

$$MA_x = G_{x1} \cos\delta - G_{y1} \sin\delta + G_{x2} + G_{x3} - Q_3 \omega_\theta^2 + \frac{l}{2}(m_2 - m_3)\dot{\omega}_\theta - Mg \cos\theta \sin\beta \tag{3-94}$$

$$MA_y = G_{x1} \sin\delta + G_{y1} \cos\delta + G_{y2} + G_{y3} + \frac{l}{2}(m_2 - m_3)\omega_\theta^2 + Q_3 \dot{\omega}_\theta + Mg \sin\theta \sin\beta \tag{3-95}$$

$$MA_z = 0 = G_{z1} + G_{z2} + G_{z3} - Mg\cos\beta \tag{3-96}$$

$$\begin{aligned} Q_4\dot{\omega}_\theta = {} & \frac{l}{2}(m_2 - m_3)A_x + Q_3 A_y + (b-c)(G_{x1}\sin\delta + G_{y1}\cos\delta) \\ & - \frac{l}{2}(G_{x2} - G_{x3}) - c(G_{y2} + G_{y3}) - Q_3 g\sin\theta\sin\beta + \frac{l}{2}(m_2 - m_3)g\cos\theta\sin\beta \end{aligned} \tag{3-97}$$

$$\begin{aligned} 0 = {} & -\frac{l}{2}(G_{z2} - G_{z3}) - h(G_{x1}\sin\delta + G_{y1}\cos\delta + G_{y2} + G_{y3}) + (D - Q_{24})A_y + Q_{24}c\dot{\omega}_\theta + Q_{25}\frac{l}{2}\omega_\theta^2 \\ & - (I_{x2}\omega_2 + I_{x3}\omega_3)\omega_\theta - (I_{x1} + I_{SAx1})(\omega_\theta + \omega_\delta)\omega_1\cos\delta - (I_{y1} + I_{SAy1})\dot{\omega}_1\sin\delta \\ & + (Q_{24} - D)g\sin\theta\sin\beta + \frac{l}{2}(m_2 - m_3)g\cos\beta \end{aligned} \tag{3-98}$$

$$\begin{aligned} 0 = {} & -(b-c)G_{z1} + c(G_{z2} + G_{z3}) - h(G_{x1}\cos\delta - G_{y1}\sin\delta + G_{x2} + G_{x3}) + r_{w2}G_{x2} + r_{w3}G_{x3} \\ & + (D - Q_{24})A_x - [D(b-c) + Q_{24}c]\omega_\theta^2 + \frac{l}{2}Q_{25}\dot{\omega}_\theta + (I_{x1} + I_{SAx1})(\omega_\theta + \omega_\delta)\omega_1\sin\delta \\ & - (I_{y1} + I_{SAy1})\dot{\omega}_1\cos\delta + (D - Q_{24})g\cos\theta\sin\beta - c(m_2 + m_3)g\cos\beta \end{aligned} \tag{3-99}$$

$$\dot{\omega}_1 = \frac{\tau_d}{I_{y1}} - \frac{r_{w1}}{I_{y1}}G_{x1} \tag{3-100}$$

$$\dot{\omega}_\theta + \dot{\omega}_\delta = \frac{1}{J_1 + J_{SA}}\tau_s \tag{3-101}$$

$$\dot{\omega}_2 = -\frac{r_{w2}}{I_{y2}}G_{x2} \tag{3-102}$$

$$\dot{\omega}_3 = -\frac{r_{w3}}{I_{y3}} G_{x3} \tag{3-103}$$

These ten equations of motion (3-94) ~ (3-103) use the 8 retained coordinates, $x,y,z,\theta,\alpha_1,\alpha_2,\alpha_3, \delta$ as follows:

- the angular velocities of the wheels $\omega_1 = \dot{\alpha}_1$, $\omega_2 = \dot{\alpha}_2$, $\omega_3 = \dot{\alpha}_3$
- the steering rate $\omega_\delta = \dot{\delta}$

Also the ten equations contain the torques τ_d and τ_s and the nine reaction forces G_{xi}, G_{yi}, G_{zi} (i=1,2,3). From these ten equations of motion, three equations (3-96), (3-98), (3-99) are used for the verification that ideal rolling (no slippage of the wheels and no loss of contact) conditions for the vehicle moving on the inclined surface are not violated. The rest of seven equations are used for the motion control of the vehicle. The eight coordinates are not independent due to the six differential constraints for accelerations (5 equations eq.(3-58) to eq.(3-62) plus the trivial constraint $A_z = 0$) which have to be added to these seven equations of motion. In this dynamic model, each of the 6 differential constraints is associated with a reaction force. We observe that one differential constraint is dependent on the other five constraints and that G_{y2} and G_{y3} are not obtainable separately, (but only as $G_{y2} + G_{y3}$), are both resulting from the holonomic constraint, $y_2 - y_3 = l$. Consequently, out of the nine reaction forces, the forces G_{y2} and G_{y3} appear in the equations of motion only as $G_{y2} + G_{y3}$ and can be obtained only as $G_{y23} = G_{y2} + G_{y3}$, reducing the number of reaction forces to eight.

In the equations of motion and the five differential constraints for control, the coordinate δ appears as δ , $\dot{\delta}$, and $\ddot{\delta}$ while all other coordinates appear only as first and second derivatives

and can be denoted as angular velocities,

$$\omega_\theta = \dot{\theta}, \qquad \omega_i = \dot{\alpha}_i \qquad i = 1,2,3 \tag{3-104}$$

A system of 16 first order differential equations can be obtained from the 10 second order equations of motion (equations (3-(94, 95, 97, 100~103)) and five differential constraints for accelerations (equations (3-(52, 53, 54, 55, 56)). After introducing the notations (3-104), this system of 16 first order equations contains six derivatives ($\dot{\delta}$, $\dot{\omega}_\theta$, $\dot{\omega}_1$, $\dot{\omega}_2$, $\dot{\omega}_3$ and $\dot{\omega}_\delta$) and can be transformed in a system of six differential and ten algebraic equations which is the suitable form for solving the equations of motion for a constrained multi-body mechanical system (Haug, E.J. (1992)). The six differential equations are,

$$\dot{\delta} = \omega_\delta \tag{3-105}$$

$$\dot{\omega}_1 = \frac{1}{I_{y1}}\tau_d - \frac{r_{w1}}{I_{y1}}G_{x1} \tag{3-106}$$

$$\dot{\omega}_2 = -\frac{r_{w2}}{I_{y2}}G_{x2} \tag{3-107}$$

$$\dot{\omega}_3 = -\frac{r_{w3}}{I_{y3}}G_{x3} \tag{3-108}$$

$$\dot{\omega}_\delta = \frac{1}{J_1 + J_{SA}}\tau_s - \dot{\omega}_\theta \tag{3-109}$$

$$\dot{\omega}_\theta = \frac{1}{c}(-r_{w2}\omega_\theta\omega_2 + A_y - \frac{l}{2}\omega_\theta^2) \tag{3-110}$$

The 10 algebraic equations are:

$$0 = G_{x1}\cos\delta - G_{y1}\sin\delta + G_{x2} + G_{x3} - MA_x - Q_3\omega_\theta^2 + \frac{l}{2c}(m_2 - m_3)(-r_{w2}\omega_\theta\omega_2 + A_y - \frac{l}{2}\omega_\theta^2) - Mg\cos\theta\sin\beta \tag{3-111}$$

$$0 = G_{x1}\sin\delta + G_{y1}\cos\delta + G_{y23} - MA_y + \frac{l}{2}(m_2 - m_3)\omega_\theta^2 + \frac{Q_3}{c}(-r_{w2}\omega_\theta\omega_2 + A_y - \frac{l}{2}\omega_\theta^2) + Mg\sin\theta\sin\beta \tag{3-112}$$

$$\begin{aligned} 0 = -\frac{1}{c}Q_4(-r_{w2}\omega_\theta\omega_2 + A_y - \frac{l}{2}\omega_\theta^2) + \frac{l}{2}(m_2 - m_3)A_x + Q_3A_y + (b-c)(G_{x1}\sin\delta + G_{y1}\cos\delta) \\ - \frac{l}{2}(G_{x2} - G_{x3}) - cG_{y23} - Q_3g\sin\theta\sin\beta + \frac{l}{2}(m_2 - m_3)g\cos\theta\sin\beta \end{aligned} \tag{3-113}$$

$$0 = -(\frac{1}{I_{y1}}\tau_1 - \frac{r_{w1}}{I_{y1}}G_{x1})r_{w1}\cos\delta + r_{w1}\omega_1(\omega_\delta + \omega_\theta)\sin\delta + A_x - (b-c)\omega_\theta^2 \tag{3-114}$$

$$0 = -(\frac{1}{I_{y1}}\tau_1 - \frac{r_{w1}}{I_{y1}}G_{x1})r_{w1}\sin\delta + \frac{b-c}{c}(-r_{w2}\omega_\theta\omega_2 + A_y - \frac{l}{2}\omega_\theta^2) - r_{w1}\omega_1(\omega_\delta + \omega_\theta)\cos\delta + A_y \tag{3-115}$$

$$\frac{r_{w2}^2}{I_{y2}}G_{x2}-\frac{l}{2c}(-r_{w2}\omega_\theta\omega_2+A_y-\frac{l}{2}\omega_\theta^2)+A_x+c\omega_\theta^2=0 \tag{3-116}$$

$$\frac{r_{w3}^2}{I_{y3}}G_{x3}+\frac{l}{2c}(-r_{w2}\omega_\theta\omega_2+A_y-\frac{l}{2}\omega_\theta^2)+A_x+c\omega_\theta^2=0 \tag{3-117}$$

$$0=G_{z1}+G_{z2}+G_{z3}-m_t g\cos(\beta) \tag{3-118}$$

$$\begin{aligned}0=&-\frac{l}{2}G_{z2}+\frac{l}{2}G_{z3}-\frac{b}{c}(d_1+d_{sa})Ay+(r_1-h)\sin(\delta)G_{x1}-h\cos(\delta)G_{y1}-hG_{y23}-\omega_\theta^2[-l\frac{(b-c)}{2c}(d_1+d_{sa})+ld_3]\\&-\omega_\theta\omega_2[-r_2\frac{(b-c)}{c}(d_1+d_{sa})+r_2(d_2+d_3)]-\tau_1\sin(\delta)+d_t g\sin(\beta)\sin(\theta)+(m_2-m_3)\frac{l}{2}g\cos(\beta)\end{aligned} \tag{3-119}$$

$$\begin{aligned}0=&(b-c)G_{z1}-cG_{z2}-cG_{z3}+d_tAx+\frac{l}{2c}(d_3-d_2)Ay-(r_1-h)\cos(\delta)G_1x_1-h\sin(\delta)G_1y_1\\&-(r_2-h)G_{x2}-(r_3-h)G_{x3}+\omega_\theta\omega_2\frac{r_2l}{2c}(d_2-d_3)+\tau_1\cos(\delta)+\omega_\theta^2[-(d_1+d_{sa})(b-c)\\&+d_2(c+\frac{l^2}{4c})+d_3(c-\frac{l^2}{4c})]+gd_t\sin(\beta)\cos(\theta)+g[-(b-c)m_{t1}+c(m_2+m_3)]\cos(\beta)\end{aligned} \tag{3-120}$$

The system of 16 differential algebraic equations for two given inputs $A_x(t)$, $A_y(t)$ which are the functions of $\omega_1(t)$, $\omega_\delta(t)$ can be solved for 16 unknowns:

- two outputs $\tau_d(t)$, $\tau_s(t)$

- six coordinates $\delta(t)$, $\omega_1(t)$, $\omega_2(t)$, $\omega_3(t)$, $\omega_\theta(t)$, $\omega_\delta(t)$
- eight reaction forces (G_{x1}, G_{x2}, G_{x3}, G_{y1}, G_{y23}, which are necessary for motion control of the vehicle, and G_{z1}, G_{z2}, G_{z3} which are necessary for verifying no slip and loss of contact conditions) for given initial conditions $\delta(t-\Delta t)$, $\omega_1(t-\Delta t)$, $\omega_2(t-\Delta t)$, $\omega_3(t-\Delta t)$, $\omega_\delta(t-\Delta t)$, $\omega_\theta(t-\Delta t)$.

IV. CONTROL ALGORITHM

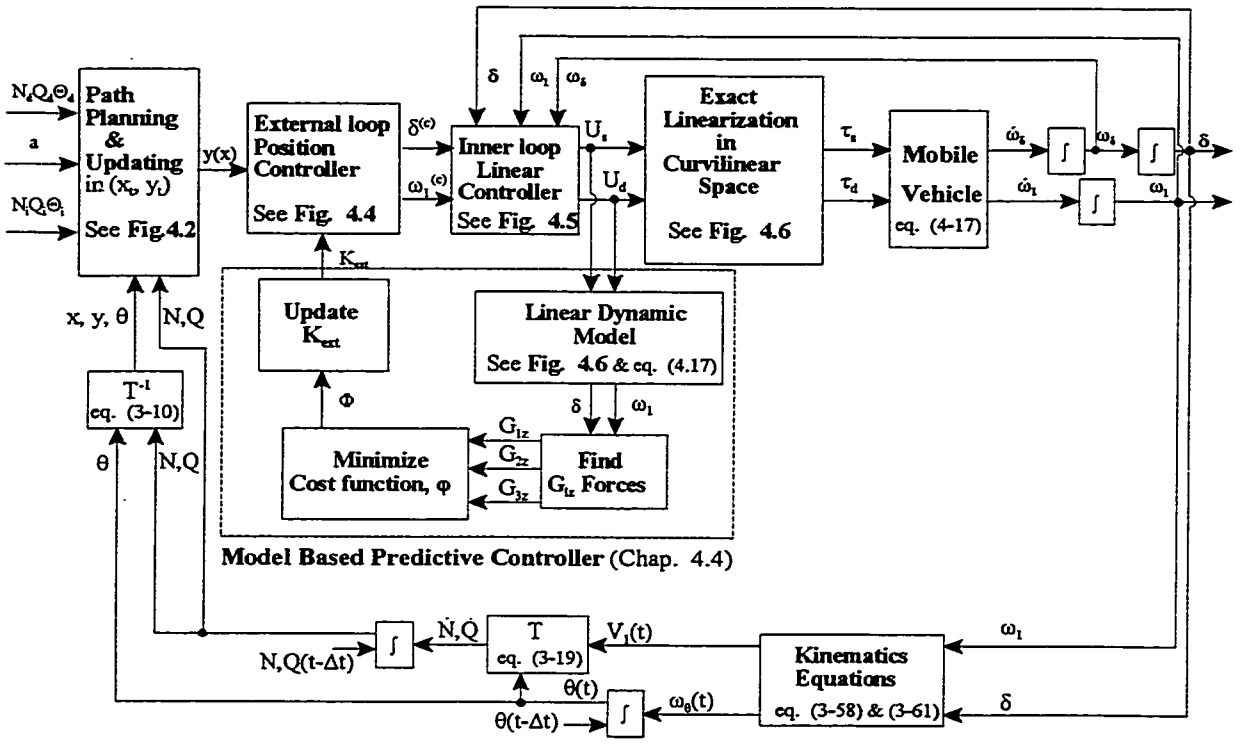

Figure 4.1 Control Block Diagram representing over-all system

The autonomous vehicle represented in (Fig. 3.2) is analyzed for the inclined plane subject

to wheel slippage and body tip-over avoidance. The control block diagram used for simulation is shown in (Fig. 4.1) and contains a three-part control scheme (an external loop controller and path planner in operational space, a model predictive control for the K_{ext} for the angular velocity command of the front wheel, and an inner loop exact input-output linearization controller in curvilinear space(s-δ)) for verifying slippage and tip-over conditions. The model based predictive control scheme improves the performance of the autonomous vehicle while avoiding slippage and loss of contact of the vehicle. Algorithm corresponding to the blocks of the control scheme are given in this chapter.

4.1 Path Planner

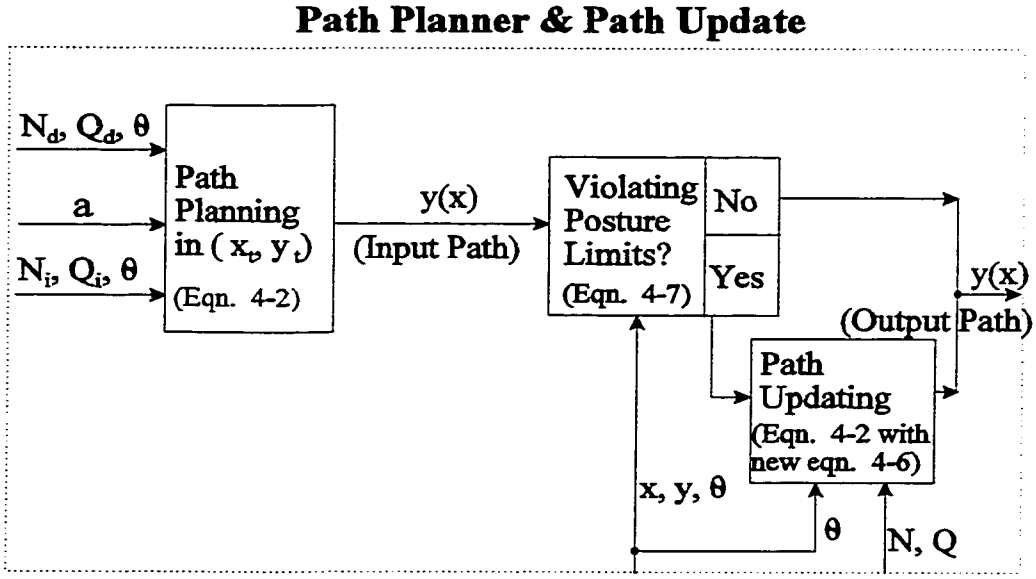

Figure 4.2 Detailed block diagram for the path planner and path update

4.1.1 Path Planning

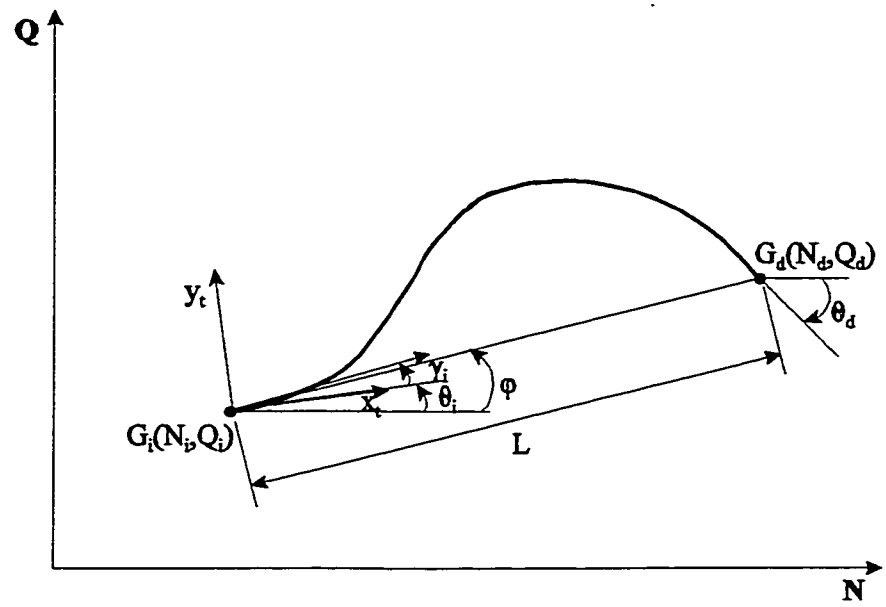

Figure 4.3 Schematic Diagram of the Path Planning in (x_t, y_t) frame.

Brokett's theorem (Brokett, R.W., 1983) states that the non-holonomic constraints of wheeled autonomous vehicles prevent them from being stabilized at a desired posture with smooth state feedback control. In order to control the motion of the vehicle about a desired posture, a particular smooth path which goes through the desired position with the desired orientation needs to be planned. By knowing the current posture of the autonomous vehicle, one can find a path constrained by the boundary conditions for the current and desired posture. The vehicle is subject to the torques τ_d and τ_s applied to the front wheel horizontal axis, y_1 and vertical axis z_1, respectively.

Two moving frames are used here (Figure 3.3):

- (x, y) which is a moving frame linked to the center of the mass of the vehicle, (Frame R)

- (x_1, y_1) which is a moving frame linked to the front wheel, (Frame R_1)

The initial and desired postures are defined by (N_i, Q_i, θ_i) and (N_d, Q_d, θ_d), respectively. The distance between the initial and desired position is defined as L. The path is calculated in (x_t, y_t) frame whose origin is G_i and where x_t is parallel to G_iG_d. γ_i is the initial angle between the velocity vector of the vehicle and its longitudinal axis x_t. φ is the angle of the tangent of the path with respect to inertial frame (N-Q-R). θ_i, θ_d are the initial and desired orientation of the vehicle with respect to inertial frame, respectively. (Figure 4.3)

A path planner using the concept of general slender beam equation (Timoshenko, S., 1985) is created to generate smooth paths. The curvature of the path can be modified by simple variation the constant "a" of the 4th order differential equation (4-1).

$$\frac{d^4y}{dx^4} - a^4 y_{(x)} = 0 \qquad (4\text{-}1)$$

This path is followed by an artificial curvilinear stiffness control which gives the time varying commands for the steering angle and angular velocity of the front wheel of the autonomous vehicle. The planned path is a steady state solution of the 4th order differential equation with four boundary conditions. Its general solution is a transcendental function of x depending on a curve parameter "a":

$$y(x) = A\cos(\alpha x) + B\sin(\alpha x) + C\cosh(\alpha x) + D\sinh(\alpha x) \qquad (4\text{-}2)$$

where, the coefficients (A,B,C,D) are obtained equating with the following four boundary conditions

with the initial and final postures of the robot described in the following section.

Assuming that the final orientation of the vehicle must coincide to the direction defined by θ_d, a path that meets the following boundary conditions must be found:

- the initial and desired positions must belong to the path;
- the tangent of the path at the initial position must coincide with the initial orientation of the vehicle.
- the tangent to the path at the desired position must coincide to the desired orientation.

The boundary conditions in (x_r, y_r) frame are expressed mathematically as follows;

$$\begin{aligned} y(0) &= 0 \\ y(L) &= 0 \\ \frac{dy}{dx}(0) &= \tan(\gamma_i + \theta_i - \varphi) \\ \frac{dy}{dx}(L) &= \tan(\theta_d - \varphi) \end{aligned} \tag{4-3}$$

These boundary conditions give a set of four equations; Assuming that the parameter "a" is chosen so that the set has a solution, the parameters A, B, C, and D are determined by solving following matrix equation.

$$\begin{bmatrix} 1 & 0 & 1 & 0 \\ 0 & 1 & 0 & 1 \\ \cos(aL) & \sin(aL) & \cosh(aL) & \sinh(aL) \\ -\sin(aL) & \cos(aL) & \sinh(aL) & \cosh(aL) \end{bmatrix} \begin{bmatrix} A \\ B \\ C \\ D \end{bmatrix} = \begin{bmatrix} 0 \\ \tan(\gamma_i + \theta_i - \varphi)/a \\ 0 \\ \tan(\theta_d - \varphi)/a \end{bmatrix} . \tag{4-4}$$

and therefore

$$A = \frac{k_1(\cos(aL)-\cosh(aL))-k_2(\sin(aL)-\sinh(aL))}{2(1-\cos(aL)\cosh(aL))}$$

$$B = \frac{k_2(\cos(aL)-\cosh(aL))+k_1(\sin(aL)-\sinh(aL))}{2(1-\cos(aL)\cosh(aL))}$$

$$C = -A$$

$$D = -B + \frac{\tan(\gamma_i+\theta_i-\varphi)}{a}$$

with

$$k_1 = \frac{-\tan(\gamma_i+\theta_i-\varphi)\sin(aL)}{a}$$

$$k_2 = \frac{\tan(\theta_d-\varphi)-\cosh(aL)\tan(\gamma_i+\theta_i-\varphi)}{a}$$

The solution of y(x) for the calculated coefficients A, B, C, D is the planned path. "a" is a curve parameter for y(x) and will be used for controlling the motion of the vehicle in difficult conditions.

4.1.2 Path Updating

To obtain a closed loop system, and compensate for potential errors, the path is updated using the current and desired position. To avoid any divergence problems, the new path must have the same shape and must be as close as possible as the former one. That is why the paths chosen for updates

are the solutions of the same beam differential equation in the frame defined by the initial position of the vehicle and not by the current one.

A new path is thus periodically computed to fit the current boundary conditions

$$\begin{aligned} y(x_{robot}) &= y_{robot} \\ y(L) &= 0 \\ \frac{dy}{dx}(x_{robot}) &= \tan(\gamma_{robot} + \theta_{robot} - \varphi) \\ \frac{dy}{dx}(L) &= \tan(\theta_d - \varphi) \end{aligned} \tag{4-5}$$

for which the parameters A, B, C, D are recalculated and "L" is changing with time.

We thus get for the parameters A, B, C, D the following constraints:

$$\begin{bmatrix} \cos(ax_{rob}) & \sin(ax_{rob}) & \cosh(ax_{rob}) & \sinh(ax_{rob}) \\ -\sin(ax_{rob}) & \cos(ax_{rob}) & \sinh(ax_{rob}) & \cosh(ax_{rob}) \\ \cos(aL) & \sin(aL) & \cosh(aL) & \sinh(aL) \\ -\sin(aL) & \cos(aL) & \sinh(aL) & \cosh(aL) \end{bmatrix} \begin{bmatrix} A \\ B \\ C \\ D \end{bmatrix} = \begin{bmatrix} y_{rob} \\ \dfrac{\tan(\gamma_i + \theta_i - \varphi)}{a} \\ 0 \\ \dfrac{\tan(\theta_d - \varphi)}{a} \end{bmatrix} \tag{4-6}$$

The inversion of this set of equations gives the new sets of coefficients A, B, C, and D for equation (4-2).

As a result of delays in steering dynamics, the vehicle trajectory can be apart from the planned

path. The path is updated whenever the vehicles position or direction are no longer consistent with the current path. These two conditions can be written as,

$$\begin{aligned} |y_{robot} - y(x_{robot})| > d \\ |\gamma_{robot} - \gamma(x_{robot})| > \psi \end{aligned} \tag{4-7}$$

where, d and ψ are real parameters which depend on the precision required.

The period of path updating is, moreover, limited to avoid instability problems. In an extreme case, where an updating is carried out after each calculation step, the autonomous vehicle will simply follow a straight line. The planned track being tangent to the initial speed of the robot, the direction of the velocity will indeed never be modified. In an ideal case, where we control δ and ω_1 the period of path updating must at least be limited to two steps of calculation. For the autonomous vehicle where δ and ω_1 are controlled from the torques applied on the front wheel, delays appear and this period has to be limited to the response time on δ.

Moreover because of these delays and of all others imprecisions, the autonomous vehicle may not reach exactly the desired point. It may, for instance, go further than this position and reach an area where the differential equations can no longer have solutions. To avoid this problem, we check that the vehicle is not in one of these areas before updating the path. While the vehicle is in one of these areas it is only compelled to remain on the last computed track.

The path, which has been presented, does not allow the robot to reach any point from every initial position. To find a path, defined by a function y=f(x), which satisfies the boundary conditions of equation(4-1), the following inequalities in (x_t, y_t) frame have to be verified:

$$-\frac{\pi}{2} \le \gamma_i + \theta_i - \varphi \le \frac{\pi}{2}$$

$$-\frac{\pi}{2} \le \theta_d - \varphi \le \frac{\pi}{2} \tag{4-8}$$

If the conditions are not satisfied, the vehicle is forced to move on a circle centered on the desired point, until the current and desired orientations verify these inequalities. When the vehicle follows on such a circle, its velocity is kept as constant and orthogonal to the vector GG_d. The curve parameter "a" must be chosen so that the set of four equations that is used to compute the constants A, B, C, and D is always invertible. The determinant of this set of equations should not be equal to zero, i.e. :

$$Det = 2\{1 - \cos[a(x-L)]\cosh[a(x-L)]\} \neq 0 \tag{4-9}$$

4.2 External Loop Position Controller

From the non-holonomic constraint of the autonomous vehicle,

$$\tan(\delta) = \frac{b}{c}\frac{Vy}{Vx} \tag{4-10}$$

we can define the angle γ between the velocity of the robot and its axis as,

$$\gamma = atan(\frac{c}{b}\tan(\delta)) \tag{4-11}$$

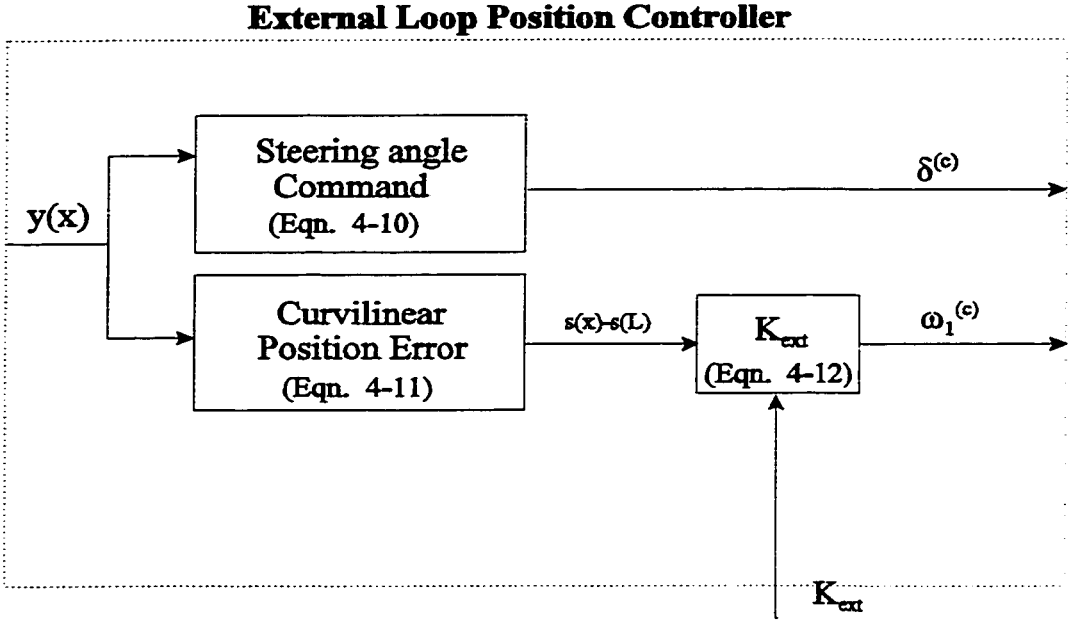

Figure 4.4 Detailed Block Diagram for the External Loop Position Controller

The steering angle command is given by,

$$\delta^{(c)} = atan(\frac{b}{c}\tan(\gamma)) \tag{4-12}$$

If the vehicle follows exactly the planned path, its current position x in (X_t, Y_t) frame can be found by the curvilinear length s between the current position and its initial position x=0 of the center of mass of the vehicle.

$$S(x) = \int_0^x \sqrt{(1+(\frac{dy}{dx})^2)}\ dx \tag{4-13}$$

For x=L, S(L)is the curvilinear length of the path.

To bring the vehicle to the desired position, an angular velocity proportional to the curvilinear position error S(L)-S(x) is applied. This suggests the following P-control for ω_1.

$$\omega_1^{(c)} = K_{ext}[S(L) - S(x)] \tag{4-14}$$

4.3 Inner Loop Input-Output Linearization Controller

Inner Loop Linear Controller is chosen as PD control for δ and P-control for ω as,

$$\begin{bmatrix} u_s \\ u_d \end{bmatrix} = \begin{bmatrix} K_2[(\delta^{(c)} - \delta) - K_1 \omega_\delta] \\ K_3(\omega_1^{(c)} - \omega_1) \end{bmatrix} \tag{4-15}$$

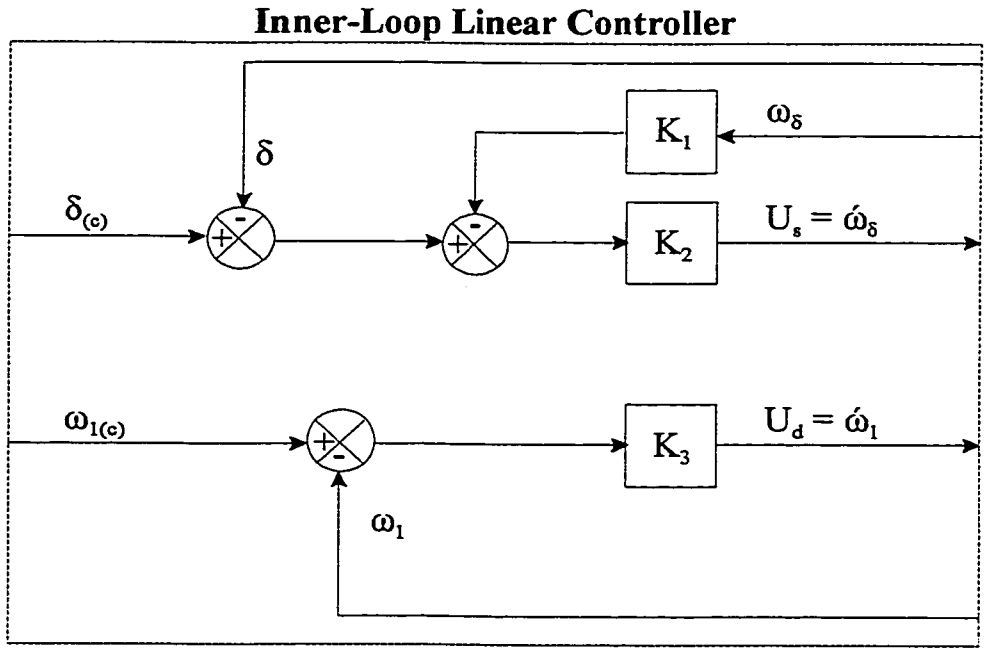

Figure 4.5 Detailed Block Diagram for Inner Loop Linear Controller

The dynamic model, given by the 16 differential-algebraic equations (3-105) - (3-120) is used for output torques τ_d and τ_s for the driving and steering servomotors, commands exact linearization. The exact linearization in curvilinear space is given by,

$$\begin{bmatrix}\tau_d\\ \tau_s\end{bmatrix}=Ad^{-1}\left(\begin{bmatrix} f(\omega_1,\omega_\delta,\delta,\theta,\beta)\\ -F(\omega_1,\omega_\delta,\delta,\theta,\beta)\end{bmatrix}+\begin{bmatrix}u_s\\ u_d\end{bmatrix}\right) \tag{4-16}$$

Exact Linearization in Curvilinear Space

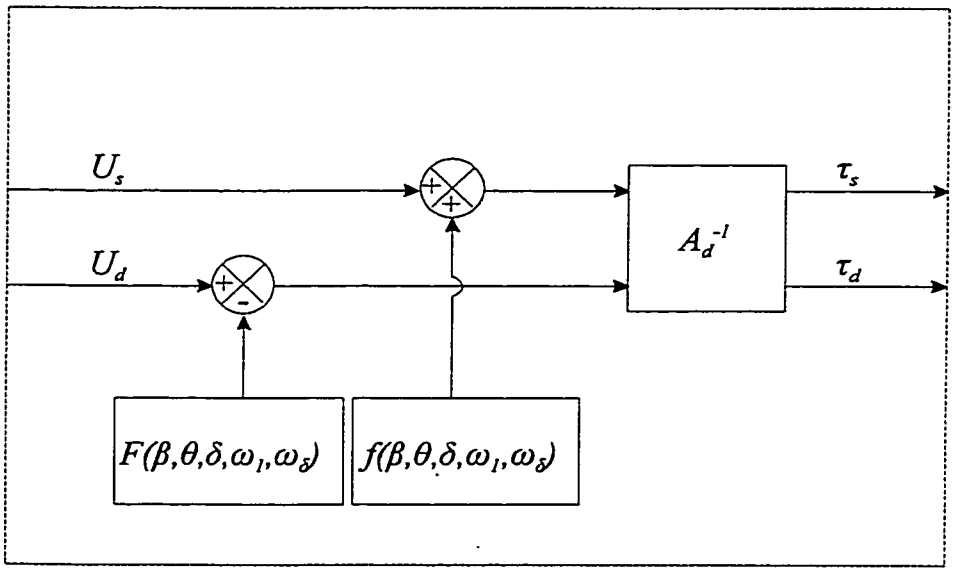

Figure 4.6 Detailed Block Diagram for Exact Linearization Scheme

No-slip conditions are defined by the condition that all reaction forces G_{x1}, G_{x2}, G_{x3}, G_{y1} and G_{y23} smaller than the corresponding maximum frictional forces. In the case that no-slip conditions are satisfied, the commands τ_d and τ_s are applied to the servomotors and the angular speed ω_1 and steering angle δ are measured and fed back for the external controller.

The kinematics equations (3-46), (3-47), and (3-49) give the relationships between the inputs ω_1, δ and the outputs $V(t)=[V_x, V_y]^T$, ω_e. Slippage and loss of contact conditions can be verified by

calculating the wheel-ground contact forces (G_{xi}, G_{yi}, G_{zi}, i=1,2,3) from ten algebraic dynamic equations (eqns. (3-111) ~ (3-120)).

The dynamic model (eqns.(3-105) ~ (3-120)) of the autonomous vehicle is modified as,

$$\begin{bmatrix}\dot{\omega}_\delta\\ \dot{\omega}_1\end{bmatrix}=\begin{bmatrix}f(\omega_1,\omega_\delta,\delta,\theta,\beta)\\ F(\omega_1,\omega_\delta,\delta,\theta,\beta)\end{bmatrix}+Ad\begin{bmatrix}\tau_d\\ \tau_s\end{bmatrix} \tag{4-17}$$

where, τ_d, τ_s are the driving and steering torques, respectively. $\dot{\omega}_1$, $\dot{\omega}_\delta$ are the driving and steering angular accelerations, respectively, and

$$f(\omega_1,\omega_\delta,\delta,\theta,\beta)=[r_l^2\{\frac{l}{2b}Q_1(\sin^2(\delta)-\cos^2(\delta))+(Q_2-Q_3)\sin(\delta)\cos(\delta)\}\sin(\delta)-D\cos(\delta)]\frac{r_1}{bD}\omega_1\omega_\delta$$
$$+[bm_1\cos(\delta)\cos(\theta)-cQ_1\sin(\delta)\cos(\theta)-(cm_t+bm_1)\sin(\delta)\sin(\theta)]\frac{r_1 g\sin(\beta)\sin(\delta)}{b^2D}$$

$$F(\omega_1,\omega_\delta,\delta,\theta,\beta)=-[\frac{l}{2b}Q_1(\sin^2(\delta)-\cos^2(\delta))+(Q_2-Q_3)\sin(\delta)\cos(\delta)]\frac{r_1^2}{D}\omega_1\omega_\delta$$
$$-[bm_1\cos(\delta)\cos(\theta)-cQ_1\sin(\delta)\cos(\theta)-(cm_t+bm_1)\sin(\delta)\sin(\theta)]\frac{g\sin(\beta)}{bD}$$

$$Ad=\begin{bmatrix}-\frac{r_1}{bD}\sin(\delta) & \frac{1}{J_1}+\frac{r_1^2}{b^2D}\sin^2(\delta)\\ \frac{1}{D} & -\frac{r_1}{bD}\sin(\delta)\end{bmatrix} \tag{4-18}$$

where

$$D=I_1+r_1^2\left[Q_3\cos^2(\delta)+Q_2\sin^2(\delta)-\frac{1}{b}Q_1\cos(\delta)\sin(\delta)\right]$$

where, m_t is the total mass of the autonomous vehicle and m_i (i=1,2,3) are the masses of or each of

the three wheels, and m_{1t} is the combined mass of front wheel and the streering assembly, respectively

J_i is the moments of inertia about the vertical axis Z_i, and I_i (i=1,2,3) are the moments of inertia about Y_i axis, respectively

r_1 is the radius of front wheel, b is the vehicle length from the origin of front wheel to the center of rear axle, and c is the distance from the center of mass to the center of rear axle, and l is the length of the rear axle, respectively

To simplify the expression of the above equations the following notations Q_1, Q_2, Q_3 are introduced :

$$Q_1 = \frac{I_2}{r_2^2} + \frac{I_3}{r_3^2} + m_t$$

$$Q_2 = \frac{I_2}{r_2^2} - \frac{I_3}{r_3^2} + m_2 - m_3$$

$$Q_3 = \frac{l^2}{4c}\left(\frac{I_2}{r_2^2} + \frac{I_3}{r_3^2}\right) - cm_{1t} - 2c(m_2+m_3) + 2bm_{1t} + \frac{1}{c}[J_f + J_2 + J_3 + (b-c)^2 m_{1t} + (c^2 + \frac{l^2}{4})(m_2+m_3)$$

The detailed derivation of equation (4-17) is described in appendix A.

4.4 Model Predictive Controller

Feedback linearization is a powerful technique for facilitating the design of the controller using for a linearized form of the autonomous vehicle. Basically, as it is shown in section 4.3, it consists of applying a nonlinear feedback to the system to compensate its nonlinearity, so that the dynamics

of the new composed system appears linear. Any linearization requires that all of the necessary variables be estimated accurately. Some conditions must be fulfilled to be able to use feedback linearization, first of all the smoothness of the system.

Unfortunately, almost any real system is not smooth outside a limited operating region, in particular any real system has some hard bounds on the inputs. Under feedback control this means that the input signal to any actuator lies between the bounds (i.e., in the unsaturated region) for a part of the state space, while for the saturated regions the input is either at the maximum or at the minimum value. Feedback linearization tends to increase the dynamic range of the input, and therefore may reduce the unsaturated region and increase the danger of running into the bounds. Reaching the bounds changes the structure of the controlled system, destroys the linearity of the composite system and, as discussed in (Canudas de Wit, C. and Sordalen, O.J., 1992), can even lead the plant to instability. Therefore, it may be worth limiting the range of allowable reference values so that the state trajectory does not leave the unsaturated region. The sufficient smoothness condition for applying feedback linearization has to be continuously observed and this requires the avoidance of actuators torque saturation, wheel-ground longitudinal and lateral slippage and tip-over of the vehicle for motion on horizontal plane as well as inclined surfaces. Obviously, avoiding this limiting conditions improves also the general performance of the vehicle.

Model Predictive Control (MPC) provides a unified solution to the problems of free motion, and contact motion controls. In the model predictive control, the knowledge is represented by analytical models of the autonomous vehicle and the environment. These models are used to predict, from current measurements, the motion over a receding horizon extending from the current time over

a fixed interval in the future.

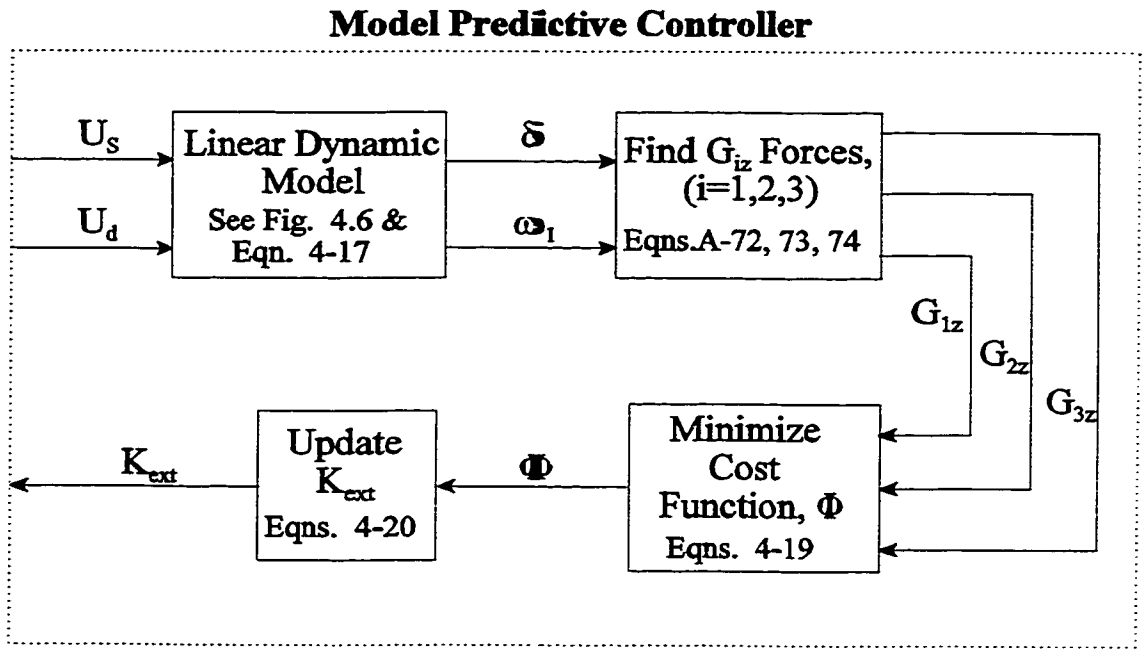

Figure 4.7 Detailed Schematic Block Diagram for Model Predictive Control

The actual control command is decided upon some control objectives over the receding horizon. In order to define how well the predicted process output tracks the reference trajectory, a criterion function is used (eqn. 4-19).

$$\Phi_k = \sum_{i=0}^{Nh} [\gamma_1(N_{dk+i} - N_{k+i})^2 + \gamma_2(Q_{dk+i} - Q_{k+i})^2 + \gamma_3(\dot{N}_{dk+i} - \dot{N}_{k+i})^2 + \gamma_4(\dot{Q}_{dk+i} - \dot{Q}_{k+i})^2 \\ \gamma_5^*(G_{z1k+i})^2 + \gamma_6^*(G_{z2k+i})^2 + \gamma_7^*(G_{z3k+i})^2] \quad (4\text{-}19)$$

where, Nh is the receding horizon

γ_i (i = 1~7) are weight factors selected during the MPC design

The variables N and Q are defined in Fig. 3.1.

$$\gamma_5^* = \begin{cases} 0, & for G_{z1} < 0 \\ \gamma_5, & otherwise \end{cases}$$

$$\gamma_6^* = \begin{cases} 0, & for G_{z2} < 0 \\ \gamma_6, & otherwise \end{cases}$$

$$\gamma_7^* = \begin{cases} 0, & for G_{z3} < 0 \\ \gamma_7, & otherwise \end{cases}$$

Usually the control objectives are given in terms of the minimization of an optimization criterion defined over the receding horizon (eqn. 4-20).

$$u^* = \arg\min_u \Phi_k \tag{4-20}$$

Now the controller output sequence $u^* = K_{ext}^*$ over the prediction horizon, Nh, is obtained by minimization of Φ_k with respect to $u=K_{ext}$. Then u^* is optimal with respect to the criterion function that is minimized. This unified approach of MPC is based on the concept found in (Soeterboek, R., 1992).

In this thesis this Model based Predictive Control, as shown in Fig. 4.7, is used for avoidance of wheel-ground longitudinal and lateral slippage and loss of wheel-ground contact of the vehicle for motion on horizontal plane as well as inclined surfaces by modifying the input commands such that the geometric path planning result is conserved and the smoothness condition for exact linearization is not violated.

V. EXPERIMENTAL SETUP

5.1 Hardware - Autonomous Vehicles

The schematic diagrams shown in Fig. 5.1 and Fig. 5.2 illustrate the components used in the experimental study. The autonomous vehicles, dSPACE digital signal processor, SYSTEM 7 direct drive motor driver, A/D, D/A, and encoder cards, batteries, analog filters, and a PC are the components needed to perform the experiment. The dSPACE DSP runs on a TMS320C30 processor chip. It is connected to the personal computer by an expansion PHS-bus. In this chapter, the dimensions and dynamic properties of the two versions of experimental autonomous vehicles are described.

There are two versions of the autonomous vehicle designed and constructed in our laboratory. Both versions have a tricycle configuration equipped with a driving and steering front wheel and two idle rear wheels. These designs are inspired by the base frame configuration of HERO1 Mobile robot (Robillard, M., 1983).

The first version has been developed for experimental testing of the sensor fusion of odometers and accelerometers in case of vehicle slippage while the robot is in operation. In the first

version, two direct drive (brushless) dc motors made by Parker Hannifin Ltd. in U.K. are installed at the front wheel of the robot, one on top of the steering assembly for steering purpose and the other on right hand side of the wheel for driving. A counterbalancing steel is attached on the other side of the driving motor.

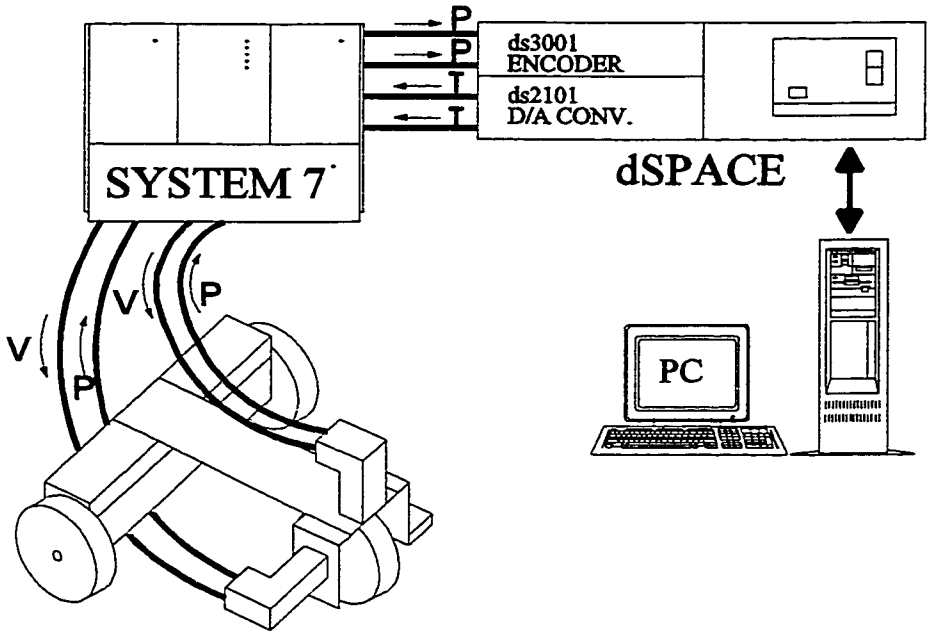

Figure 5.1 Schematic diagram of the experimental setup of the autonomous vehicle driven by two direct drive motors

This version of autonomous vehicle has a frame with dimension of 0.4 x 0.3 x 0.4 m. The vehicle was connected to System 7 motor driver which was supplied with the motors by the manufacturer (Fig. 5.1). The signals establish communication with the dSPACE DSP (digital signal processor). The dSPACE DSP generated the analogue torque commands outputs (τ_d, τ_s) by DS2101 D/A converter control board while communicating with PC and receives the angular displacement

signals (θ_d, θ_s) from DS3001 incremental encoder board.

The servomotor type is an important factor in autonomous vehicle design. Desirable servos are light weight, compact, easily integrated, efficient, controllable, and nearly maintenance free. Especially for the application at unmanned environment, easy servo maintenance is a desirable feature. Although the direct drive motor outperforms the dc motor with brush in the matter of torque control, it is realized that it is not suitable for autonomous vehicle application because of a heavy and bulky motor driver unit which increases the size and weight of the vehicle. It was also realized that the thickness of vehicle frame affects the dynamic characteristics of the rigid body assumption. The thickness of the vehicle frame of above version is only 3 mm. These two main factors gave us enough reason to construct the second generation vehicle with thicker and more sturdy frames and dc motors replacing direct drive motors.

A second autonomous vehicle, the CLAMOR, was constructed by (Victor Lonmo, 1996). The vehicle has a dimension of 0.51 x 0.51 x 0.53 m and weighs 24.5 Kg with two batteries installed. The servomotors are DC motors(Pitmo 14202 series, Pittman corporation) capable of position and torque control modes. These DC servomotors have 75.1:1 planetary gears and have a torque output of max. 10 Nm. Power for the motors is supplied by two 12 V, 10 Ah batteries connected in series. Each servomotor has a built-in optical incremental encoder which has 1000 steps per revolution at motor shaft resulting in 75100 steps per revolution for output shaft. The frame is made of ½" x 3" aluminum stock for strength. The plate metal used for the box near the rear wheels is 3/32" thick aluminum. The dSPACE controller is DSP based (TMS320C30) and contains D/A and incremental encoder boards (Fig. 5.2). The identification of dry friction torques gave approximately 1.1 Nm.

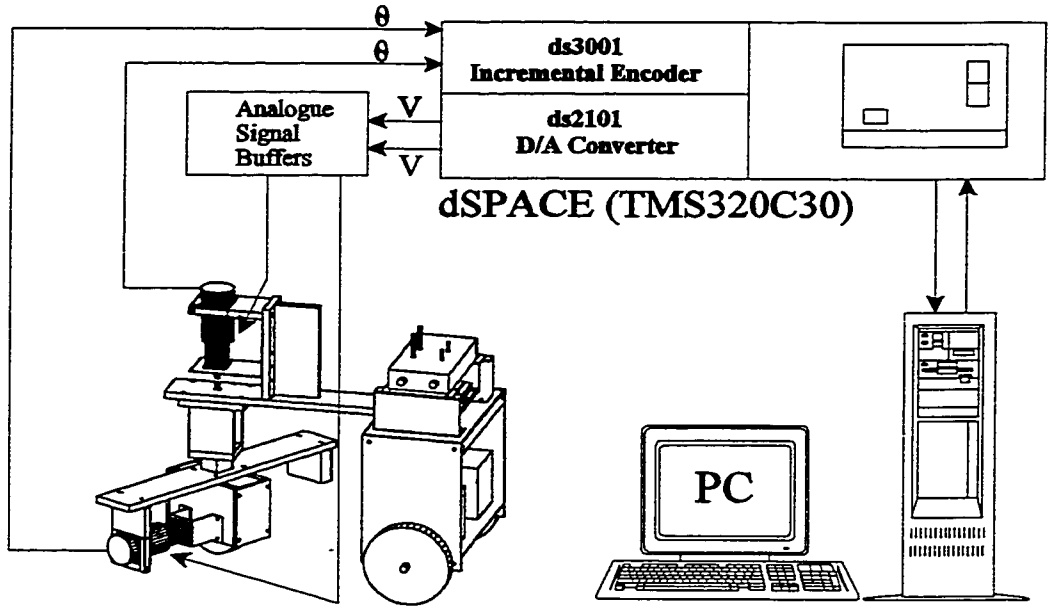

Figure 5.2 Schematic diagram of the experimental setup of the autonomous vehicle driven by two dc servomotors

The computer controlling of the vehicle is actually not on board which makes the vehicle not truly autonomous. A laptop computer and a portable dSPACE DSP can however easily be employed to make the vehicle autonomous.

5.2 Software

The software associated with the dSPACE DSP consist of SED30, MON30, TRACE30, and C code compilation.

5.2.1 SED30

This is a setup editor software which is used to create and edit system setup files and the application specific setup files. It also configures all the boards, verify the presence of a ds1002 processor board, displays a list of all boards found in the computer currently executing the setup editor, and generate the setup file. Once a C code is compiled, it needs to go through the SED30 to be properly setup.

5.2.2 MON30

MON30 is a utility program that performs the actual loading and evaluation of the system setup file and of DSP object code modules and their corresponding application specific setup files. It allows the user to control the TMS320C30 DSP operation by use of RESET and HOLD signals. It permits initialization of the I/O channels by allowing access to the peripheral board registers through the PHS-bus.

5.2.3 TRACE30

This program provides real-time trace capabilities for any application running on a ds1002 digital signal processor board, which is a member of the DSP-CITpro hardware family and contains

a TMS320C30 floating-point DSP. TRACE30 allows to record and graphically display all signals and parameters represented as single-precision float variables or integer variables in the ds1002's memory. The number of traced variables is unlimited. TRACE30 thus provides extremely good insight into any application while it is executed in real-time by the DSP.

5.2.4 User C code

Using any ANSI C code editor, a C code for the controller should be constructed. Unlike the computer simulation, the generated C code can only be compiled by the DSP compiler and all the variables are properly addressed. It is necessary to perform the computer simulation and verify the ability of the program. If the control program is considered to be safe to operate the real experimental setup, the C program can easily be modified for the experiment.

VI. SIMULATION AND EXPERIMENTAL RESULTS

The simulation and experimental results on motion control problems of the autonomous vehicle including sensor fusion, path planning, path tracking, and the verification of the vehicle slippage and tip-over condition over the flat and inclined plane using Input-Output Linearization scheme and with a Model Based Predictive Control scheme are presented in this chapter. The simulation and experiment are performed referring to the vehicle CLAMOR as shown in Fig. 5.2. The vehicle parameters for the simulations have been designed to represent the actual dimension of the vehicle platform as closely as possible. The properties of CLAMOR which have been measured and used in simulations and experiments are given in chapter 5. A Model based Predictive Controller is employed for improving the performance of the vehicle by avoiding loss of wheel ground contact of the vehicle.

6.1 Simulation results

For the purpose of supporting the simulation results, a static force analysis was performed for the experimental autonomous vehicle shown in Fig. 5.2. It was found that the mobile vehicle is about to be tipped-over at the angle of inclination of the plane $\beta = 43.45°$ when the initial orientation of the mobile vehicle $\theta_0 = 0°$, and $\beta = 65.3°$ when $\theta_0 = 90°$. These results show that the vehicle is in danger of being tipped-over whenever the inclination slope β is over 43.45° when the vehicle is not in motion. In the dynamic case, the tip-over angle β is further reduced by the effect of centrifugal forces exerted on the vehicle when it is in motion. The analysis has shown that the centrifugal force with the radius of curvature ρ = 0.5m and velocity of 0.5m/s has the effect of increasing the magnitude and the angle of the force vector exerted on the slope by the vehicle by 8.58 N and 2.047°, respectively. The simulation models were developed using C-language. The cycle time used for the simulation was 1ms using a pentium 200 Mhz PC. This duration permits a real-time implementation with at least 1000 control cycle per second. This high control cycle rate is sufficient for the most applications of the autonomous vehicles using a similar microprocessors.

6.1.1 Avoidance of slippage and tip-over conditions via the analysis of the curve parameter "a" of path planning

The block diagram used for simulation is shown in Fig. 4.1, and contains the two-part control scheme besides the model predictive control scheme.

The implementation of the above controller is based on an operational space controller which generates a path meeting the initial and final vehicle position N, Q and orientation θ. The curve

parameter "a" shown in eqn. (4-2) plays an important role deciding the shape of planned path. The curve parameter "a" should be chosen so that the eqn. (4-16) always be invertible and eqn.(4-2) has a solution. The determinant of the path planning algorithm, eqn (4-9), shouldn't be zero. The smallest positive solution of the equation cos(x)cosh(x)=1 is x≈4.73. The curve parameter "a" is thus chosen so that aL<4.73. Figure 6.1 shows the planned paths for different values of "a". For larger values of "a", the planned path becomes oscillatory in space. For the present simulation study, a=0.1 was chosen such that the planned path is stiff enough to prevent to have too much curvature in the vehicle's trajectory.

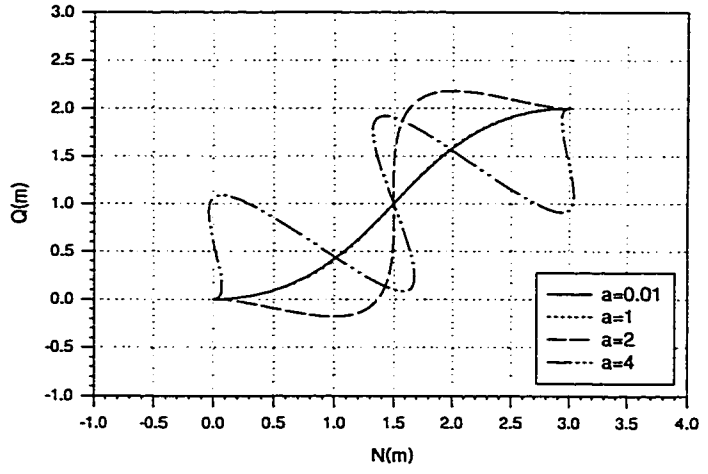

Figure 6.1 Planned Path for $N_i = 0$, $Q_i = 0$, $\theta_i = 0°$, and $N_d = 3$, $Q_d = 2$, $\theta_d = 0°$ with different curve parameters "a".

The simulations were performed using this controller implementation for a slope β=15°, initial posture of $N_i = 0$, $Q_i = 0$, and $\theta_i = 0°$, and desired posture of $N_d = 3$, $Q_d = 2$, and $\theta_d = 0°$. As it is shown in Fig. 6.1, the planned paths are significantly different for the different values of the curve parameter "a". When "a" is increased, the planned path becomes oscillatory in space(Fig. 6.1).

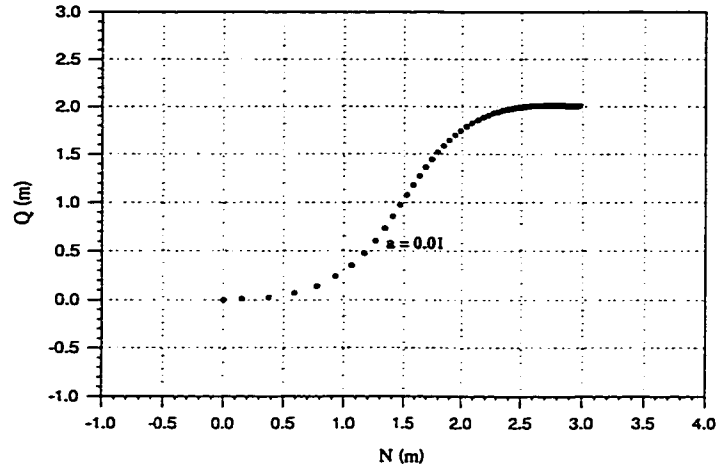

Figure 6.2 Trajectory of the vehicle generated with curve parameter a = 0.01

Fig. 6.2 shows a smooth trajectory generated by the vehicle following a planned path with the parameter a = 0.01

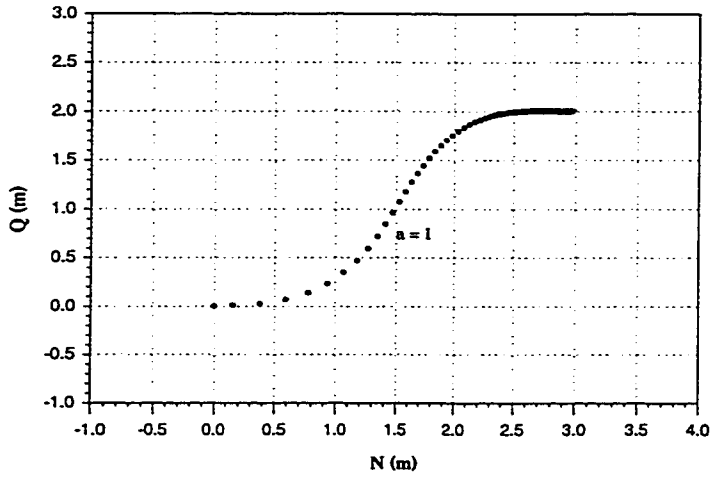

Figure 6.3 Trajectory of the vehicle generated with curve parameter a = 1

Fig. 6.3 also shows a smooth trajectory generated by the vehicle following a planned path with the curve parameter a = 1 which differs insignificantly for the previous case for a = 0.01. As it is observed by Figures. 6.1, 6.2, and 6.3, the vehicle follows the planned trajectory well as far as the curve parameter "a" is maintained small enough, in other word the planned path is stiff enough.

Unlike the above trajectories, by applying the curve parameter a = 2 the vehicle's actual trajectory is quite different from the planned one (Fig. 6.1 and Fig. 6.4). This fact explains that the generated trajectory, taking into account the dynamics of the vehicle, tries to meet the flexibility of the planned path and updates the path accordingly. Analysis of the wheel-ground contact forces shows that this path plan with a=2 is still feasible for the vehicle not to slip and not to tip-over.

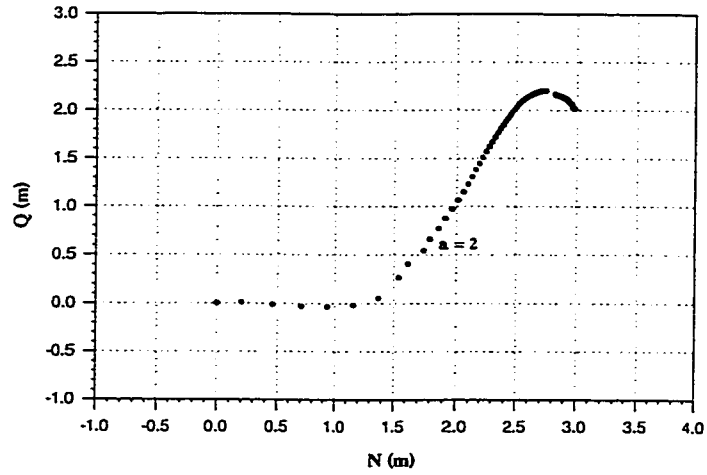

Figure 6.4 Trajectory of the vehicle generated with curve parameter a = 2

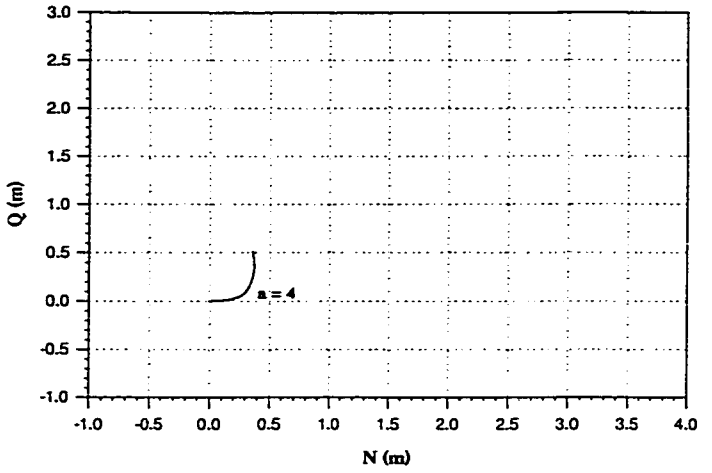

Figure 6.5 Trajectory of the vehicle generated with curve parameter a = 4

Fig. 6.5 indicates that having too high value of "a", for the planned path, makes the vehicle unable to follow the planned path and update it. The vertical wheel ground contact forces show values which change the sign indicating that the vehicle tips over at that time.

These results show that the parameter "a" should be chosen small enough to prevent the vehicle (which is following the planned path) from slipping and/or tipping-over. Increasing the slope angle β of the inclined plane, on which the vehicle moves, leads to more frequent situations in which slippage or tip-over can occur.

6.1.2 Analysis of loss of contact conditions via the conditions of the wheel-ground contact forces (G_{xi}, G_{yi}, G_{zi} , i=1,2,3)

Wheel-ground contact loss and no slip conditions can be written as,

$$G_{iz} \geq 0 \qquad i=1,2,3$$

$$(G_i^2 x + G_i^2 y) \leq \mu^2 G_i^2 z \qquad i=1,2,3$$

where μ is a friction coefficient chosen as 0.7 throughout the simulation.

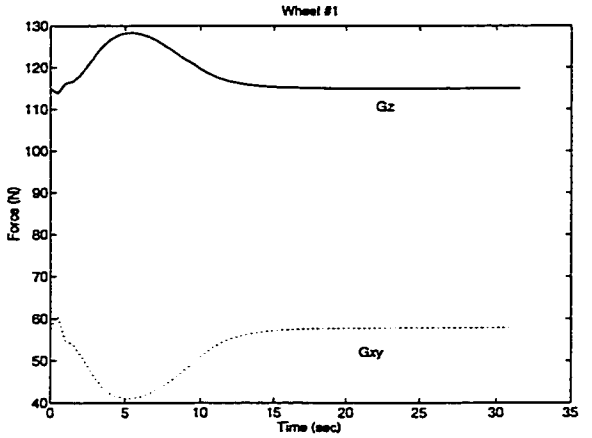

Figure 6.6 Wheel-ground contact forces for the front wheel when no slippage, no loss of contact occurs ($K_{ext} = 2.0$)

Simulation results for initial posture of $N_i = 0$, $Q_i = 0$, and $\theta_i = 0°$, desired posture of $N_d = 3$, $Q_d = 2$, and $\theta_d = 0°$, slope of β=15°, curve parameter a = 1.0, and $K_{ext} = 2.0$ show that wheel-ground contact forces have a magnitude $(G_{xi}^2 + G_{yi}^2)^{1/2}$ which is lower than the friction forces μG_{zi} for μ=0.7, i.e. no slippage occurs. Also, the G_{zi} forces do not change the sign during the motion, i.e. no loss of contact occurs, (Fig. 6.6, 6.7, 6.8).

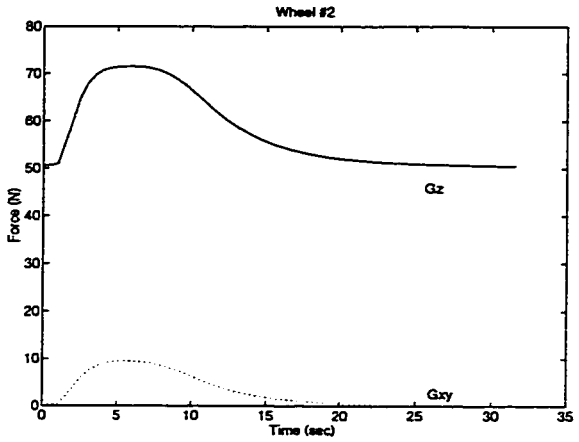

Figure 6.7 Wheel-ground contact forces for the wheel #2, no slippage, no loss of contact occurs

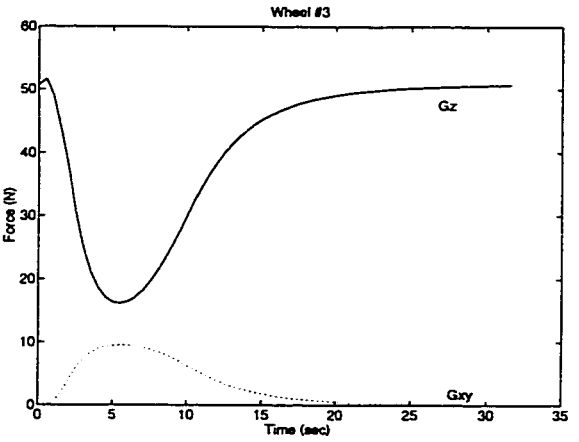

Figure 6.8 Wheel-ground contact forces for the wheel #3, no slippage, no loss of contact occurs

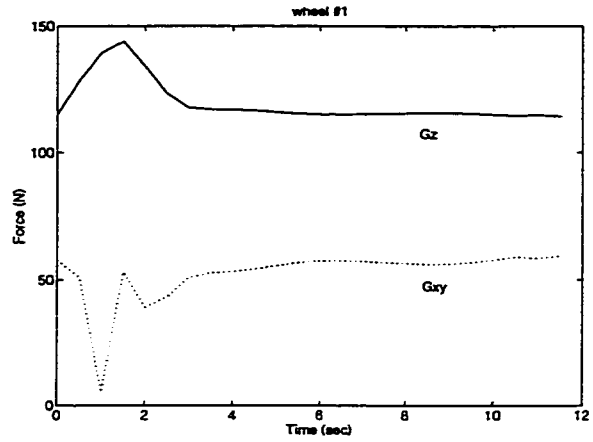

Figure 6.9 Wheel-ground contact forces for the front wheel for $K_{ext} = 4.0$

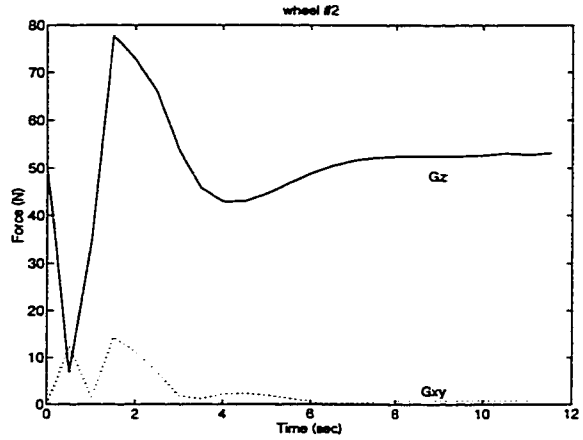

Figure 6.10 Wheel-ground contact forces for the wheel #2 showing it slipped but not lost contact with no $G_z < 0$

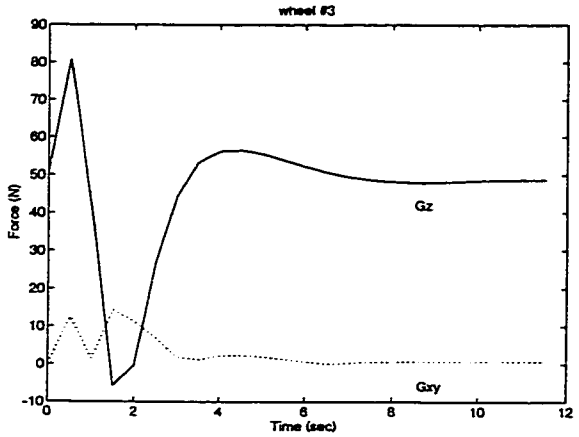

Figure 6.11 Wheel-ground contact forces for the wheel #3 when slippage and loss of contact occur

In figures 6.9 to 6.11, the results for a larger K_{ext} ($K_{ext} = 4.0$) are shown. In this case, larger centrifugal forces are generated and, consequently, wheel ground contact forces become larger than friction forces and wheel slippage occurs (for example, for wheel #2 in figure 6.10, at time = 0.5 sec., G_{z2}= 5 N and G_{xy2} = 13 N signals the wheel #2 is being slipped). Also, as shown in figure 6.11, the resulting large centrifugal force leads to a reduction of G_{z3} and even to sign reversal indicating loss of wheel-ground contact for the vehicle at time = 1.4 to 2 sec.. Increasing the slope angle β of the inclined plane, on which the vehicle moves, leads to more frequent situations in which slippage or tip-over can occur.

6.1.3 Comparison of the Performances of Model Predictive Control Scheme and Input-Output Linearization Control Scheme by the Analysis of Tip-over Conditions via the External Loop Proportional Controller Design (K_{ext}) of the autonomous vehicle

The operational space controller which generates a path meeting the initial and final vehicle position N, Q and orientation θ, uses a proportional (K_{ext}) control law for operational space errors (see Fig. 4.3). The nonlinear controller is used for linearization with regard to δ and ω_1 .

Rewriting the proportional controller of $\omega_1^{(c)}$ from eqn.(4-14),

$$\omega_1^{(c)} = K_{ext}[S(L) - S(x)] \tag{6-1}$$

K_{ext} determines the response time of the external loop. The value of K_{ext} must be high enough to have a reasonable duration of travel from initial to the desired points. The velocity of the autonomous vehicle is proportional to K_{ext}. This gain can be reduced to avoid tip-over of the vehicle.

The main control task here is finding right K_{ext} such that the vehicle will not lose wheel-ground contact. Combination of Model Predictive Control and Input-Output Linearization control is chosen for solving difficulties of the Input-Output Linearization control alone.

The simulations were first performed using the Input-Output Linearization control only and using Model Predictive Control on a horizontal surface for initial posture of N_i=0(m), Q_i=0(m), and θ_i=-15°, and desired posture of N_d=2.0(m), Q_d=2.0(m), and θ_d=90°. The curve parameter "a" is maintained as a=1.0 such that the planned path is non-oscillatory in space. The results are later compared with those from Input-Output Linearization and Model Predictive Control to show the improvement on the performance of the vehicle.

6.1.3.1 Performance of the Input-Output linearization control scheme for various external loop proportional control gain, K_{ext}

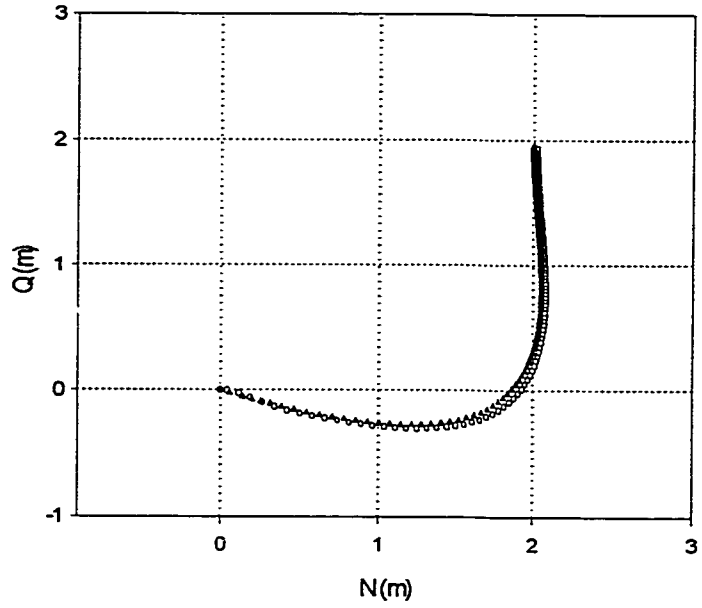

Figure 6.12 Planned Path(▲) and the trajectory(∘) of the vehicle with K_{ext}=2.0 and a=1.0

Figure 6.12 shows a smooth trajectory of the vehicle following the planned path very well without tip-over for initial posture of N_i=0(m), Q_i=0(m), and θ_i=-15°, and desired posture of N_d=2.0(m), Q_d=2.0(m), and θ_d=90° with K_{ext}=2.0 and a=1.0. Figures 6.13 and 6.14 show the N and Q coordinates versus time for the planned and the generated trajectory. These figures confirm the well tracked path of the above result, figure 6.12.

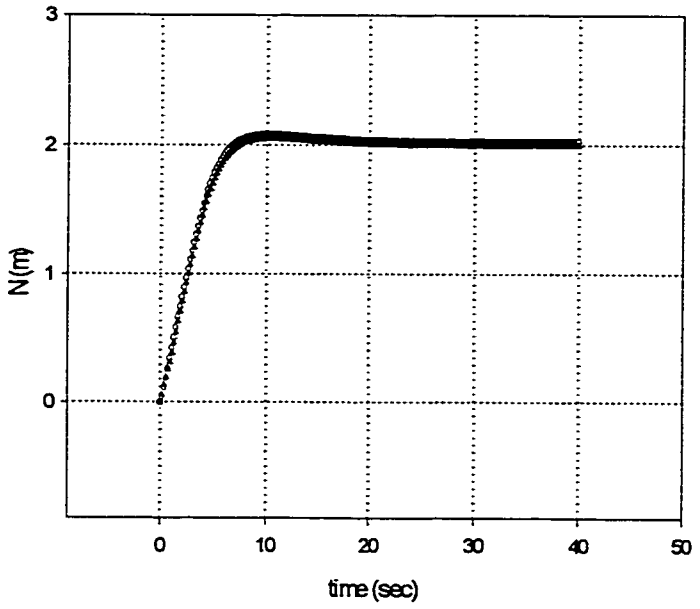

Figure 6.13 The time behavior of N position (planned (▲) and generated(○)) for figure 6.12

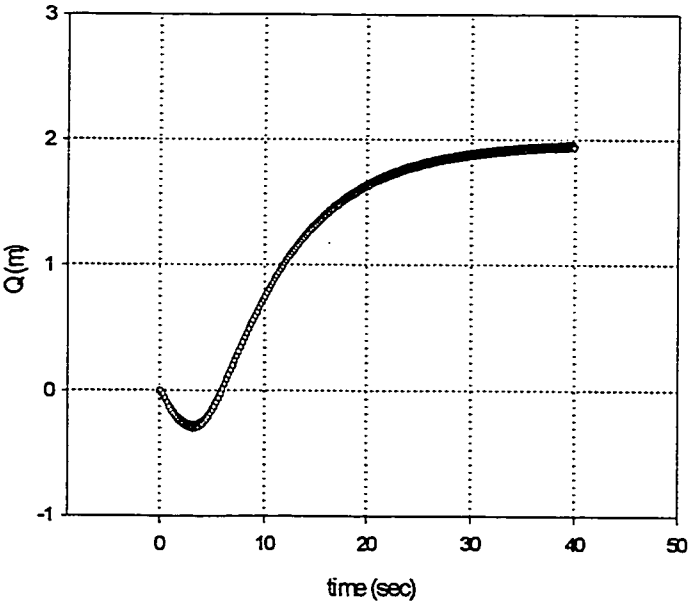

Figure 6.14 The time behavior of Q position (planned (▲) and generated(○)) for figure 6.12

Figure 6.15 shows the time variation of the orientation angle, θ of the vehicle, which reaches the desired 1.57 rad(=90°). In figure 6.16, the steering angle, δ of the vehicle settles down close to 0°, also as desired. Figure 6.17 shows the time variation of driving wheel velocity, ω_1, which reaches zero when the vehicle approaches the desired position. By examining figures 6.18, 6.19, 6.20 which show the vertical reaction forces (G_{1z}, G_{2z}, and G_{3z}) of the wheels to the ground, we can find out if the loss of wheel ground contact had occurred by the following tip-over condition,

$$G_{iz} \geq 0, \qquad for \quad i=1,2,3 \tag{6-2}$$

In the present case, it is seen that no vertical reaction force becomes negative in time, i.e., there is no loss of contact between the wheels and the ground. Figures 6.21, 6.22, 6.23 show the traction forces for wheel #1, #2, and #3, respectively. They show smooth force variation for driving the vehicle. Matching the figures 6.18, 6.19, 6.20 to 6.21, 6.22, 6.23, respectively in terms of the no slip condition,

$$G_{xyi}^2 = (G_{ix}^2 + G_{iy}^2) \leq \mu^2 G_{iz}^2, \qquad for \quad i=1,2,3 \tag{6-3}$$

where the friction coefficient is assumed equal to 0.7. The results show that the traction force of wheel #1 does not become lower than friction force, i.e. no slippage occurred between the driving wheel and the ground.

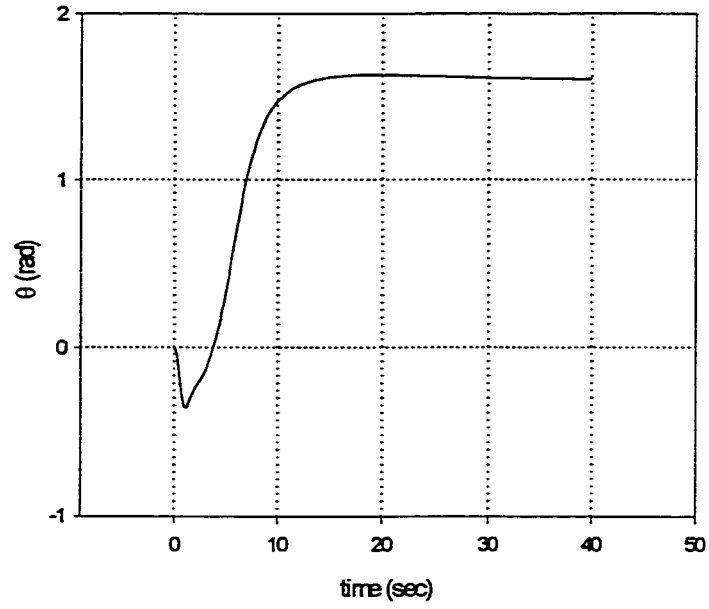

Figure 6.15 The time behavior of the orientation angle(θ) of the vehicle for figure 6.12

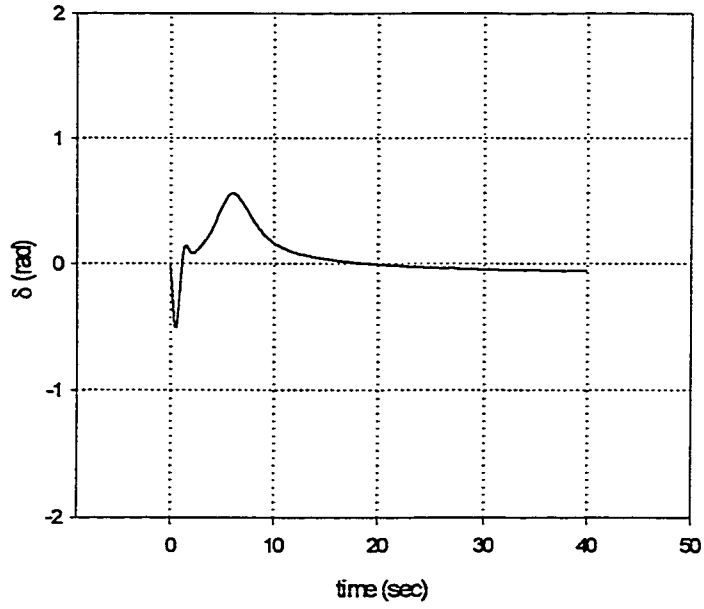

Figure 6.16 The time behavior of the steering angle(δ) of the vehicle for figure 6.12

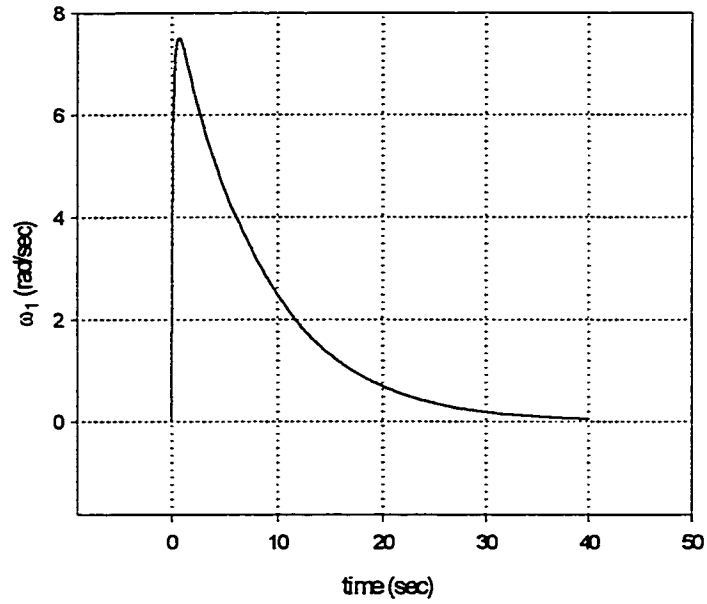

Figure 6.17 The time behavior of the angular velocity of the front wheel of the vehicle(ω_1) for figure 6.12

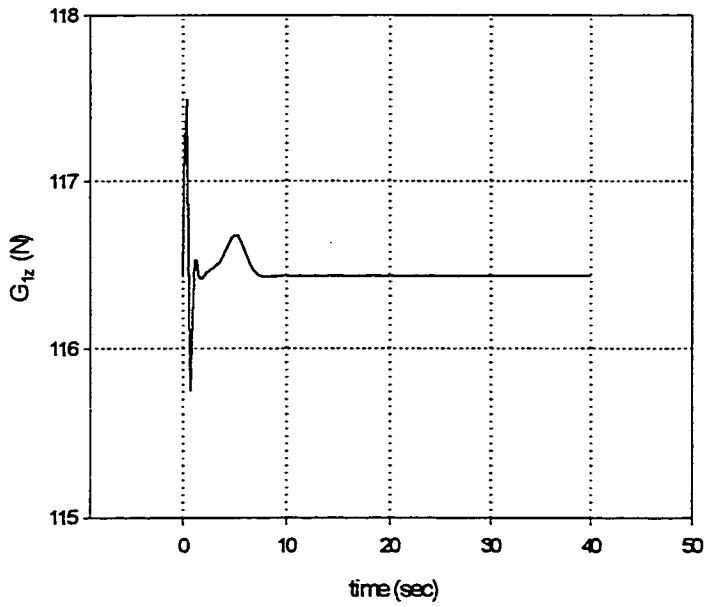

Figure 6.18 The time behavior of the vertical force of the front wheel(#1) of the vehicle for figure 6.12

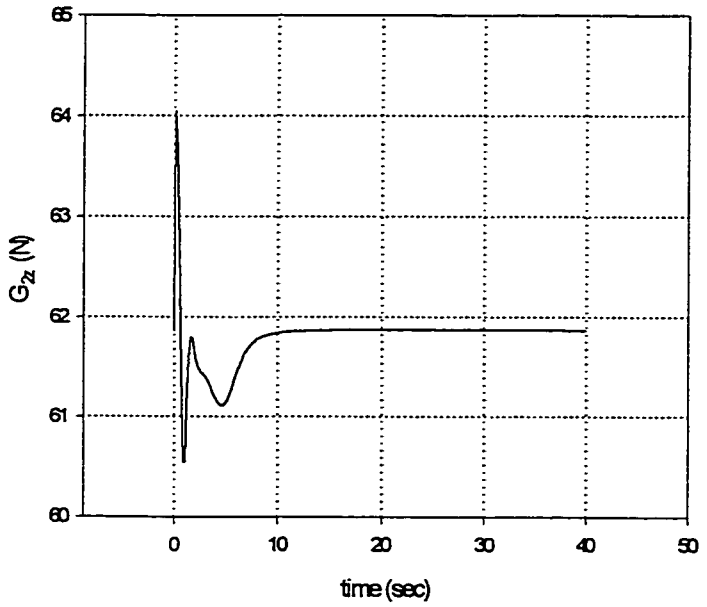

Figure 6.19 The time behavior of the vertical force of wheel#2 of the vehicle for figure 6.12

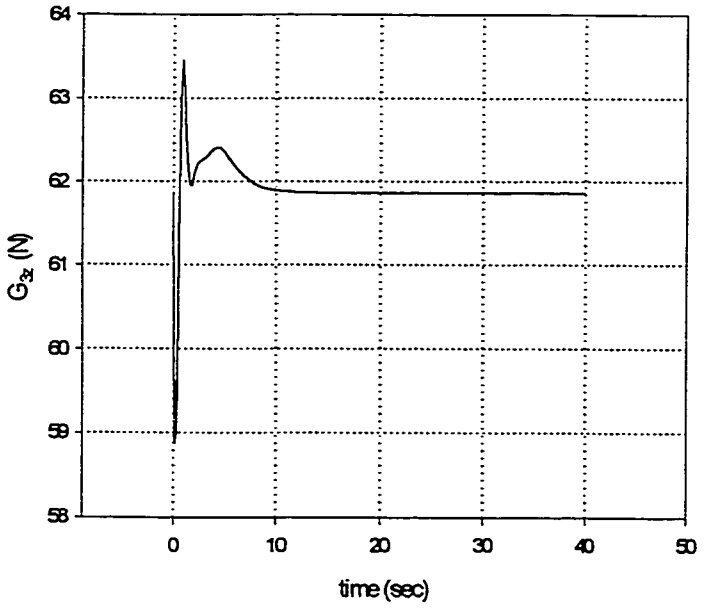

Figure 6.20 The time behavior of the vertical force of wheel#3 of the vehicle for figure 6.12

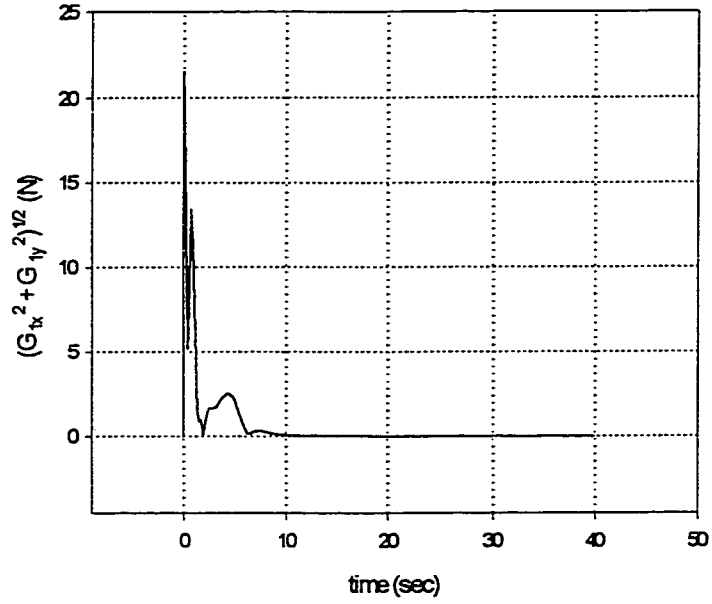

Figure 6.21 The time behavior of the traction force of the front wheel(#1) of the vehicle for the trajectory from figure 6.12

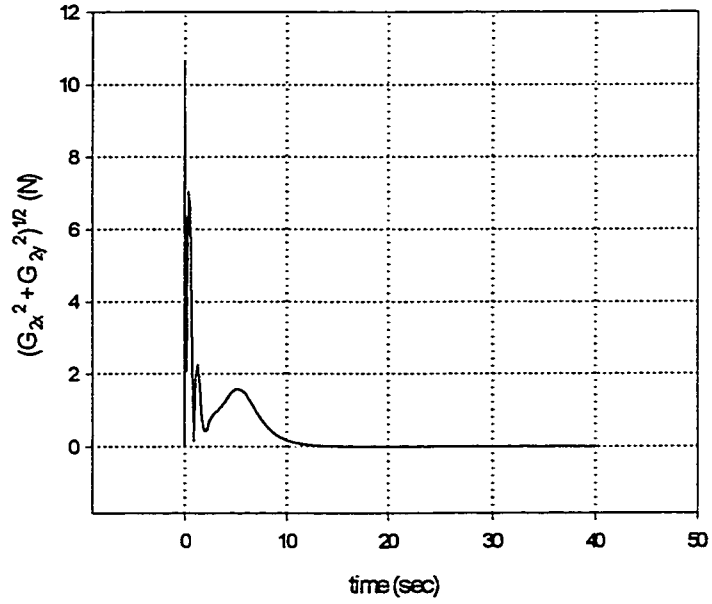

Figure 6.22 The time behavior of the G_{xy} force of wheel #2 of the vehicle for the trajectory from figure 6.12

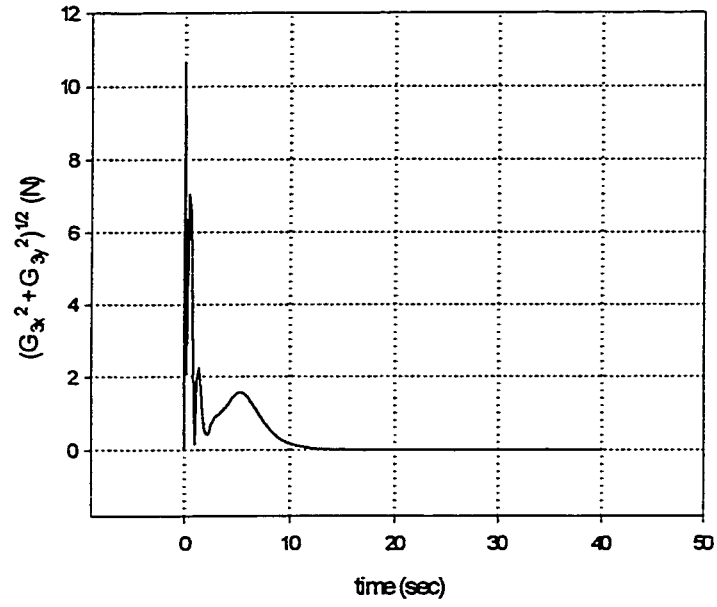

Figure 6.23 The time behavior of the G_{xy} force of wheel #3 of the vehicle for the trajectory from figure 6.12

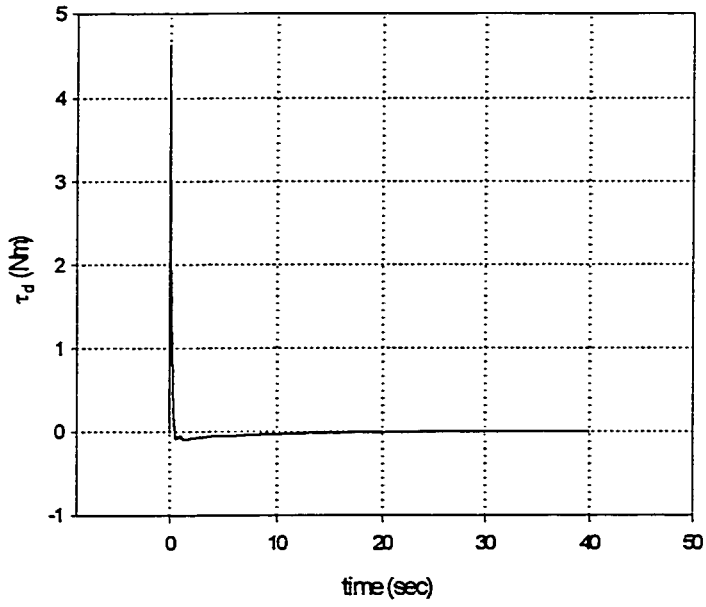

Figure 6.24 The time behavior of the driving torque of the vehicle for figure 6.12

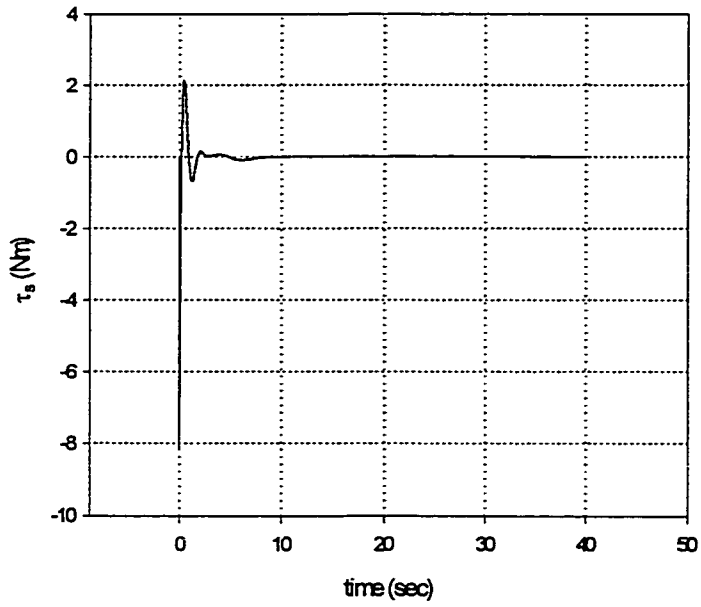

Figure 6.25 The time behavior of the steering torque of the vehicle for figure 6.12

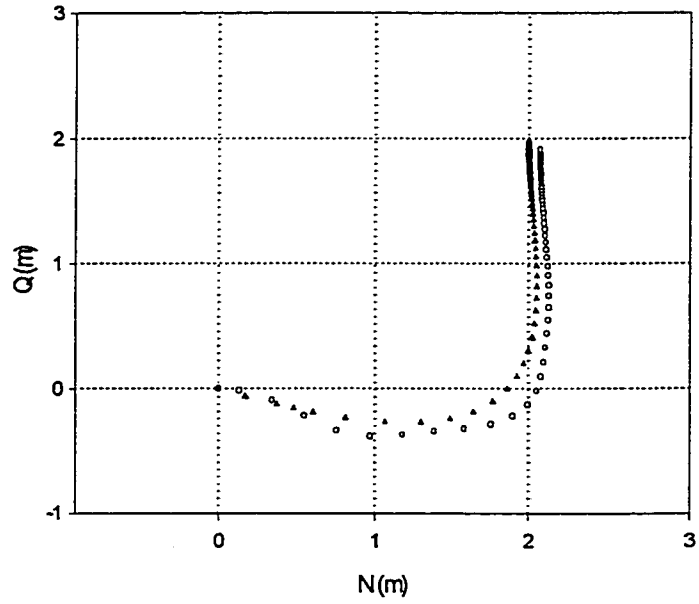

Figure 6.26 Planned Path(▲) and the trajectory(∘) of the vehicle with K_{ext}=3.0 and a=1.0

Figures 6.24 and 6.25 show the high initial torques followed after a few seconds of oscillating torques and then by zero torques. Figure 6.26 show the planned path and the trajectory of the vehicle when K_{ext} is increased to 3.0 while other conditions are same as before. The figure shows a curved trajectory followed by the vehicle, parallel to the planned one. Figure 6.26 also shows that the vehicle didn't reach to the target(N_d=2.0(m), Q_d=2.0(m)). This result can be explained by the fact that only one control variable, in this case $\omega_1^{(c)}$, can be closed loop controllable while the other variable $\delta^{(c)}$ is open loop controllable because of the non-holonomic constraint, eqn.(3-51). $\omega_1^{(c)}$ is function of the curvilinear position error as shown by eqn.(4-14). Figures 6.27 and 6.28 show the time history of the position of the vehicle, and steady-state errors can be noticed. As shown in figures 6.29 and 6.30, the orientation angle(θ) and the steering angle(δ) of the vehicle reache to the desired values after

some oscillations in the beginning. The vertical reaction forces of the three wheels to the ground shown in figures 6.32, 6.33, and 6.34 reveals no loss of wheel-ground contact given that no force changes sign. The G_{xy} forces of the three wheels shown in figures 6.35, 6.36, and 6.37 showed oscillatory behavior. The front wheel force G_{xyl} is high and drives the vehicle without slippage. Figures 6.38 and 6.39 show the time variation of the driving and steering torques which move toward zero after oscillations for a few seconds.

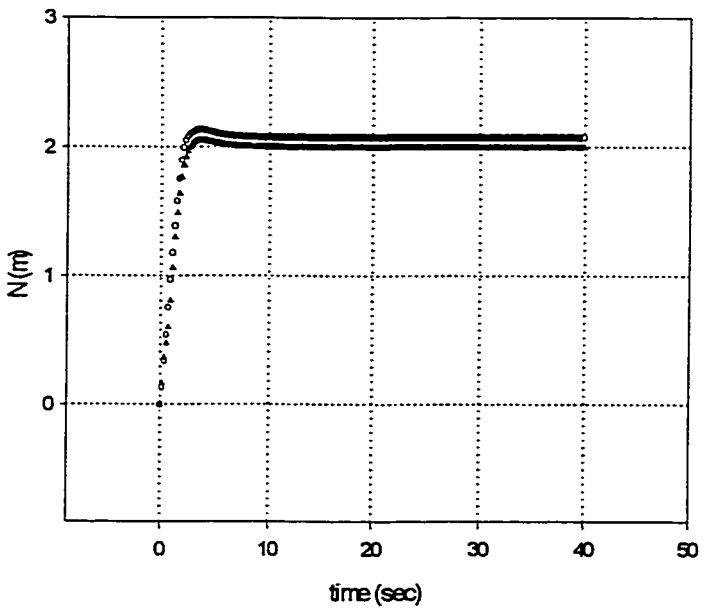

Figure 6.27 The time behavior of N position (planned (▲) and generated(○)) for figure 6.26

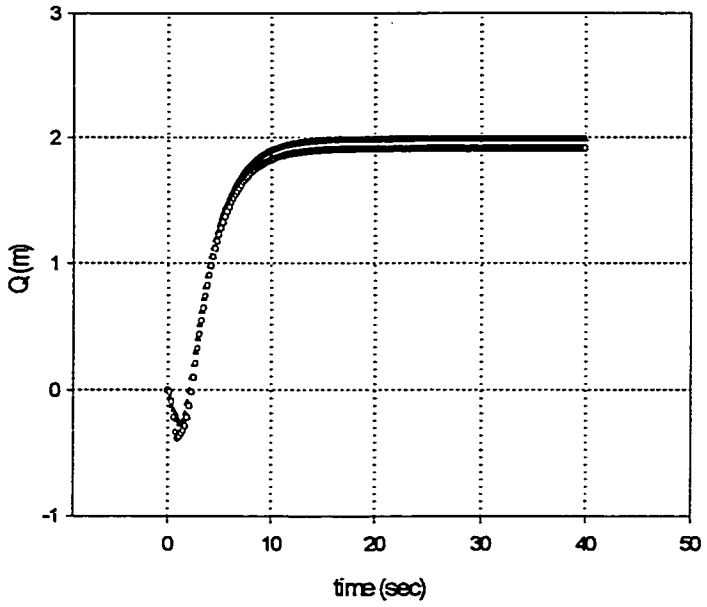

Figure 6.28 The time behavior of Q position (planned (▲) and generated(○)) for figure 6.26

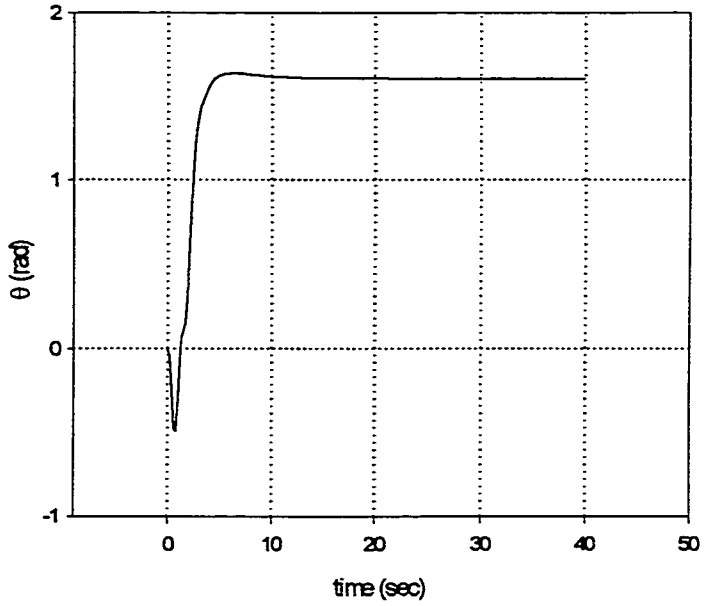

Figure 6.29 The time behavior of the orientation angle(θ) of the vehicle for figure 6.26

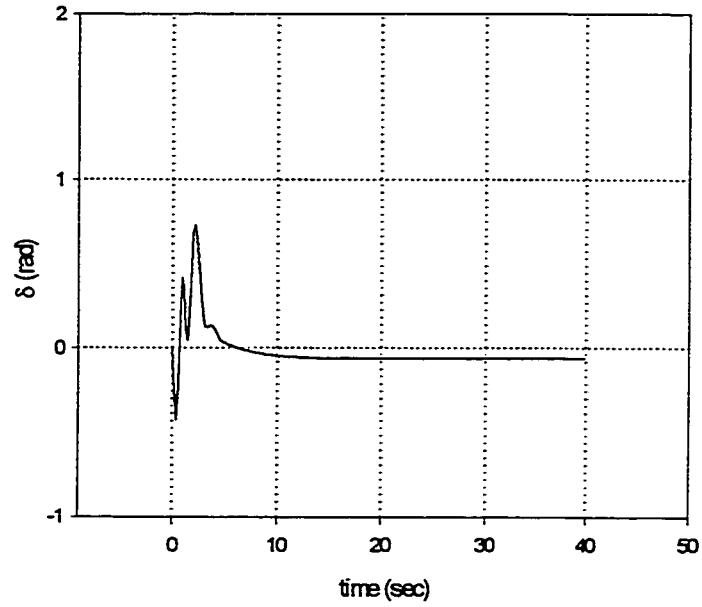

Figure 6.30 The time behavior of the steering angle(δ) of the vehicle for figure 6.26

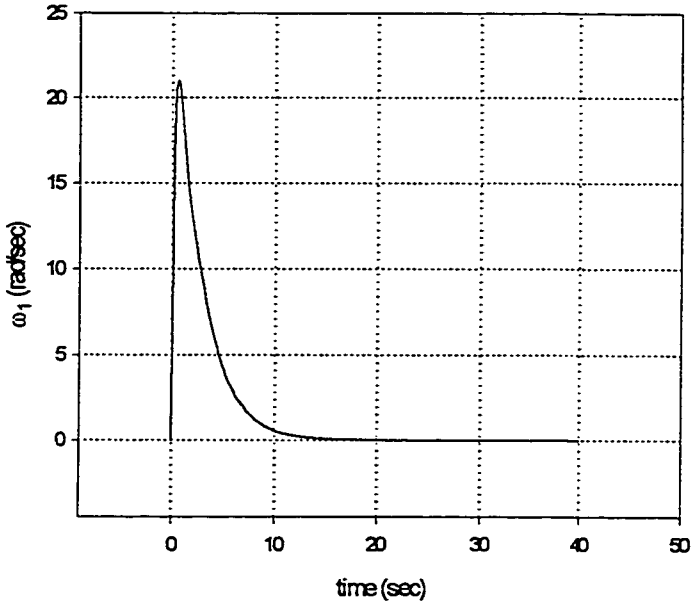

Figure 6.31 The time behavior of the angular velocity of the front wheel of the vehicle(ω_1) for figure 6.26

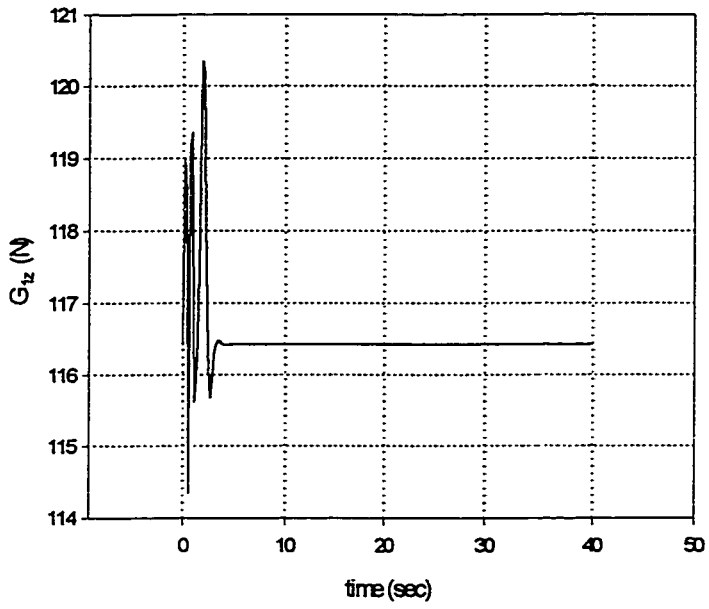

Figure 6.32 The time behavior of the vertical force of the front wheel(#1) of the vehicle for figure 6.26

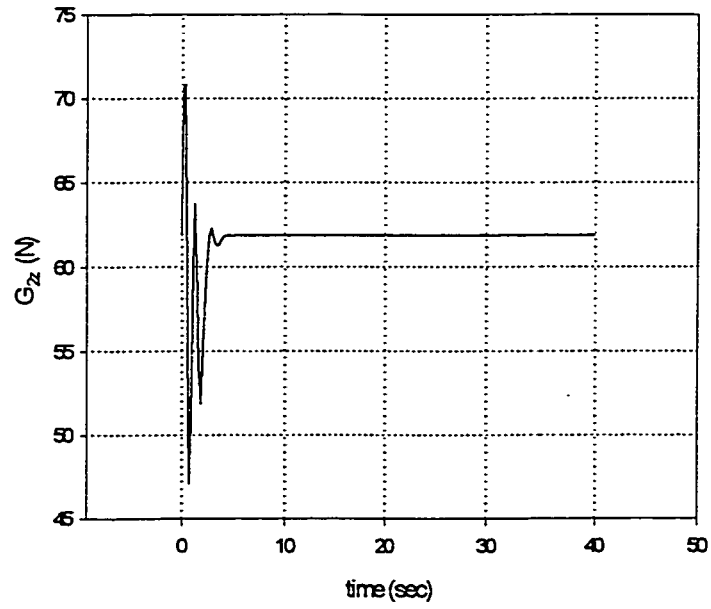

Figure 6.33 The time behavior of the vertical force of wheel #2 of the vehicle for figure 6.26

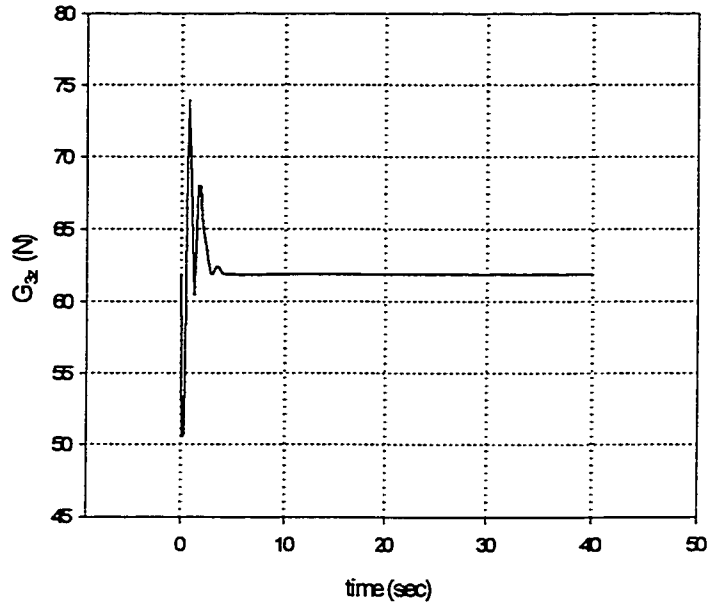

Figure 6.34 The time behavior of the vertical force of wheel #3 of the vehicle for figure 6.26

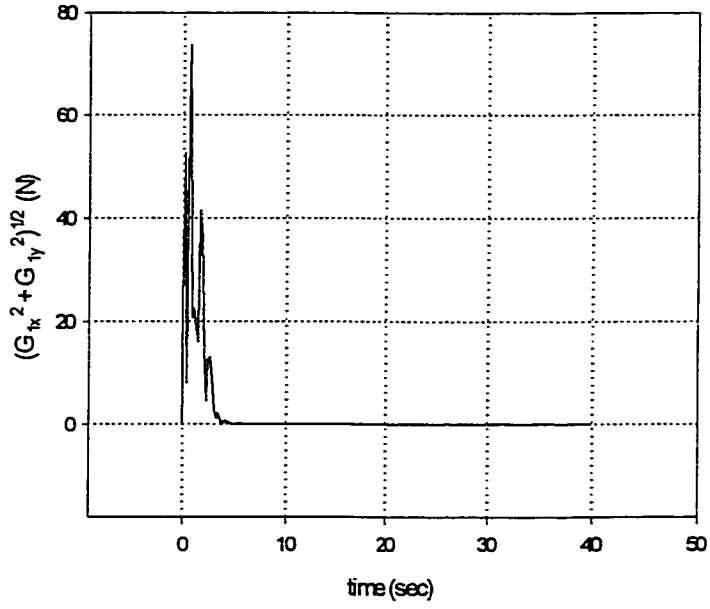

Figure 6.35 The time behavior of the traction force G_{xy1} of the front wheel(#1) of the vehicle for figure 6.26

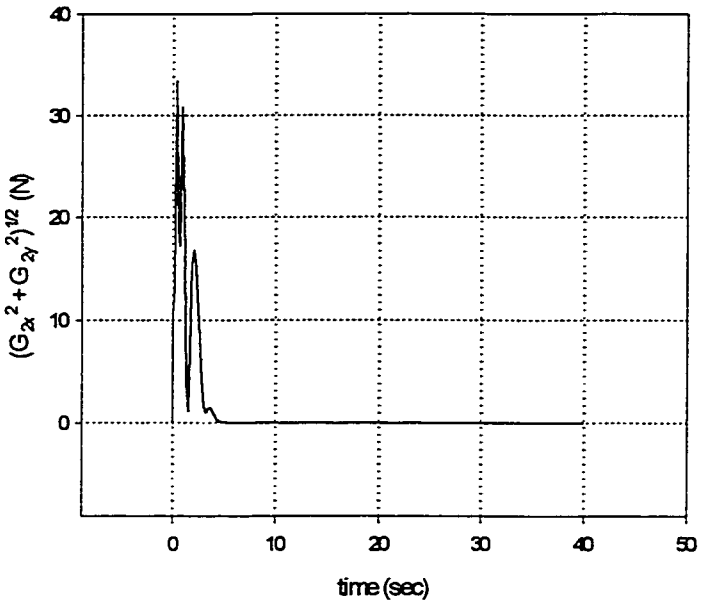

Figure 6.36 The time behavior of the G_{xy2} force of wheel #2 of the vehicle for figure 6.26

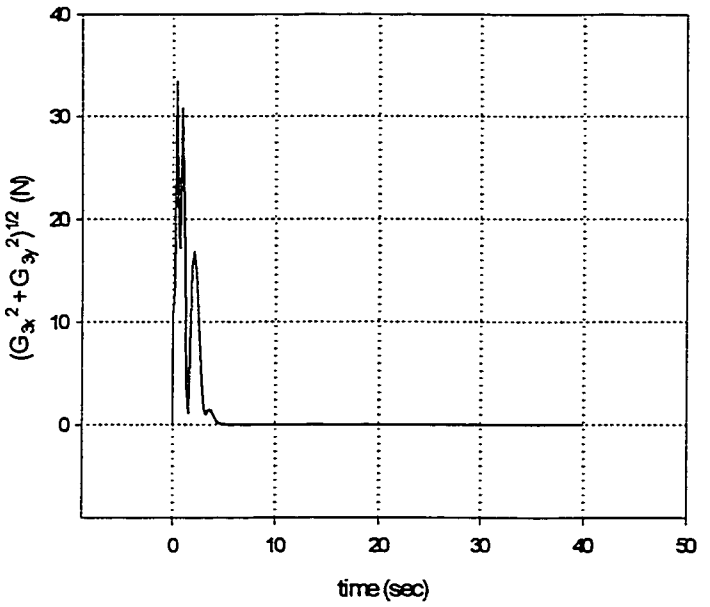

Figure 6.37 The time behavior of the G_{xy3} force of wheel #3 of the vehicle for figure 6.26

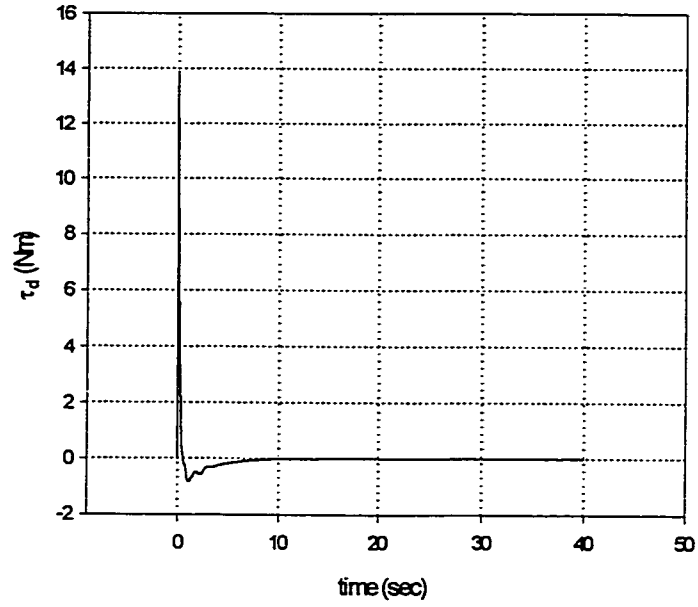

Figure 6.38 The time behavior of the driving torque of the vehicle for figure 6.26

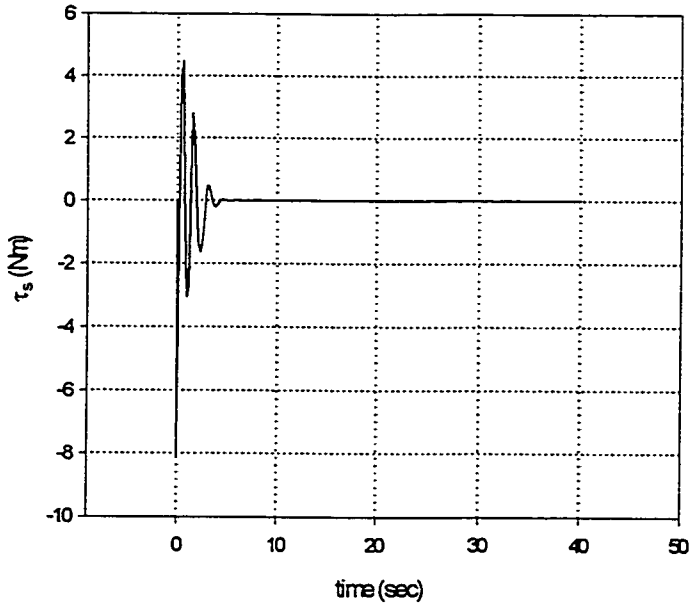

Figure 6.39 The time behavior of the steering torque of the vehicle for figure 6.26

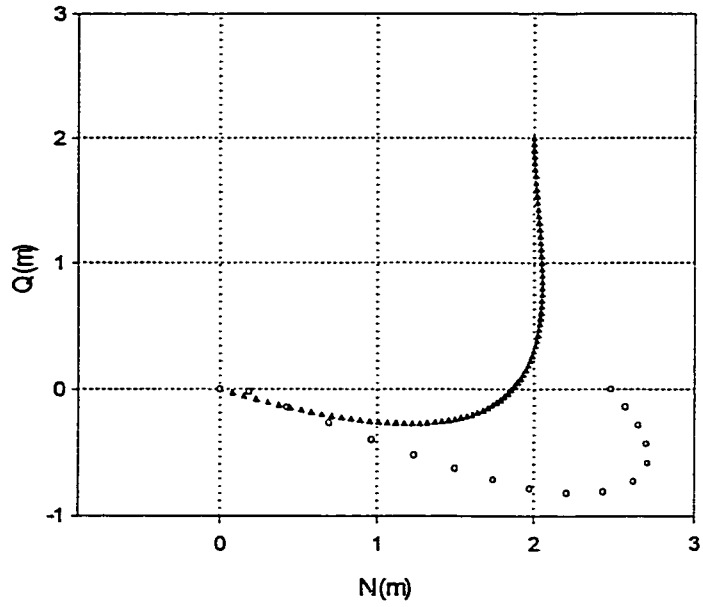

Figure 6.40 Planned path(▲) and the trajectory(○) of the vehicle with K_{ext}=4.0 and a=1.0

Figure 6.40 shows the planned path and the trajectory of the vehicle for K_{ext} increased to 4.0 while other conditions are same as before. The figure shows a prematurely stopped trajectory of the vehicle when attempting to follow the same planned path. The trajectory of the vehicle had stopped abruptly when one of the vertical forces of the three wheels changed sign and become negative. This phenomena means that loss of contact had occurred. The figure shows that the vehicle negotiated the first sharp corner but the centrifugal forces of the vehicle are already out of range of the safe region of not being tipped-over. Eventually tipping over on the other side occurs, and the end position is far from the desired one. Figures 6.41 and 6.42 show the same phenomena in time history of the position of the vehicle. Tipping-over occurred at about eight seconds after the initial

movement of the vehicle. From figures 6.43 and 6.44, the orientation angle(θ) and the steering angle(δ) of the vehicle show the erratic oscillations after the first 8 seconds of motion with full wheel-ground contact. The vertical reaction forces of the three wheels to the ground for the present case shown in figures 6.46, 6.47, and 6.48 reveal loss of ground contact of the wheel #3 leading the vehicle to be tipped-over. While G_{1z} and G_{2z} are maintained above zero, as shown in figures 6.46 and 6.47, G_{3z} shown in figure 6.48 becomes less than zero after 8 seconds of execution. The propulsion forces of the three wheels shown in figures 6.49, 6.50, and 6.51 show that the vehicle was going well until the forces on wheel #2 and #3 became zero then the forces oscillate erratically. We can see same phenomena on both driving and steering torques of the vehicle as shown in figures 6.52 and 6.53, respectively.

In fact, the autonomous vehicle model is derived only for the case of full wheel-ground contact. The moment the contact is lost, the model is not valid any more, such that all these results after 8 sec. should be ignored.

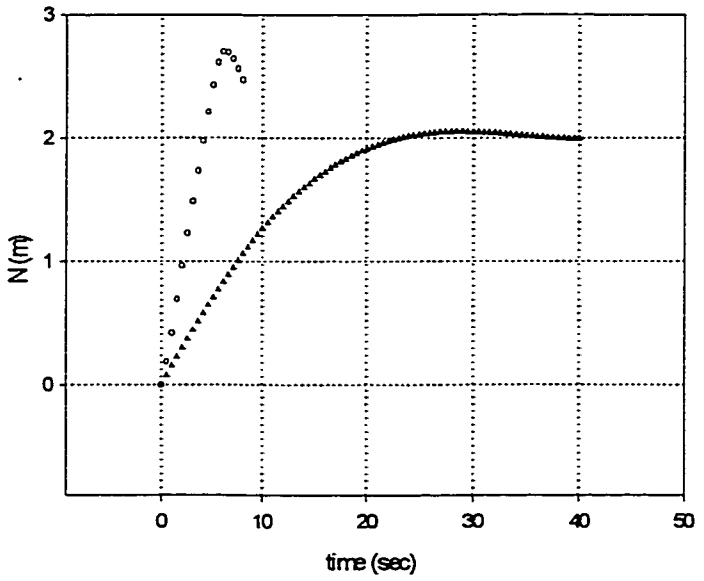

Figure 6.41 The time behavior of N position (planned (▲) and generated(◦)) for figure 6.40

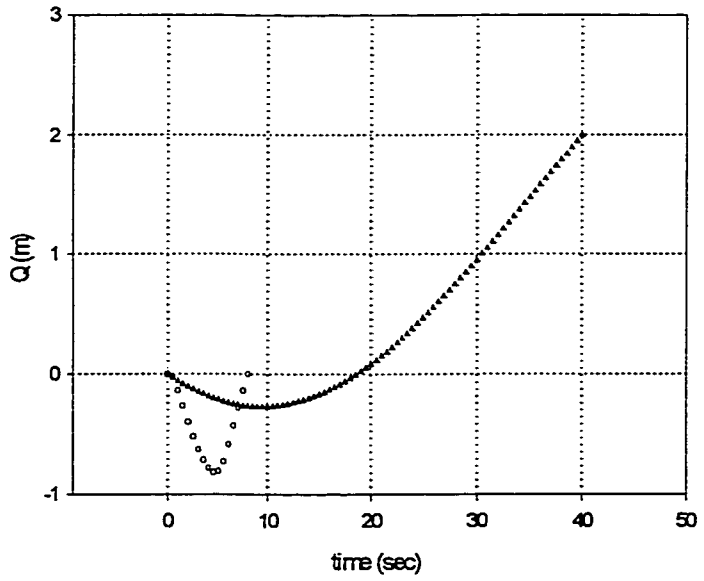

Figure 6.42 The time behavior of Q position (planned (▲) and generated(◦)) for figure 6.40

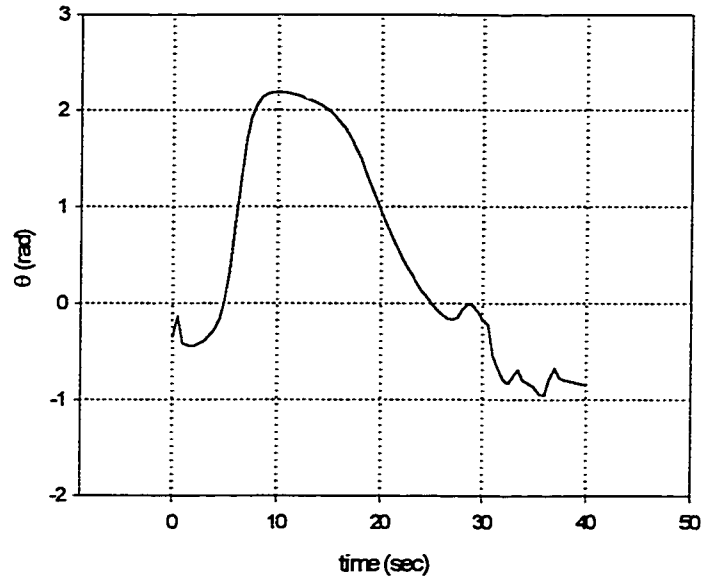

Figure 6.43 The time behavior of the orientation angle(θ) of the vehicle for figure 6.40

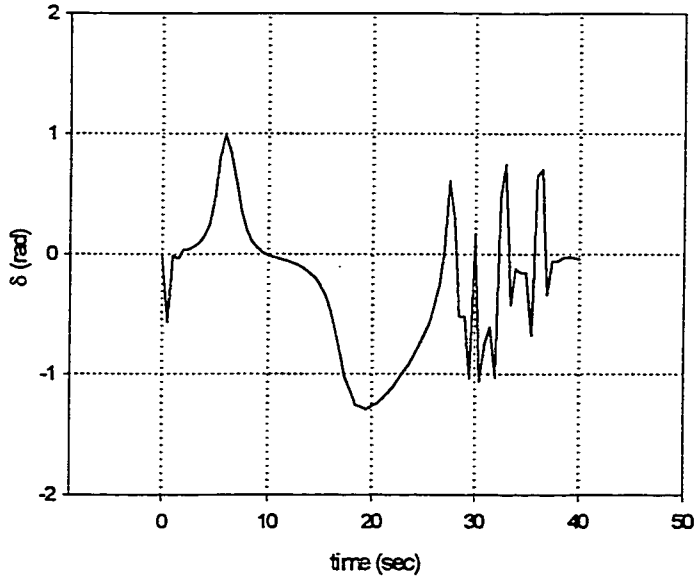

Figure 6.44 The time behavior of the steering angle(δ) of the vehicle for figure 6.40

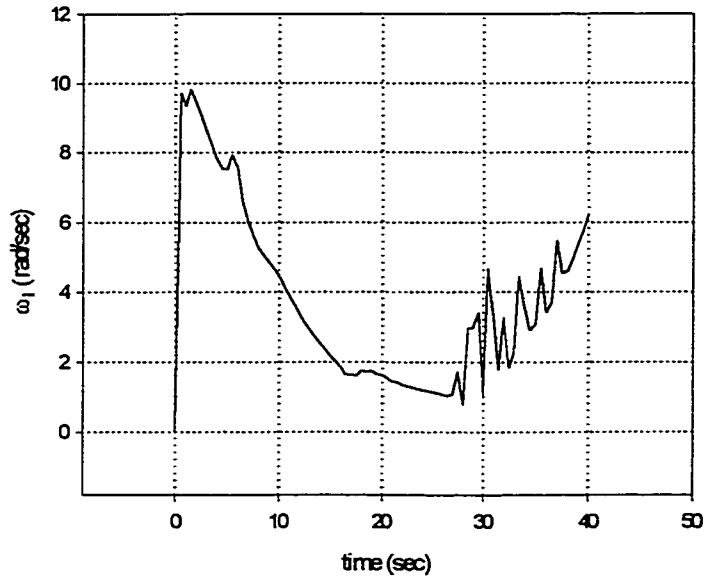

Figure 6.45 The time behavior of the angular velocity of the front wheel of the vehicle(ω_1) for figure 6.40

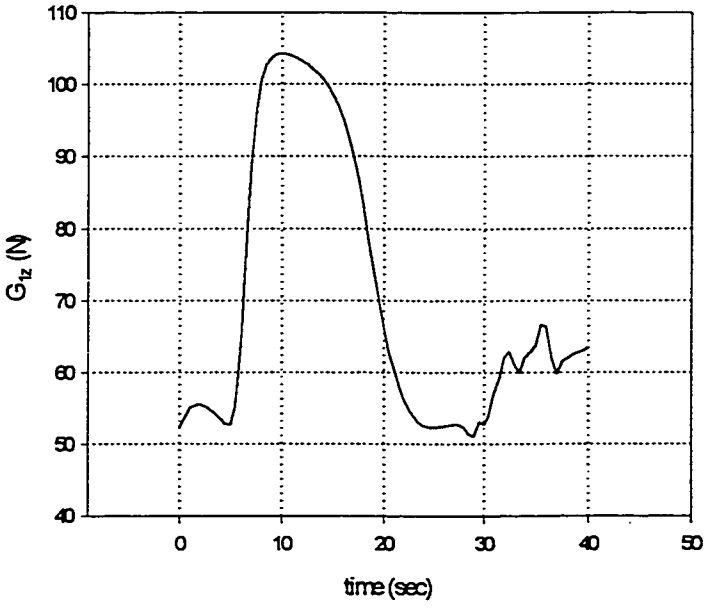

Figure 6.46 The time behavior of the vertical force of the front wheel(#1) of the vehicle for figure 6.40

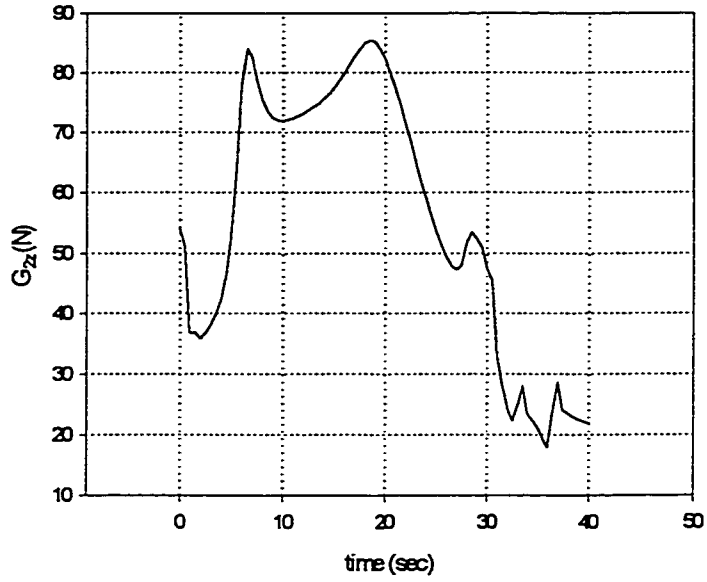

Figure 6.47 The time behavior of the vertical force of wheel#2 of the vehicle for figure 6.40

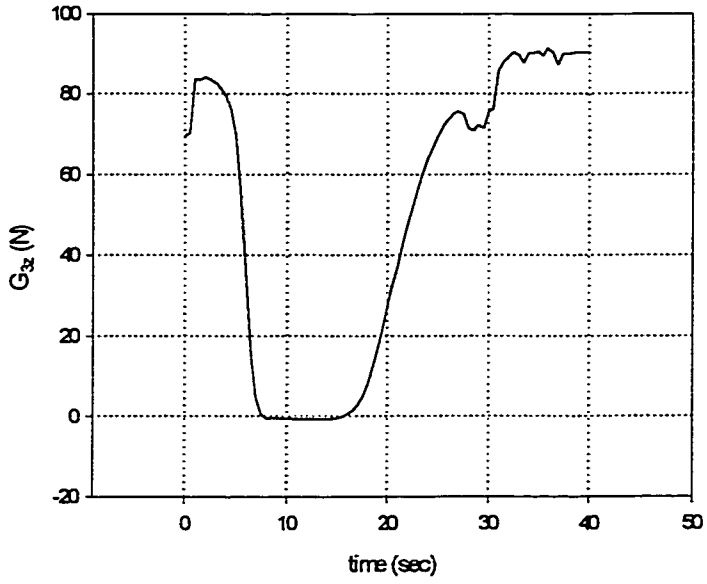

Figure 6.48 The time behavior of the vertical force of wheel#3 of the vehicle for figure 6.40

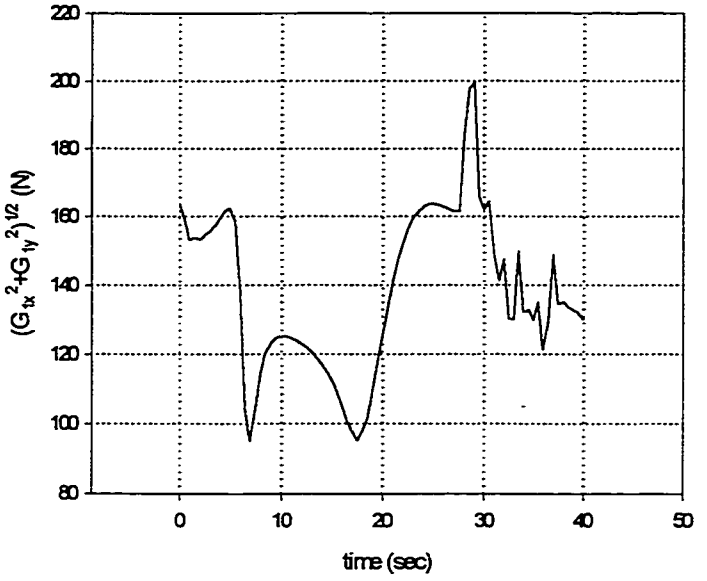

Figure 6.49 The time behavior of the traction force G_{xy1} of the front wheel(#1) of the vehicle for figure 6.40

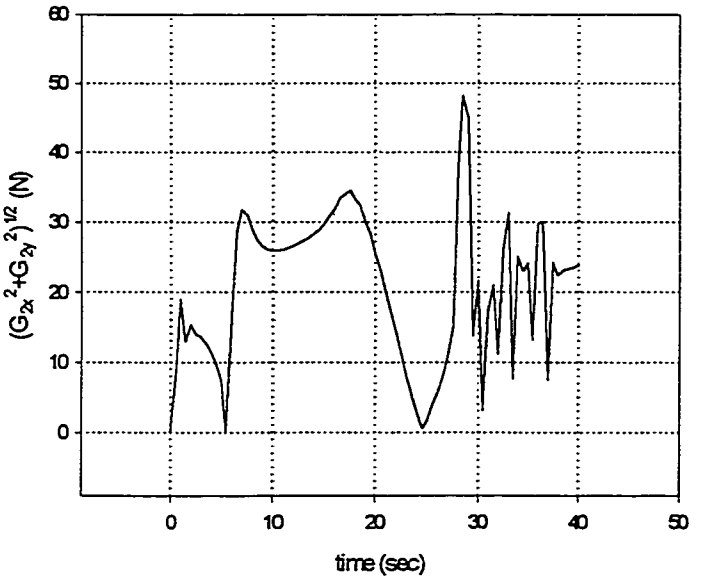

Figure 6.50 The time behavior of the G_{xy2} force of wheel #2 of the vehicle for figure 6.40

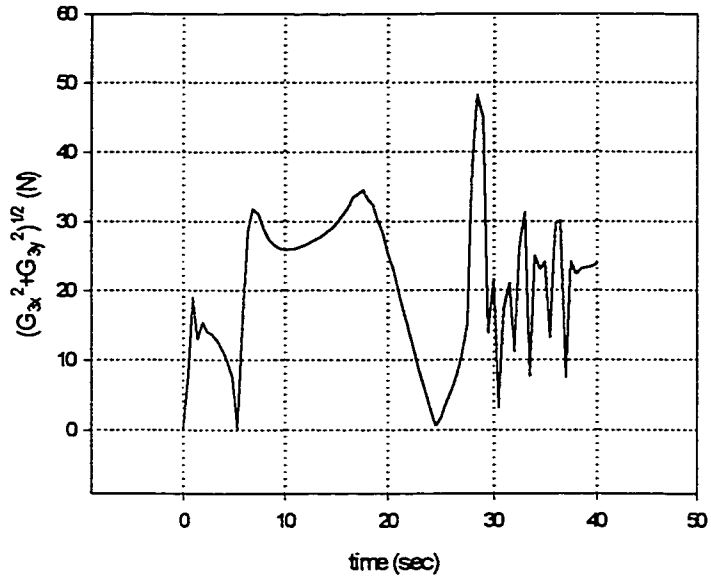

Figure 6.51 The time behavior of the G_{xy3} force of wheel #3 of the vehicle for figure 6.40

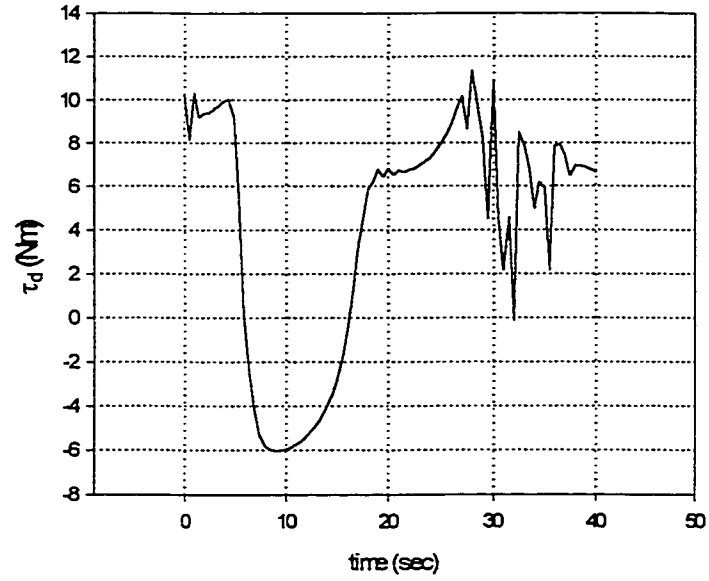

Figure 6.52 The time behavior of the driving torque of the vehicle for figure 6.40

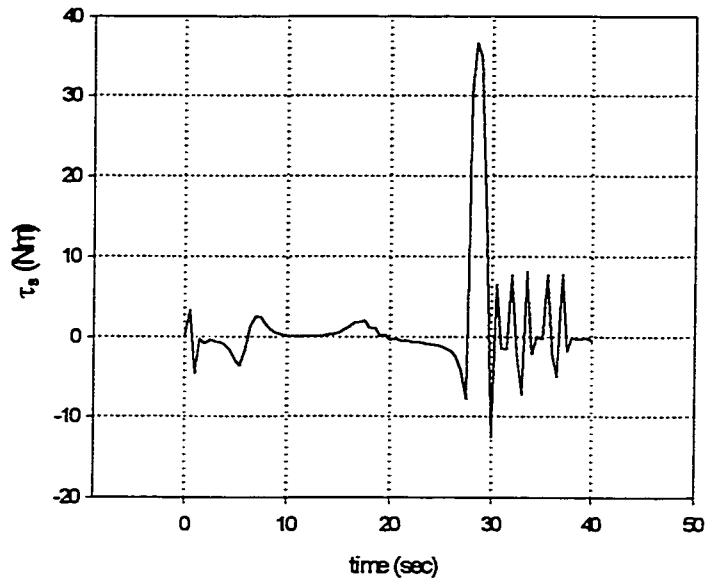

Figure 6.53 The time behavior of the steering torque of the vehicle for figure 6.40

6.1.3.2 Performance of the Model Predictive Control (MPC) with the Input-Output Linearization (IOL) control scheme for external loop proportional control gain, K_{ext}=4.0

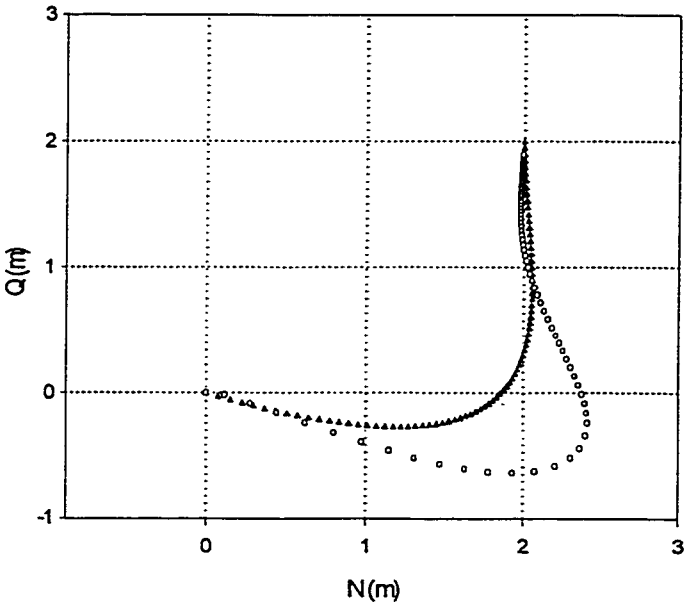

Figure 6.54 Planned Path(▲) and the trajectory(○) of the vehicle with K_{ext}=4.0 and a=1.0 using MPC

The result shown in figure 6.54 obtained with MPC and IOL compared to the result shown in figure 6.40 for only IOL represents a clear improvement on the performance of the vehicle tracking the planned path. The Model Predictive Controller is used for finding safe K_{ext} by predicting the violation of the loss of contact condition in combination with the Input-Output Exact Linearization controller. A smooth trajectory with a little more curvature is generated by the vehicle with the Model Predictive Controller (fig. 6.54) while with just Input-Output Exact Linearization scheme (fig. 6.40) the vehicle was shown to be in danger of being tipped-over. All results, shown in figures 6.55 to 6.67 confirm the improvement achieved by combining MPC and IOL Control. The graph of G_{3z}

vs. time (fig. 6.62) clearly shows the performance of the Model Predictive Controller in negotiating not to go in the region of negative values. Since all the vertical forces of the wheels to the ground stay at positive area, no loss of contact occurs.

Figures 6.55 and 6.56 show the same phenomena in time history of the position of the vehicle. From figures 6.57 and 6.58, the orientation angle(θ) and the steering angle(δ) of the vehicle, show the smooth variation and reaching to the desired values which are quite smoother than the ones with the Input-Output Linearization control scheme only (figs. 6.43, 6.44). All the other results also show the improvement of the performance of the vehicle in comparison with the corresponding results of the former case.

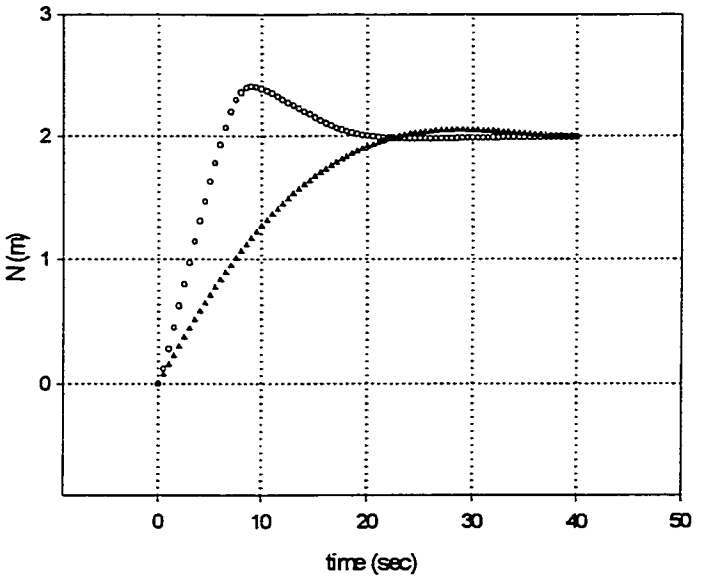

Figure 6.55 The time behavior of N position (planned (▲) and generated(○)) for figure 6.54

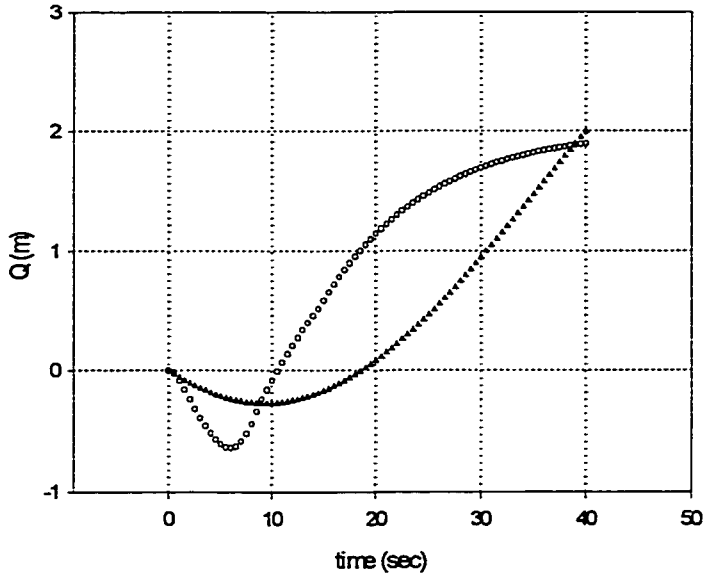

Figure 6.56 The time behavior of Q position (planned (▲) and generated(○)) for figure 6.54

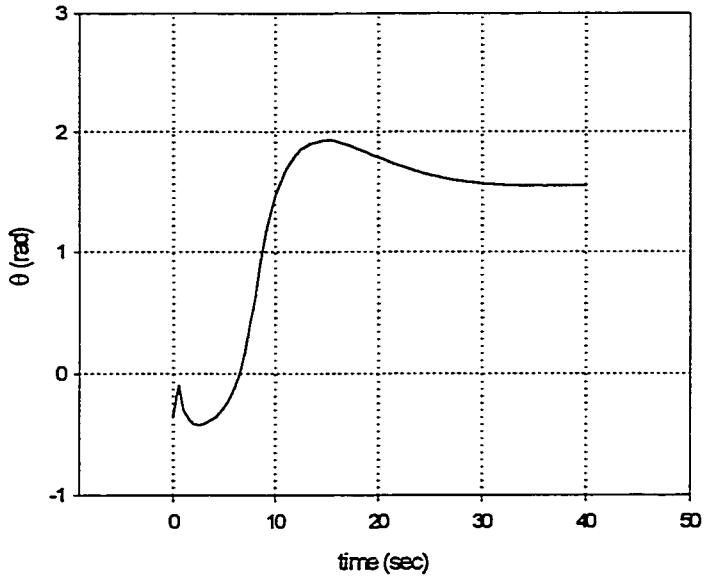

Figure 6.57 The time behavior of the orientation angle(θ) of the vehicle for figure 6.54

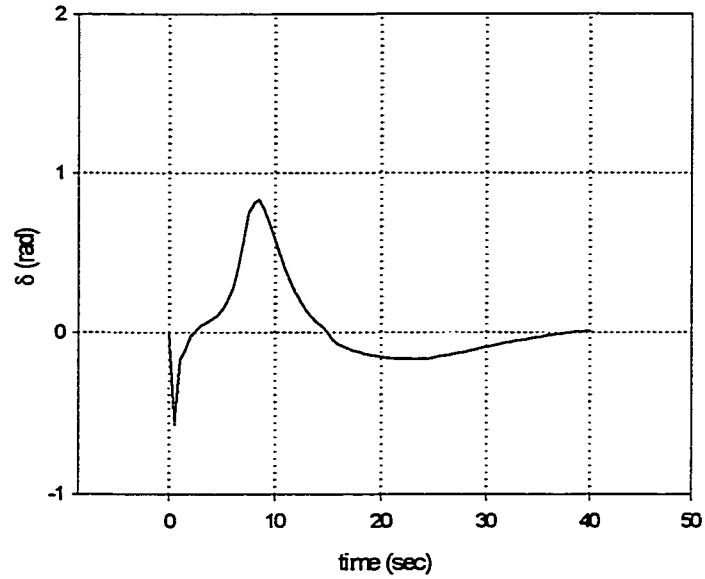

Figure 6.58 The time behavior of the steering angle(δ) of the vehicle for figure 6.54

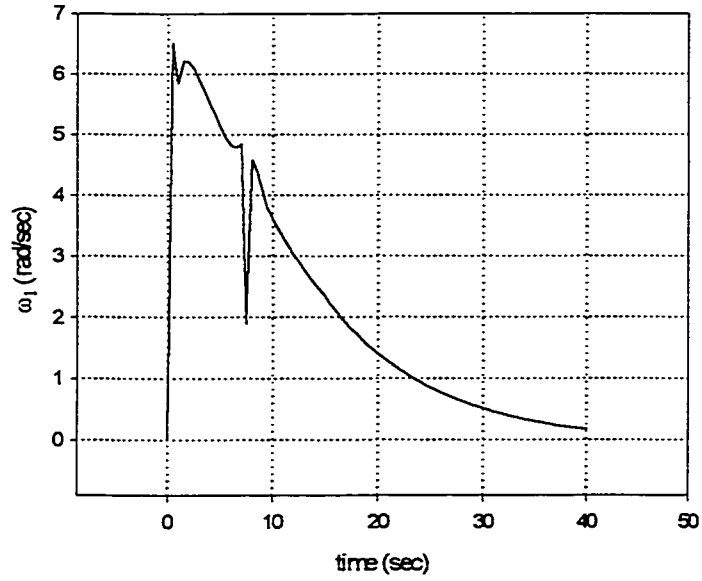

Figure 6.59 The time behavior of the angular velocity of the front wheel of the vehicle(ω_1) for figure 6.54

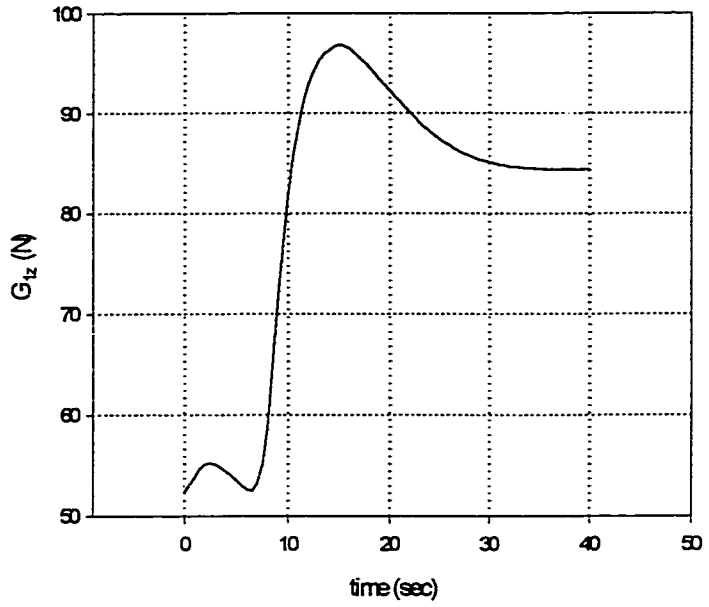

Figure 6.60 The time behavior of the vertical force of the front wheel(#1) of the vehicle for figure 6.54

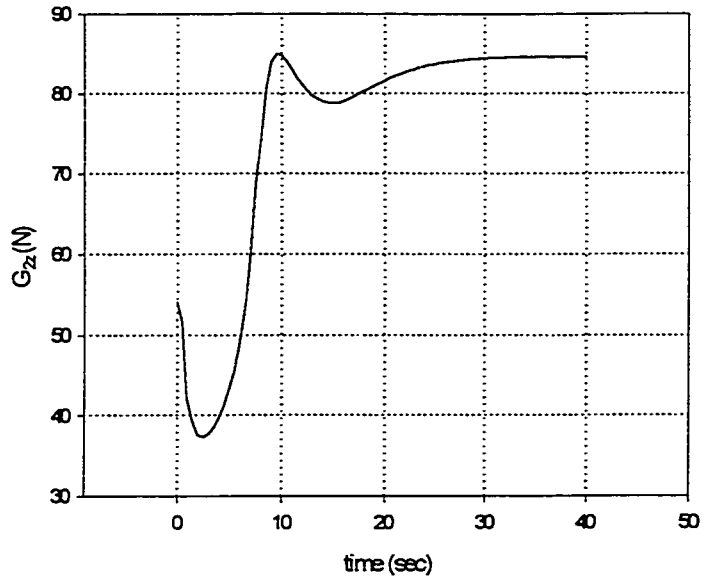

Figure 6.61 The time behavior of the vertical force of wheel#2 of the vehicle for figure 6.54

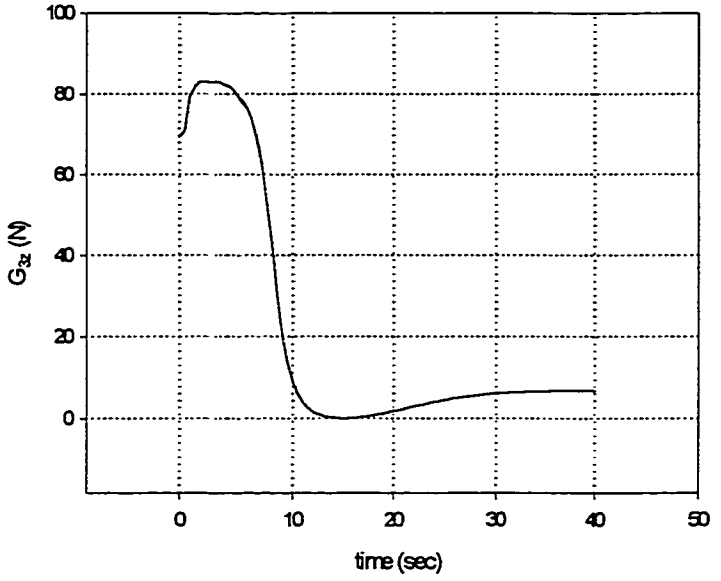

Figure 6.62 The time behavior of the vertical force of wheel#3 of the vehicle for figure 6.54

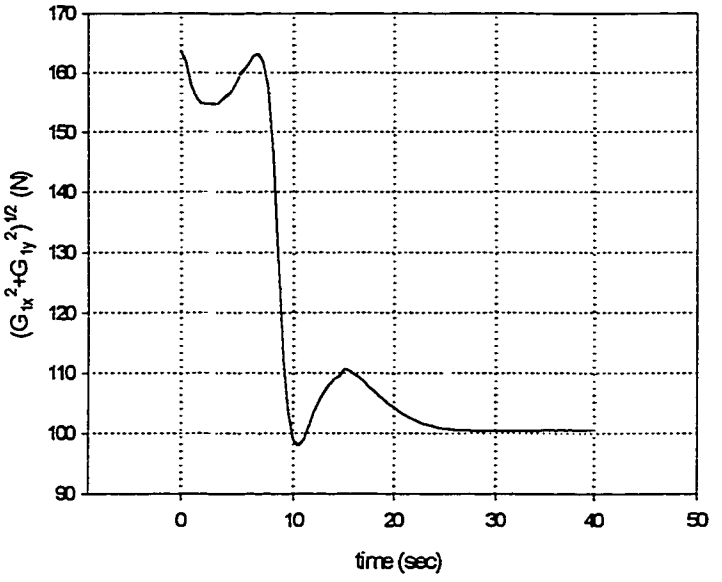

Figure 6.63 The time behavior of the traction force G_{xy1} of the front wheel(#1) of the vehicle for figure 6.54

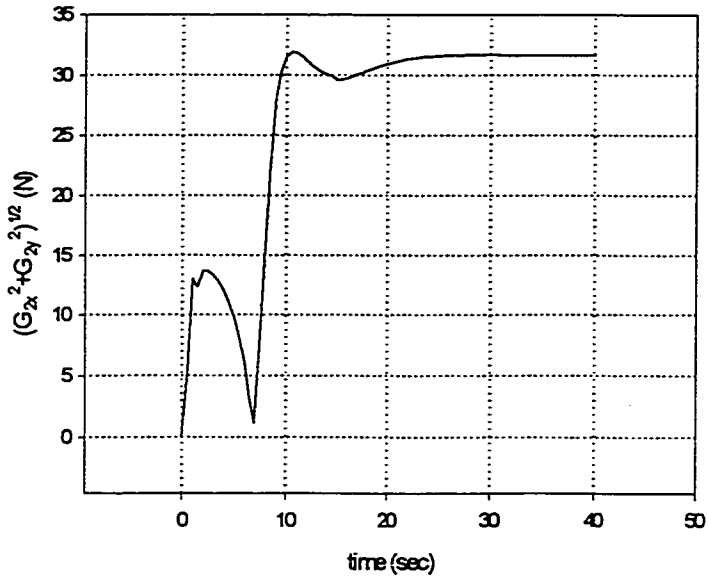

Figure 6.64 The time behavior of the G_{xy2} force of wheel #2 of the vehicle for figure 6.54

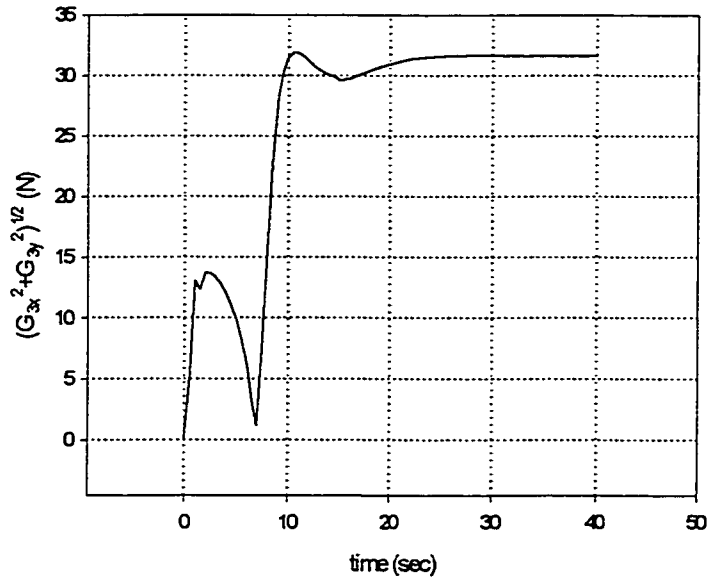

Figure 6.65 The time behavior of the G_{xy3} force of wheel #3 of the vehicle for figure 6.54

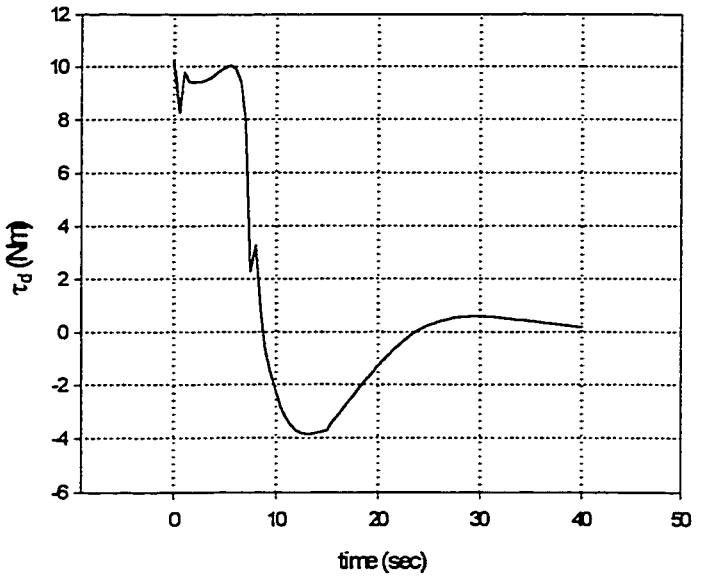

Figure 6.66 The time behavior of the driving torque of the vehicle for figure 6.54

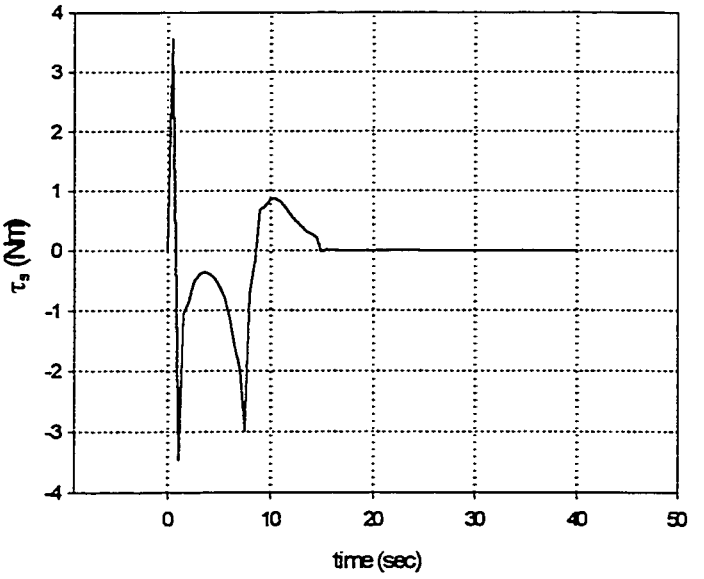

Figure 6.67 The time behavior of the steering torque of the vehicle for figure 6.54

6.2 Experimental Results

An experimental study was performed with the autonomous vehicle shown in Fig. 5_1, is equipped with two direct drive motors on board (System 7 User Guide, 1992). An optical position encoder was used to measure the rotational (and inferred linear) displacement of the driving wheel. A linear accelerometer was mounted on the steering mechanism near the driving wheel to measure the longitudinal acceleration of the vehicle. A counter weight was extended from the rear of the vehicle to lower the drive traction and induce wheel slippage (Loose paper was also placed on the floor to increase the probability of wheel slippage). The total mass of the vehicle assembly was 11 kg, and the maximum torque available at the driving wheel was 2 Nm.

The linear displacement was closed-loop controlled by a PD controller using feedback signal from the incremental encoder attached at the driving motor. The vehicle was commanded to drive in a straight line to a position 2m from the starting point. The bandwidth of the vehicle system was determined, from experiment, to be $f_b \approx 0.35$ Hz. The signals from the encoder and the accelerometer were each sampled at a rate of $f_s = 100$ Hz, simultaneously. The signal from the accelerometer was used to observe the wheel slippage. The resulting discrete data streams, referred to simply as the encoder and INS measurement signals, were then used in the verification of the slippage of the wheels and the development and testing of the data fusion technique. The detailed analysis of the sensor fusion can be found in the David Green's M.Eng. thesis (Green, D., 1993). Figures 6.14–6.16 illustrate results from a typical test run, where signals other than the encoder position and INS acceleration were obtained through derivation and integration.

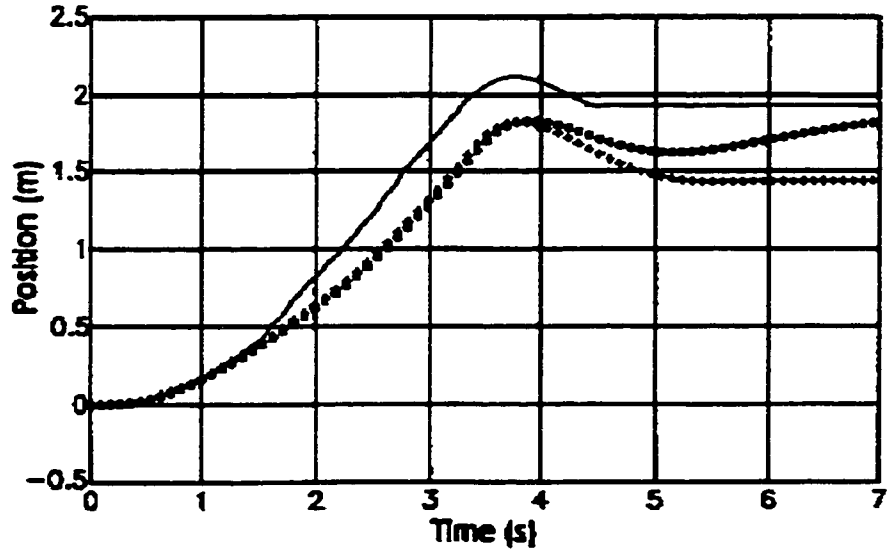

Figure 6.68 Encoder(-), INS(o) and fused(+) position signals

In Figure 6.68, it can be seen that, according to the encoder signal, the vehicle overshoots and reverses to settle at a position just short of the 2m set-point. (The steady-state error is due to internal mechanical friction). The double integrated accelerometer signal denoted as INS signal indicates that the vehicle position increases more slowly, overshooting at a somewhat lower position, and then continuing to increase without apparent bound. These differences are explained with reference to the velocity responses.

Figure 6.69 shows the velocity, derived from the encoder signal, and from integration of accelerometer signal. The encoder derived signal can be seen to increase and then oscillate above the INS signal, in the regions of about t = 1.2(sec) to t = 3.4(sec) and 4.3 (sec) to 5.4 (sec). This phenomenon was caused by slip-induced oscillations in the feedback-control system. The INS signal, although not subject to the effects of wheel slip, suffered from the problem of integration error. After about t = 5.4(sec), the vehicle was observed to have come to a complete stop, while the INS velocity signal indicates that the vehicle continued to move forward at a significant speed.

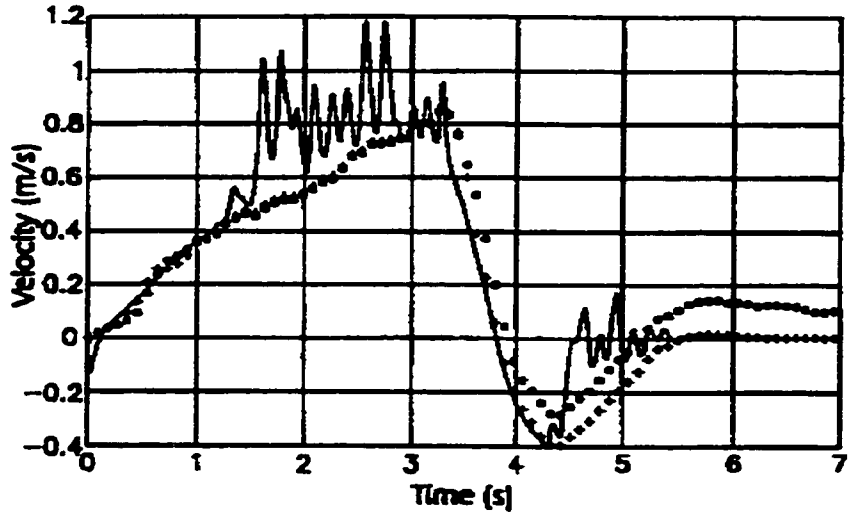

Figure 6.69 Encoder(-), INS(o) and fused(+) velocity signals

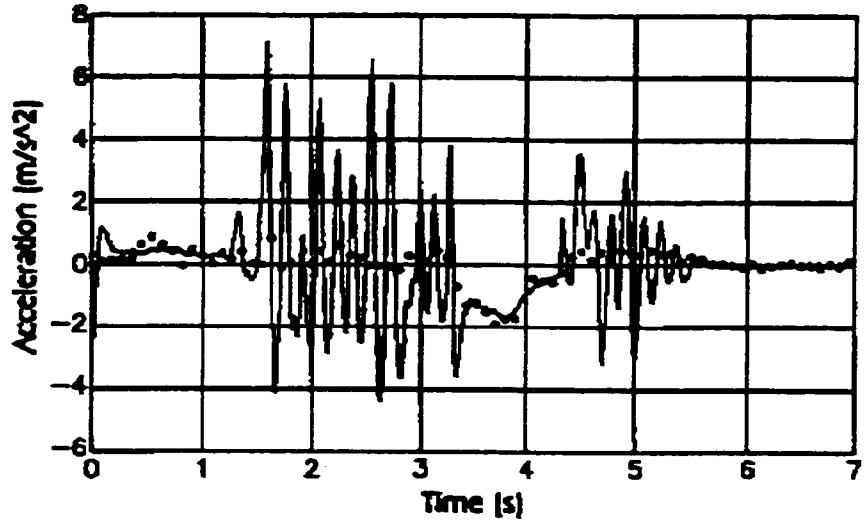

Figure 6.70 Encoder(-) and INS(o) acceleration signals

Figure 6.70 shows the accelerations, derived from encoder signal and measured from accelerometer signal. Neither the encoder nor the INS signals suffer from an accumulating (integration) error, so it is, at this level, the wheel slippage can be detected reliably. It is easily seen from the Figure 6.16 that there is a considerable difference between the encoder derived signal and

the accelerometer signal during the periods of t = 1.2(sec) to t = 3.4(sec) and t = 4.3(sec) to t = 5.5(sec), where the large changes in the encoder signal are assumed to indicate the presence of wheel slippage. In other areas, the acceleration data from the encoder and the accelerometer matches very well which indicates no driving wheel slippage during that period. The position data (Figure 6.68), calculated from the signal from the accelerometer accumulate, however, noise since signal is twice integrated. Because of this noise accumulation, we can not estimate position only from the accelerometer signal. Therefore, as far as we do not integrate the signal from the accelerometer, it gives us very good signals.

In summary, when no driving wheel slippage is observed, the encoder-based estimates appear to be valid. But when significant slip occurs, the encoder tends to overestimates the change in position, which also yields an erroneous velocity estimation. On the other hand, although the INS based estimates suffer from an increasing error in integration caused by noise, the INS system is itself free from the effects of wheel slippage. The complementary nature of the observed characteristics suggests that fusion of the encoder and INS signals will result in an overall improvement in the estimates of position and velocity.

These experimental results verify the assumption of this work that the fusion of inertial and kinematic navigation system is possible and beneficial for controlling autonomous vehicles during non-slippage as well as during slippage conditions.

VII. CONCLUSIONS AND RECOMMENDATIONS

7.1 Conclusions

A. Analytical and simulation studies permit to conclude that the autonomy of a vehicle moving on uneven and inclined surfaces can be achieved by the proposed dynamic based control approach which uses interactively a Model Predictive Control (MPC) combined with the Input-Output Linearization Control for avoiding Input-Output Linearization smoothness condition violations.

B. The autonomous motion control can be achieved by a multi-loop controller consisting of:

- a linear proportional controller for position errors in curvilinear coordinates;
- a Model Predictive Controller(MPC) for verifying smoothness conditions i.e., that in

the immediate future, wheel-ground contact loss and tip-over will not occur;

- an Input-Output Linearization (IOL) scheme to facilitate autonomous vehicle curvilinear motion control.

Besides the three loops, the proposed control system contains two updating procedures:

- in case of predicted violation of the smoothness conditions, iterative modification of the proportional gain for curvilinear errors is applied until the violation no longer exists;
- in case of significant sideway position and orientation errors, the path is updated to fit current and destination postures.

C. Complete three- dimensional kinematic and dynamic models as well as path planning, path following, and path updating schemes developed in the thesis were designed for real time control for autonomous motion of a non-holonomic vehicle on uneven surfaces.

D. Computer simulation studies verify that vehicle motion control is successful in avoiding slippage on a horizontal surface and loss of wheel-ground contact on inclined plane motion.

E. Simulation results permit the improvement of the structural design of the vehicle and the development and tuning the controller by testing the vehicle for various conditions of the road and in particular for various slopes.

F. The simulation model is useful for developing future autonomous mobile vehicles and for off-road tele-operated vehicles design.

7.2 Contributions

The major contributions of this research can be summarized as follows:

- A complete 3-D dynamic model for a three wheeled vehicle with front wheel steering and driving which can be computed by a PC in real-time
- A multi-loop control system which satisfies the requirements of autonomous motion of a non-holonomic vehicle on uneven surfaces.
- New solution with full linearization using IOL approach combined with MPC for observing, in real time, the smoothness conditions. In the literature search this solution was not found in publications.
- A form of the dynamic model of the autonomous vehicle which is solvable in real time by reducing to two differential equations those solved in the closed loop part of the controller and separating the rest of the differential equations to be solved only when needed, off loop, for contact forces verification. This analytical reduction of dynamic model contributes to reduce significantly the computing time such that it makes the model based motion controller of the vehicle executable in real time.
- Simulation study proving that the performance of the proposed Model Predictive Control (MPC) approach combined with the Input-Output Linearization (IOL) control are successful in avoiding the loss of contact of the vehicle in inclined plane

motion by modifying the input commands such that the geometric path planning result is conserved and the smoothness condition for exact linearization is not violated.

7.3 Recommendations for Further Studies

Stability of the proposed proportional error gain updating as well as path updating schemes require further theoretical study. An experimental study is also needed for evaluating the domain of applicability for various levels of slippery and uneven-inclined terrains. An experimental study of the proposed control system would be revealing and beneficial for the validity of simulation results regarding the ability of avoiding loss of wheel-ground contact and vehicle tip-over.

REFERENCES

Adam, A., Rivlin, E., and Rotstein, H. (1999), " Fusion of Fixation and Odometry for Vehicle Navigation," IEEE Transactions on Systems, Man, and Cybernetics, Vol. 29, No. 6, Nov. 1999, pp. 593-603

Aguilar, L.E., et al. (1997), "Robust Path Following Control for Wheeled Robot via Sliding Mode Techniques," Proceedings of 1997 IEEE/RSJ International Conference of Intelligent Robotic Systems IROS'97, Sept. 1997, pp. 1389-1395

Alexander, J.C. and Maddocks, J.H.(1990), "On the Kinematics of Wheeled Mobile Robots," International Journal of Robotics Research, Vol. 8, No. 5, Oct. 1990

Allgöwer, et al. (1999), " Nonlinear Predictive Control and Moving Horizon Estination-An Introductory Overview," Advances in Control: Highlights of ECC'99, P.M. Frank, Ed., London: Springer, 1999, pp. 391-449

Anand, D. K. and Cuniff, P.F. (1984), "Engineering Mechanics, Dynamics.", Allyn and Bacon, 1984

Arkin, R.C. (1989), "Motor Schema-Based Mobile Robot Navigation," The International Journal of Robotics Research, Aug. 1989, pp 92-112

Balaguer, C., Gimenez, A., Pastor, J.M., Padron, V.M., and Abderrahim, M. (2000), " A Climibing Autonomous Robot for inspection Applications in 3D Complex Environments," Robotica, Vol. 18, Part 3, May/June 2000, pp. 287-297

Balaram, J.(2000), " Kinematic State Estimation for a Mars Rover," Robotica, Vol. 18, Part 3, May/June 2000, pp. 251-262

Barraquand, J. and Latombe, J.C. (1990), "Controllability of Mobile Robots with Kinematic Constraints", Technical Roport No. STANCS-90-1317, Stanford University, June, 1990

Bloch, A. M. and McClamroch N. H. (1989), "Control of a Mechanical System with Classical Nonholonomic Constraints," Proceedings of the 28th Conference on Decision and Control Tampa, Florida, December, 1989, pp. 201-205.

Bloch, A. M., McClamroch N. H., and Reyhanoglu M. (1990), "Controllability and Stabilizability Properties of a Nonholonomic Control System," Proceedings of the 29th Conference on Decision and Control Honolulu, Hawaii, December, 1990, pp. 1312-1314.

Bloch, A., Reyhanoglu, M., and McClamroch, N.H. (1992), "Control and Stabilization of nonholonomic dynamic systems," IEEE Transactions on Automatic Control, Vol. 37, No. 11, 1992, pp. 1746-1757

Borenstein, J. and Koren, Y. (1989), "Real-time Obstacle Avoidance for Fast Mobile Robots," IEEE Trans. on System and Cybermation, Vol. 19, No. 5, 1989, pp 1179-1187

Borenstein, J. and Koren, Y. (1990), "Real-time Obstacle Avoidance for Fast Mobile Robots in Cluttered Environments," Proc. IEEE International Conference on Robotics and Automation, Vol. 1, Cincinnati, Ohio, May 13-18, 1990, pp 572-577

Brockett, R.W. (1983), " Asymptotic Stability and Feedback Stabilization," Differential Geometric Control Theory, Editors: Brockett, R.W., Millman, R.S., and Sussmaan, H.J., Birkhauser, 1983

Brooks, R.A. (1986), "A Robust Layered Control System for A Mobile Robot," IEEE Journal on Robotics and Automation, Vol. RA-2, No.1, 1986, pp 14-23

Camacho, E.F. and Bordons, C. (1995), " Model Predictive Control in the Process Industry," Springer, 1995

Campion, G. et al (1988), "External Linearization Control for a MobileRobot," IFAC, Syroco, 1988

Campion, G. et al (1990), "Controllability and State Feedback Stabilization of Non-holonomic Mechanical Systems," International Workshop in Adaptive and nonlinear Control Issues in Robotics, Nov 21-23, 1990, Granoble, France, pp 106-124

Campion, G., d'Andrea-Novel, B., and Bastin, G.(1991), "Controllability and state feedback stabilizability of nonholonomic mechanical systems," Advanced Robot Control, C. Canudas de Wit, editor, LNCIS 162, Springer, 1991, pp 106-124

Canudas de Wit, C., and Roskam, R. (1991), "Path following of 2-DOF Mobile Robot under Path and Input Torque Constraints," Proc. 1991 IEEE Conference on Robotics and Automation, Vol. 2, Sacramento, California, April 9-11, 1991, pp 1142-1147

Canudas de Wit, C. and Sordalen, 0.J. (1992), "Exponential Stabilization of Mobile Robots with Nonholonomic Constraints," IEEE Trans. On Automatic Control, Vol. 37, No. 11, Nov. 1992, pp 1791-1797

Carlisle, B. (1983), "An Omni-directional Mobile Robot," Development in Robotics, IFS, 1983, pp 79-87

Chacal, J.A. and Sira-Ramirez, H. (1994), "On the Sliding Mode Control of Wheeled Mobile Robots ," Proceedings of IEEE International Conference on Systems, Manufacturing and Cybernetics, Sept. 1994, pp. 1938-1943

Clark, M.R., Anderson, G.T., and Skinner, R.D. (2000), " Coupled Oscillator Control of Autonomous Mobile Robots," Autonomous Robots, Vol. 9, No. 2, Sept. 2000, pp. 189-198

Clarke, D. W., et al (1975), "A self-tuning controller," Proc. Inst. Elect. Eng., Vol. 122, 1975, p. 929

Clarke, D. W., et al (1987), "general Predictive Control," Automatica, pt. I and II, Vol. 23, No. 3, 1987, pp. 137-160

Clarke, D.W., Mohtadi, C., Tuffs, P.S. (1987), " Generalized predictive control," Automatica. 23, 1987, pp. 137-160

Clake, D.W. (1988), "Application of Generalized Predictive Control to Industrial Processes," IEEE Control Systems Magazine, 1988, pp. 49-55

Clarke, D.W., Mohtadi, C. (1989), "Properties of Generalized predictive control," Automatica. 25, No. 6, 1989, pp. 859-875

Clarke, D. (1994), " Advances in Model-Based Predictive Control," Oxford University Press, 1994

Colbaugh, R., Barany, E., and Trabatti, M. (1999), " Control of Nonholonomic Mechanical Systems using Reduction and Adaptation," Robotica, Vol. 17, Part 3, May/June 2000, pp. 249-260

Colbaugh, R., Trabatti, M., and Glass, K. (1999), " Redundant Nonholonomic Mechanical Systems: Characterization and Control," Robotica, Vol. 17, Part 2, Mar./Apr. 2000, pp. 203-217

Cox, I. J, Wilfong, G. T. (1990), "Autonomous Robot Vehicles," Springer-Verlag., 1990

Cozman, F., Krotkov, E., and Guestrin, C. (2000), " Outdoor Visual Position Estimation for Planetary Rovers," Autonomous Robots, Vol. 9, No. 2, Sept. 2000, pp. 135-150

Crowley. J.L. (1989), "Asynchronous Control of Orientation and Displacement in Robot Vehicle," Proc. IEEE International Conference on Robotics and Automation. Vol. 3. Scottsdale. Arizona, May 14-19, 1989, pp 1277-1282

Cutler, C.R. and Ramaker, B.L. (1980), " Dynamic matrix control - A computer control algorithm," Proc. JACC, San Francisco, U.S.A., 1980

Cybermation (1988), "K2A Mobile Platform", Commercial offer, 5457 JAE Valley Road, Roanoke, Virginia 24014, 1988

Dahl, 0., and Nielson, L. (1989), " Torque Limited Path Following by On-Line Trajectory Time - Scaling " , Proc. IEEE International Conference on Robotics and Automation, Vol. 3, Scottsdale, Arizona, May 14-19, 1989, pp. 1122-1128

Dahl, 0., and Nielson, L. (1990), "Stability Analysis of an On-Line Algorithm for Torque Limited Path Following", Proc. IEEE International Conference on Robotics and Automation, Vol. 2, Cincinnati, Ohio, May 13-18, 1990, pp 1216-1222.

d'Andrea-Novel, B., et al (1992), " Dynamic Feedback Linearization of Nonholonomic Wheeled Mobile Robots", Proc. IEEE International Conference on Robotics and Automation, Vol. 3, Nice, France, May 1992, pp 2527-2532.

Daniel, D.J. et al (1985), "Kinematics and Open-loop Control of An Illonator-based Mobile Platform," Proc. IEEE International Conference on Robotics and Automation, St.Louis, MO., Mar 1985, pp 346-353

De Keyser, R. and Van Cauwenberghe, A. (1985), "Extended Prediction self-adaptive control," Proc. 7th IFAC Symposium on Identification and System Parameter Estimation, York, U.K., 1985, pp. 1255-1260

Demircioglu, H. and Karasu, E. (2000), " Generalized Predictive Control," IEEE Control Systems Magazine, Vol. 20, No. 3, Oct. 2000, pp. 36-47

Deng, Z., and Brady, M. (1993), "Dynamic Tracking of a Wheeled Mobile Robot", Proc. of the IEEE\RJS International Conf. on Intelligent Robots and Systems, Yokohama, Japan, July 26-30, 1993, pp 1295-1298.

DeSouza, F.A. and Greg, V.K. (1984), "Advanced Dynamics: Modeling and Analysis," Prentice Hall, 1984

Denning Mobile Robots, Inc. (1991), "Securing the Future", Commercial offer Manual, 21 Cunnings Park, Woburm, MA. 01801, 1991

Divelbiss, A. W., and Wen, J. (1992), " A Global Approach to Nonholonomic Motion Planning", The 31th IEEE Conference on Decision and Control, Dec. 1992, pp. 1597-1602

Djath, K., Siadat, A., Dufaut, M., and Wolf, D. (1999), " Navigation of a Mobile Robot by Locally Optimal Trajectories," Robotica, Vol. 17, Part 5, Sept./Oct. 2000, pp. 553-563

Durfee, E.H., Kenny, P.G., and Kluge, K.C. (1998), " Integrated Premission Planning and Execution for Unmanned Ground Vehicles," Autonomous Robots, Vol. 5, Nov. 1998, pp. 97-110

Ellis, J.R. (1969), "Vehicle Dynamics," Business Books, London, 1969

Feng, D. et al (1989), "The Servo-Control System for An Omnidirectional Mobile Robot," Proc. IEEE International Conference on Robotics and Automation, Vol. 3, Scottsdale, Arizona, May 14-19, 1989, pp 1566-1571

Fukao, T., Nakagawa, H., and Adachi, N. (2000), " Adaptive Tracking Control of a Nonholonomic Mobile Robot," IEEE Transactions on Robotics and Automation, Vol. 16, No. 5, Oct. 2000, pp. 609-615

Garcia-Alegre, M. C. and Recio, F. (1997), " Basic Visual and Motor Agents for Increasingly Complex Behavior Generation on a Mobile Robot," Autonomous Robots, Vol. 5, 1998, pp. 19-28

Ge, S.S. and Cui, Y.J. (2000), " New Potential Functions for Mobile Robot Path Planning," IEEE Transactions on Robotics and Automation, Vol. 16, No. 5, Oct. 2000, pp. 615-620

Giralt, G. et al (1984), "An Integrated Navigation and Motion Control System for Autonomous Multisensory Mobile Robots," The First International Symposium on Robotics Research, MIT Press, 1984, pp 191-214

Gomez-Ortega, J. and Camacho, E.F. (1994), " Neural Network MBPC for Mobile Robot Path Tracking," Robotics & computer-Integrated Manufacturing, Vol. 11, 1994, pp. 271-278

Gomez-Ortega, J. and Camacho,. E.F. (1996), " Mobile Robot Navigation in a Partially Structured Static Environment using Neural Predictive Control," Control Engineering Practice, Vol. 4, 1996, pp.1669-1678

Gomez-Ortega, J. et al (1997), " Fuzzy Predictive controller for Mobile Robot Path-Tracking," Proc. SICICA'97, Annecy (France), July 1997, pp. 283-288

Graettinger, T.J. and Krogh. B.H. (1989), "Evaluation and Time Scaling of Trajectories for Wheeled Mobile Robots", ASME Journal of Dynamic Systems Measurement and Control. Vol. 111, June 1989. pp 222-231

Green, D.N. (1993), " Guidance and Control of an Autonomous Planetary Rover," M.Eng. Thesis, Carleton University, Nov. 1993

Gurvits, L. (1992), "Averaging Approach to Nonholonomic Motion Planning", Proc. IEEE International Conference on Robotics and Automation, Vol. 3, Nice, France, May 1992, pp. 2541-2546

Hamel, T. and Meizel, D. (1996), " Robust Control Laws for Wheeled Mobile Robots," International Journal of System Science, Vol. 27, No. 8, 1996, pp. 695-704

Hatwal, H. and Mikulcik, E.C. (1986), "Some Inverse Solutions to an Automobile Path-Tracking Problem with Input Control of Steering and Brakes," Vehicle System Dynamics, Vol. 15, 1986, pp 61-71

Haug, E.J. (1992), " Intermediate Dynamics," Prentice Hall, 1992

Hemami, A. et al (1990), "A New Control Strategy for Tracking in Mobile Robots and AGV's," Proc. IEEE International Conference on Robotics and Automation, Vol. 2, Cincinnati, Ohio, May 13-18, 1990, pp 1122-1127

Hemami, A. et al (1992), "Synthesis of an Optimal Control Law for Path Tracking in Mobile Robots," Automatica, Vol. 28, No. 2, 1992, pp 383-387.

Holland, J.M. (1989), "A Mobile Platform for Industrial Research", Robotics Research Conference, Scottsdale, Arizona, SME Technical Paper, No. MS80–786, 1989, p. 13

Hoppenot, P., Colle, E., and Barat, C. (2000), " Off-line Localization of a Mobile Robot using Ultrasonic Measurements," Robotica, Vol. 18, Part 3, May/June 2000, pp. 315-323

Houston, R.L. (1990), " Multibody Dynamics," Butterworths-Heinemann, 1990, Boston

Isidori, A. (1989), "Nonlinear Control Systems," 2nd edition, Springer, 1989

Jeng, J. and Lee, T., " A Neural Gain Scheduling Network Controller for Nonholonomic Systems," IEEE Transactions on Systems, Man, and Cybernetics, Vol. 29, No. 6, Nov. 1999, pp. 654-661

Jiang, Z.P. and Pomet, J.B. (1994), " Combining Backstepping and Time-varying Techniques for a new set of Adaptive Controllers," Proceedings of IEEE International Conference of Decision & Control, Dec. 1994, pp. 2207-2212

Kagami, Y., Emura, T., and Hiyama, M. (2000), " Vision-based Playback Method of Wheeled Mobile Robots," Robotica, Vol. 18, Part 3, May/June 2000, pp. 281-286

Kanayama, Y., and Miyake, N. (1986), " Trajectory Generation for Mobile Robots," Journal of Robotics Research, Vol. 3, 1986, pp. 333-340

Kanayama, Y., et al (1988), " A Locomotion Control Method for Autonomous Vehicles," Proc. 1988 IEEE International Conference on Robotics and Automation, Vol. 2, 1988, pp. 1315-1317

Kanayama, Y., and Hartman, B.I. (1989), "Smooth Local Path Planning for Autonomous Vehicles",Proc. 1989 IEEE International Conference on Robotics and Automation, Vol. 2, 1989, pp 1265-1270.

Kanayama, Y. et al (1990), "A Stable Tracking Control Method for An Autonomous Mobile Robot," Proc. 1990 IEEE International Conference on Robotics and Automation, Vol. 1, Cincinnati, Ohio, May 13-18, 1990, pp 384-389

Kanayama, Y. and Hartman, B. I. (1997), " Smooth Local-Path Planning for Autonomous Vehicles," International Journal of Robotics Research, Vol. 16, No. 3, June 1997, pp. 263-284

Kang, D. S., Anderson, J. M., and DeBitetto, P. A.(2000), " Draper Unmanned Vehicle Systems," Robotica, Vol. 18, Part 3, May/June 2000, pp. 263-272

Kapitanovsky, A., Goldenberg, A.A., and Mills, J.K. (1993), "Dynamic control and motion planning technique for a class of nonlinear systems with drift," Systems & Control Letters, Vol. 21, 1993, pp. 363-369

Katende, E. and Jutan, A. (1993), "A New constrained Self-tuning PID Controller," Canadian Journal of Chemical Engineering, Vol. 71, 1993, p. 625

Katende, E. and Jutan, A. (2000), "Nonlinear Predictive Control of Complex Processes," Ind. Eng. Chem., Vol. 35, 1996, pp 3539-3546

Katende, E. and Jutan, A. (2000), "Experimental Evaluation of Predictive Temperature Control for a Batch Reactor System," IEEE Transactions on Control Systems Technology, Vol. 8, No. 1, Jan. 2000, pp 2-13

Kelly, A. and Stentz, A. (1998), " Rough Terrain Autonomous Mobility - Part 1: A Theoretical Analysis of Requirements," Autonomous Robots, Vol. 5, Nov. 1998, pp. 129-161

Khatib, O. (1986), "Real-time Obstacle Avoidance for Manipulators and Mobile Robots," The International Journal of Robotics Research, Vol. 5, No. 1, Spring 1986, pp 396-404

Kinnaert, M. (1989), "Adaptive generalized predictive controller for MIMO systems," Int. J. Control, Vol. 50, No. 1, 1989, pp. 161-172

Krogh, B.H. (1984), "A Generalized Potential Field Approach to Obstacle Avoidance Control," Proc. SME Conference Robotics Research: The next five years and Beyond, Bethlehem, PA., Aug. 1984, pp 1-15

Krogh, B.H. and Thorpe, C.E. (1986), "Integrated Path Planning and Dynamic Steering Control for Autonomous Vehicles," Proc. 19th IEEE International Conference on Robotics and Automation, San Francisco, CA., Apr 7-10 1986, pp 1664-1669

Kwon, W.H. (1994), " Advances in Predictive Control: Theory and Application," Proc. 1st Asian Control Conference, Tokyo, 1994

Lafferriere, G.A. (1991), "A general strategy for computing steering controls of systems without drift," Proc. of the 30th IEEE Conf. On Decision and Control, 1991, pp. 1115-1120

Lafferriere, G.A. and Sussmann, H. (1993), "A differential geometric approach to motion planning," Nonholonomic Motion Planning, Kluwer, 1993, pp. 235-270

Latombe, J.C. (1991), "Robot Motion Planning," Kluwer Academic Publishers, 1991

Lee, D. and Recce, M. (1997), " Quantitative Evaluation of the Exploration Strategies of a Mobile Robot," International Journal of Robotics Research, Vol. 16, No. 4, Aug. 1997, pp. 413-447

Lee, J.H. and Cooley, B. (1997), " Recent Advances in Model Predictive Control and Other related areas," Proc. Chemical Process Control - V, J.C. Kantor, C.E. Garcia, and B. Carnahan, Eds., CACHE, AIChE, 1997, pp. 201-216

Li, Z., and Canny, J. F. (1993), " Nonholonomic Motion Planning," Kluwer Academic Publishers, 1993

Lim, D. and Seraji, H. (1997), " Configuration Control of a Mobile Dexterous Robot: Real-time Implementation and Experimentation," International Journal of Robotics Research, Vol. 16, No. 5, Oct. 1997, pp. 601-618

Linkers, D.A. and Mahfonf, M. (1994), "Generalized Predictive Control in Clinical Anaesthesia," in Advances in Model-Based Predictive Control, Oxford University Press, 1994

Lonmo, V. (1996), "Dynamics based control of a mobile robot with non-holonomic constraints," M.A.Sc. Thesis, University of Ottawa, 1996

Lopez-Sanchez, M., Esteva, F., Lopez de Mantaras, R., Sierra, C., and Amat, J. (1998), " Map Generation by Cooperative Low-Cost Robots in Structured Unknown Environments," Autonomous Robots, Vol. 5, Nov. 1998, pp. 53-61

Mahadevan, S., Theocharous, G., and Khaleeli, N. (1998), " Rapid Concept Learning for Mobile Robots," Autonomous Robots, Vol. 5, Nov. 1998, pp. 239-251

Mashke, B.M., and Van der Shaft, A.J. (1994), "A hamiltonian approach to stabilization of nonholonomic mechanical systems," Proc. Of the 33rd IEEE Conference on Decision and Control, 1994, pp 2950-2954

Mayne, D.Q. (1997), "Nonlinear Model Predictive Control: An assessment," Proc. Chemical Process Control - V, J.C. Kantor, C.E. Garcia, and B. Carnahan, Eds., CACHE, AIChE, 1997, pp. 217-231

McGee, R.B. et al (1979), "Adaptive Locomotion of a Multilegged Robot over Rough Terrain," IEEE Trans. Syst., Man., and Cyber., Vol. SMC9, 1979

McKerrow, P. J. (1991), "Introduction to Robotics," Addison-Wesley Publishers Ltd., 1991

Meng, Q., Liu, D., Zhang, M., and Sun, Y. (1999), " Wall-following by an Autonomously Guided Vehicle (AGV) using New Fuzzy-I (Integration) Controller," Robotica, Vol. 17, Part 1, Jan./Feb. 2000, pp. 79-86

Meng, Q., Sun, Y., and Cao, Z. (2000), " Adaptive Extended Kalman Filter (AEKF)-based Mobile Robot Localization using Sonar," Robotica, Vol. 18, Part 5, Sept/Oct. 2000, pp. 459-473

Miura, J. and Shirai, Y. (1997), " Vision and Motion Planning for a Mobile Robot under Uncertainty," International Journal of Robotics Research, Vol. 16, No. 6, Dec. 1997, pp. 806-825

Mukhedee , R. , and Anderson , D. P.(1993) , " Nonholonomic Motion Planning Using Stokes's Theorem", Proc. 1993 IEEE International Conference on Robotics and Automation, Vol. 3, 1993, pp. 802-809

Muir, P.F. and Newman, C.P. (1987), "Kinematic Modeling for Feedback Control of An Omnidirectional Wheeled Mobile Robot," Proc. 1987 IEEE International Conference on Robotics and Automation, Vol. 3, Raleigh, North Carolina, Mar 31- Apr 3, 1987, pp 1772-1778

Murphy, R. R. (1999), " Case Studies of Applying Gibson's Ecological Approach to Mobile Robots," IEEE Transactions on Systems, Man, and Cybernetics, Vol. 29, No. 1, Jan. 1999, pp. 105-111

Murphy, R. R. and Hershberger, D. (1999), " Handling Sensing Failures in Autonomous Mobile Robots," International Journal of Robotics Research, Vol. 18, No. 4, Apr. 1999, pp. 382-400

Murray, R.M., and Sastry, S.S. (1990), "Steering Nonholonomic Systems Using Sinusoids", The 29th IEEE Conference on Decision and Control, Dec. 1990, pp. 2097-2100

Murray, R.M., and Sastry, S.S. (1991), "Steering Nonholonomic Systems in Chained Form", The 30th IEEE Conference on Decision and Control, Dec. 1991, pp. 1121-1126

Murray, R.M., Li, Z. and Sastry, S.S. (1994), "A Mathematical Introduction to Robotic Manipulation," CRC Press, 1994

Nakamura, Y. and Mukherjee, R. (1990), "Nonlinear Control for the Nonholonomic Motion of Space Robot Systems," International Workshop in Adaptive and Nonlinear Control: Issues in Robotics, Nov 21-23, 1990, Granoble, France

Necsulescu, D.S. and Kim, B. (1992), "Free Motion, Collision Avoidance and Contact Motion Control for Mobile Robots", 7th IFAC Symposium on Information Control Problems in Manufacturing Technology, Toronto, Ont., May 25-28, 1992, pp 331-336

Necsulescu, D.S., Kim, B., and Kalaycioglu, S. (1993), "Dynamics Control of an Autonomous Wheeled Ground Vehicle," Transactions of CSME, Vol.17, No.4B, pp735-758

Necsulescu, D.S., et al (1993), " Fusion of Inertial and Kinematic Navigation Systems for Autonomous Vehicles," Proc. IEE-IEEE Vehicle Navigation & Information Systems Conference VNIS'93, Ottawa, Canada Oct. 12-14, 1993, pp. 462-465

Necsulescu, D.S., and Kim, B. (1998),"Autonomous mobile vehicles for motion on uneven and inclined surfaces," ELECTROMOTION Vol.5, pp126-130

Nelson, W.L. and Cox, I.J. (1988), "Local Path Control for An Autonomous Vehicle," Proc. of the 1988 IEEE International Conference on Robotics and Automation, Vol. 3, Philadelphia, Penn., 1988, pp 1504-1510

Nelson, W.L. (1989), "Continuous-Curvature Paths for Autonomous Vehicles" , Proc. 1989 IEEE International Conference on Robotics and Automation, Vol. 2, 1989, pp. 1260-1264

Nijmeijer, H., and Van der Schaft, A.J. (1990), "Nonlinear Dynamical Control Systems," Springer-Verlag, 1990.

Nilsson, N.J. (1969), "A Mobile Automation: An Application of Artificial Intelligence Techniques," Proc. of the lst IJCAI, Washington, D.C., May, 1969

Oriolo, G. and Makamura, Y. (1993), "Control of mechanical systems with second-order nonholonomic constraints: Underactuated manipulators," Proc. Of the 30th IEEE Conf. On Decision and Control, 1993, pp 306-308

Piche, S., Sayyar-Rodsari, B., Johnson, D., and Gerules, M. (2000), " Nonlinear Model Predictive Control using Neural Networks," IEEE Control Systems Magazine, June 2000, pp. 53-62

Prasad, D. and Burns, A. (2000), " A Value-based Scheduling Approach for Real-Time Autonomous Vehicle Control," Robotica, Vol. 18, Part 3, May/June 2000, pp. 273-279

Qin, S.J. and Badgwell, T.A. (1997), " An overview of Industrial Model Predictive Control Technology," Proc. Chemical Process Control - V, J.C. Kantor, C.E. Garcia, and B. Carnahan, Eds., CACHE, AIChE, 1997, pp. 232-256

Rawlings, J.B. (2000), " Tutorial Overview of Model Predictive Control," IEEE Control Systems Magazine, June 2000, pp. 38-52

Richalet, J. et al (1978), " Model predictive heuristic control: applications to industrial processes," Automatica, Vol. 14, No. 5, 1978, pp. 413-428

Richalet, J. et al (1987), " Predictive Functional Control: Applications to fast and accurate robots," Proc. 10th IFAC World Congress, Munich, Germany, 1987

Richalet, J. (1993), " Industrial Applications of Model Based Predictive Control," Automatica, Vol. 29, No. 5, 1993, pp. 1251-1274

Robillard, M.J. (1983), " HERO 1: Advanced Programming and Interfacing," Howard W. Sams & Co., Inc., 1983

Rowe, N. C. (1997), " Obtaining Optimal Mobile-Robot Paths with Nonsmooth Anisotropic Cost Functions using Qualitative-State Reasoning," International Journal of Robotics Research, Vol. 16, No. 3, June 1997, pp. 375-399

Ryu, B. and Yang, H.S. (1999), " Integration of Reactive Behaviors and Enhanced Topological Map for Robust Mobile Robot Navigation," IEEE Transactions on Systems, Man, and Cybernetics, Vol. 29, No. 5, Sept. 1999, pp. 474-485

Sagues, C. and Guerrero, J.J. (1999), " Motion and Structure for Vision-based Navigation," Robotica, Vol. 17, Part 4, July/Aug. 2000, pp. 355-364

Saha, S. K. and Angeles, J. (1989), "Kinematics and Dynamics of a Three Wheeled AGV," Proc. 1989 IEEE International Conference on Robotics and Automation, Vol. 3, Scottsdale, Arizona, May 14-19, 1989, pp 1572-1577

Salichs, M.A. and Moreno, L. (2000), " Navigation of Mobile Robots: Open Question," Robotica, Vol. 18, Part 3, May/June 2000, pp. 227-234

Samson, C. (1990a), "Velocity and Torque Feedback Control of a Nonholonomic Cart," Proc. of the International Workshop on Nonlinear and Adaptive Control Issues in Robotics, Grenoble, France, Nov. 21-23, 1990, pp 125-151

Samson, C., and Ait-Abderrahim, K. (1990b), "Mobile Robot Control, Part 1: Feedback Control of a Nonholonomic Wheeled Cart in Cartesian Space", Internal Report, INRIA, France, June 8, 1990.

Samson. C. (1991), "Time-Varying Feedback Stabilization of A Nonholonomic Car-like Mobile Robot," The 30th IEEE Conference on Decision and Control, 1991, pp 1-24

Sarkar, N., Yun, X. and Kumar, V. (1993), "Dynamic path following: A new control algorithm for mobile robots," Proc. 32nd IEEE Conf. On Decision and Control, 1993, pp. 2670-2675

Sarkar, N. et al (1994), " Control of Mechanical Systems With Rolling Constraints Application to Dynamic Control of Mobile Robots", The Int. Journal of Robotics Research, Vol. 13, No. 1, Feb. 1994, pp 55-69.

Sasiadek, J.Z., et al (1993), " Dead Reckoning for Mobile Robots via Sensor Fusion," Proceedings on Advanced Technologies in Knowledge Based Systems and Robotics Workshop, Ottawa, Nov. 14-17, 1993

Sekiguchi, M. et al (1989), "Behavior Control for a Mobile Robot by Multi-Hierarchical Nueral Network," Proc. 1989 IEEE International Conference on Robotics and Automation, Vol. 3, Scottsdale, Arizona, May 14-19. 1989, pp 1578-1583

Shiller, Z. and Gwo, Y.R. (1991), "Dynamic Motion Planning of Autonomous Vehicles," IEEE Trans. on Robotics and Automation, Vol. 7, No. 2, April 1991, pp 241-249

Shilling, R., "Fundamentals of Robotics: Analysis and Control," Prentice Hall Inc., 1998

Shim, H.S., et al. (1995)," Variable Structure Control of Non-holonomic Wheeled Mobile Robots," Proceedings of IEEE International Conference of Robotics & Automation, May 1995, pp. 1694-1699

Shin, D.H. et al (1991), " A Partitioned Control Scheme for Mobile Robots Path Tracking", Proc. 1991 IEEE International Conference on Robotics and Automation, Vol. 1, Sacramento, California, April 9-11, 1991, pp 338-342.

Slotine, J.E., and Li., W. (1991), "Applied Nonlinear Control", Prentice Hall, 1991.

Soeterboek, R., Verbruggen, H. (1991), and Van den Bosch, P., "Predictive Control of a nonlinear processes," Proc. of the IFAC Symposium on Intelligent Tuning and Adaptive Control ITAC 91, Singapore, 1991

Soeterboek, R. (1992), " Predictive Control - A Unified Approach," Prentice Hall, 1992

Sordalen, 0.J. and Canudas de Wit, C. (1990), "Path Following and Stabilization of A Mobile Robot," International Workshop in Adaptive and Nonlinear Control : Issues in Robotics, Granoble, France, Nov 21-23, 1990, pp. 125-151

Su, C.Y. and Stepanenko, Y. (1994), " Robust Motion/force Control of Mechanical Systems with Classical Non-holonomic Constraints," IEEE Transactions of Automatic Control, Vol. 39, No. 3, Mar. 1994, pp. 609-614

Su, C.Y., Stepanenko, Y., and Goldenberg, A. A. (1999), " Reduced Order Model and Robust Control Architecture for Mechanical Systems with Non-holonomic Pfaffian Constraints," IEEE Transactions on Systems, Man, and Cybernetics, Vol. 29, No. 3, May 1999, pp. 307-313

Sussmann, H. (1991), " Local Controllability and Motion Planning for some Classes of Systems with Drift ", The 30th IEEE Conference on Decision and Control, Dec. 1991, pp. 1110-1114

Steer, B. (1989), "Trajectory Planning for Mobile Robot," The International Journal of Robotics Research, Vol. 8. No. 5, Oct. 1989. pp. 3-14

System 7 User Guide (1992), "Hybrid and Brushless Servo Motors and Encoders,," Section G, Dorset, England, 1992

Timoshenko, S. (1985), "Mechanics of Materials," 2nd Ed. PWS Engineering, 1985

Tsoularis, A. and Kambhampati, C. (1999), " Avoiding Moving Obstacles by Deviation from a Mobile Robot's Nominal Path," International Journal of Robotics Research, Vol. 18, No. 5, May 1999, pp. 454-465

Vainio, M., Appelqvist, P., and Halme, A. (2000), " Mobile Robot Society for Distributed Operations in Closed Aquatic Environment," Robotica, Vol. 18, Part 3, May/June 2000, pp. 235-250

Valavanis, K.P., Hebert, T., Kolluru, R., and Tsourveloudis, N. (2000), " Mobile Robot Navigation in 2-D Environments using an Electrostatic Potential Field," IEEE Transactions on Systems, Man, and Cybernetics, Vol. 30, No. 2, Mar. 2000, pp. 187-196

VanAntwerp, J.G., and Braatz, R.D. (2000), "Fast Model Predictive Control of Sheet and Film Processes," IEEE Transactions on Control Systems Technology, Vol. 8, No. 3, May 2000, pp 408-417

Walsh, G.C. et al (1994), "Stabilization of trajectories for systems with nonholonomic constraints," IEEE Trans. On Automatic Control, Vol. 39, No. 1, 1994, pp. 216-222

Ward, K. and Zelinsky, A. (2000), " Acquiring Mobile Robot Behaviors by Learning Trajectory Velocities," Autonomous Robots, Vol. 9, No. 2, Sept. 2000, pp. 113-133

Warren, C. W. (1989), "Global Path Planning Using Artificial Potential Fields," Proc. 1989 IEEE International Conference on Robotics and Automation, Vol. 1, Scottsdale, Arizona, May 14-19, 1989, pp. 316-321

Yang, J.M. and Kim, J.H. (1999), "Sliding Mode Motion Control of Nonholonomic Mobile Robots," IEEE Control Systems, Apr. 1999, pp. 15-23.

Ydstie, B.E. (1984), "Extended horizon adaptive control," Proc. 9th IFAC World Congress, Budapest, Hungary, 1984

Yuh, J. (1990), "Modeling and Control of Underwater Robotic Vehicle," IEEE Trans, on Systems, Manufacturing and Cybernetics, Vol. 20, No. 6, Nov/Dec., 1990, pp. 1475-1483

Yun, X., and Yamamoto, Y. (1993), "Internal Dynamics of a Wheeled Mobile Robot", Proc. of the IEEE\RJS International Conf. on Intelligent Robots and Systems, Yokohama, Japan, July 26-30, 1993, pp. 1288-1294

Zhang, Y.L., Velinsky, S.A., and Feng, X. (1997), " On the Tracking Control of Differentially Steered Wheeled Mobile Robots," Journal of Dynamic Systems, Measurement, and Control, Vol. 199, Sept. 1997, pp. 455-461

Appendix A

The derivations of equation of motion equation (4-17) with ω_1 and ω_δ and their derivatives, in terms of the other state variables and their derivatives and the inputs, τ_s and τ_d, based on the kinematics and dynamics of the system (Necsulescu, D.S., Kim, B., and Kalaycioglu, S., 1993), are presented in this appendix. The equations are linear in internal forces F_{FSAx1}, F_{FSAy1}, F_{FSAz1}, F_{SAx1}, F_{SAy1}, F_{SAz1}, F_{Fxi}, F_{Fyi}, F_{Fzi} (i=2,3), and internal moments M_{FSAx1}, M_{FSAy1}, M_{FSAz1}, M_{SAx1}, M_{SAy1}, M_{SAz1}, M_{xi}, M_{yi}, M_{zi} (i=2,3). These internal forces and moments are needed to be eliminated from the equations of motion (3-70) ~ (3-93) using the constraints (3-63) ~ (3-69) of the associated absolute accelerations A_{xi}, A_{yi}, A_{zi} (i=1,2,3).

$$\begin{aligned} &F_{SAx1}\cos\delta - F_{SAy1}\sin\delta = \\ &-m_1 A_{x1} + G_{x1}\cos\delta - G_{y1}\sin\delta - m_1 g\sin\beta\left[\cos(\theta+\delta)\cos\delta + \sin(\theta+\delta)\sin\delta\right] \end{aligned} \tag{A-1}$$

$$\begin{aligned} &F_{SAx1}\sin\delta + F_{SAy1}\cos\delta = \\ &-m_1 A_{y1} + G_{x1}\sin\delta + G_{y1}\cos\delta - m_1 g\sin\beta\left[\cos(\theta+\delta)\sin\delta - \sin(\theta+\delta)\cos\delta\right] \end{aligned} \tag{A-2}$$

$$F_{SAz1} = G_{z1} - m_1 g\cos\beta \tag{A-3}$$

$$M_{SAx1} = -I_{x1}\left(\omega_\theta + \omega_\delta\right)\omega_1 - G_{y1}r_{w1} \tag{A-4}$$

$$M_{SAy1} = \tau_d = I_{y1}\dot{\omega}_1 + G_{x1}r_{w1} \tag{A-5}$$

$$M_{SAz1} = J_1\left(\dot{\omega}_\delta + \dot{\omega}_\theta\right) \tag{A-6}$$

$$\begin{aligned} &F_{FSAx1}\cos\delta - F_{FSAy1}\sin\delta = \\ &-m_{SA}A_{x1} + F_{SAx1}\cos\delta - F_{SAy1}\sin\delta - m_{SA}g\sin\beta\left[\cos(\theta+\delta)\cos\delta + \sin(\theta+\delta)\sin\delta\right] \end{aligned} \tag{A-7}$$

$$\begin{aligned} &F_{FSAx1}\sin\delta + F_{FSAy1}\cos\delta = \\ &-m_{SA}A_{y1} + F_{SAx1}\sin\delta + F_{SAy1}\cos\delta - m_{SA}g\sin\beta\left[\cos(\theta+\delta)\sin\delta - \sin(\theta+\delta)\cos\delta\right] \end{aligned} \tag{A-8}$$

$$F_{FSAz1} = F_{SAz1} - m_{SA}g\cos\beta \tag{A-9}$$

$$M_{FSAx1} = M_{SAx1} - I_{SAx1}\left(\omega_\theta + \omega_\delta\right)\omega_1 - S_b F_{FSAy1} - S_a F_{SAy1} \tag{A-10}$$

$$M_{FSAy1} = M_{SAy1} + I_{SAy1}\dot{\omega}_1 + S_b F_{FSAx1} + S_a F_{SAx1} \tag{A-11}$$

$$M_{FSAz1} = \tau_s = J_{SA}\left(\dot{\omega}_\delta + \dot{\omega}_\theta\right) + M_{SAz1} \tag{A-12}$$

$$F_{Fx2} = -m_2 A_{x2} + G_{x2} - m_2 g \sin\beta \cos\theta \tag{A-13}$$

$$F_{Fy2} = -m_2 A_{y2} + G_{y2} - m_2 g \sin\beta \sin\theta \tag{A-14}$$

$$F_{Fz2} = G_{z2} - m_2 g \cos\beta \tag{A-15}$$

$$M_{x2} = -I_{x2}\left(\omega_\theta \omega_2\right) - G_{y2} r_{w2} \tag{A-16}$$

$$M_{y2} = 0 = I_{y2}\dot{\omega}_2 + G_{x2} r_{w2} \tag{A-17}$$

$$M_{z2} = J_2 \dot{\omega}_\theta \tag{A-18}$$

$$F_{Fx3} = -m_3 A_{x3} + G_{x3} - m_3 g \sin\beta \cos\theta \tag{A-19}$$

$$F_{Fy3} = -m_3 A_{y3} + G_{y3} - m_3 g \sin\beta \sin\theta \tag{A-20}$$

$$F_{Fz3} = G_{z3} - m_3 g \cos\beta \tag{A-21}$$

$$M_{x3} = -I_{x3}\left(\omega_\theta \omega_3\right) - G_{y3} r_{w3} \tag{A-22}$$

$$M_{y3} = 0 = I_{y3}\dot{\omega}_3 + G_{x3} r_{w3} \tag{A-23}$$

$$M_{z3} = J_3 \dot{\omega}_\theta \tag{A-24}$$

$$\begin{aligned} F_{FSAx1}\cos\delta - F_{FSAy1}\sin\delta = &-(m_1 + m_{SA})A_{x1} + G_{x1}\cos\delta - G_{y1}\sin\delta \\ &-(m_1 + m_{SA})g\sin\beta\left[\cos(\theta+\delta)\cos\delta + \sin(\theta+\delta)\sin\delta\right] \end{aligned} \tag{A-25}$$

$$\begin{aligned} F_{FSAx1}\sin\delta + F_{FSAy1}\cos\delta = &-(m_1 + m_{SA})A_{y1} + G_{x1}\sin\delta + G_{y1}\cos\delta \\ &-(m_1 + m_{SA})g\sin\beta\left[\cos(\theta+\delta)\sin\delta - \sin(\theta+\delta)\cos\delta\right] \end{aligned} \tag{A-26}$$

$$F_{FSAz1} = G_{z1} - (m_1 + m_{SA})g\cos\beta \tag{A-27}$$

F_{SAx1} and F_{SAy1} need to be decoupled from eqns. (A-1) and (A-2),

$$F_{SAx1} = G_{x1} - m_1 A_{x1}\cos\delta - m_1 A_{y1}\sin\delta - m_1 g\sin\beta\cos(\theta+\delta) \tag{A-28}$$

$$F_{SAy1} = G_{y1} + m_1 A_{x1}\sin\delta - m_1 A_{y1}\cos\delta + m_1 g\sin\beta\sin(\theta+\delta) \tag{A-29}$$

F_{FSAx1} and F_{FSAy1} also need to be decoupled from eqns. (A-25) and (A-26),

$$F_{FSAx1} = G_{x1} - (m_1 + m_{SA})A_{x1}\cos\delta - (m_1 + m_{SA})A_{y1}\sin\delta \\ -(m_1 + m_{SA})g\sin\beta\cos(\theta + \delta) \tag{A-30}$$

$$F_{FSAy1} = G_{y1} + (m_1 + m_{SA})A_{x1}\sin\delta - (m_1 + m_{SA})A_{y1}\cos\delta \\ +(m_1 + m_{SA})g\sin\beta\sin(\theta + \delta) \tag{A-31}$$

$$M_{FSAx1} = -(I_{x1} + I_{SAx1})(\omega_\theta + \omega_\delta)\omega_1 - (r_{w1} + S_b + S_a)G_{y1} \\ -S_m A_{x1}\sin\delta + S_m A_{y1}\cos\delta - S_m g\sin\beta\sin(\theta + \delta) \tag{A-32}$$

where, $S_m = S_b(m_1 + m_{SA}) + S_a m_1$

$$M_{FSAy1} = (I_{y1} + I_{SAy1})\dot{\omega}_1 + (r_{w1} + S_b + S_a)G_{x1} - S_m A_{x1}\cos\delta \\ -S_m A_{y1}\sin\delta - S_m g\sin\beta\cos(\theta + \delta) \tag{A-33}$$

$$M_{FSAz1} = \tau_s = (J_1 + J_{SA})(\dot{\omega}_\delta + \dot{\omega}_\theta) \tag{A-34}$$

The equation (3-70), with equations (A-13), (A-19), and (A-25), becomes,

$$MA_x = G_{x1}\cos\delta - G_{y1}\sin\delta + G_{x2} + G_{x3} - Q_3\omega_\theta^2 + \frac{l}{2}(m_2 - m_3)\dot{\omega}_\theta - Mg\cos\theta\sin\beta \qquad \text{(A-35)}$$

and the equation (3-71), with equations (A-14), (A-20), and (A-26), becomes,

$$MA_y = G_{x1}\sin\delta + G_{y1}\cos\delta + G_{y2} + G_{y3} + \frac{l}{2}(m_2 - m_3)\omega_\theta^2 + Q_3\dot{\omega}_\theta + Mg\sin\theta\sin\beta \qquad \text{(A-36)}$$

and the equation (3-72), with equations (A-15), (A-21), and (A-27), becomes,

$$MA_z = 0 = G_{z1} + G_{z2} + G_{z3} - Mg\cos\beta \qquad \text{(A-37)}$$

and the equation (3-73), with equations (A-13), (A-14), (A-18), (A-19), (A-20), (A-24), and (A-26), becomes,

$$\begin{aligned} Q_4\dot{\omega}_\theta = {} & \frac{l}{2}(m_2 - m_3)A_x + Q_3A_y + (b-c)(G_{x1}\sin\delta + G_{y1}\cos\delta) - \frac{l}{2}(G_{x2} - G_{x3}) \\ & - c(G_{y2} + G_{y3}) - Q_3g\sin\theta\sin\beta + \frac{l}{2}(m_2 - m_3)g\cos\theta\sin\beta \end{aligned} \qquad \text{(A-38)}$$

the equation (3-74), with equations (A-4), (A-5), (A-14), (A-15), (A-16), (A-20), (A-21), (A-22), and (A-26), becomes,

$$0 = -\frac{l}{2}(G_{z2}-G_{z3}) - h(G_{x1}\sin\delta + G_{y1}\cos\delta + G_{y2} + G_{y3}) + (D-Q_{24})A_y + Q_{24}c\dot{\omega}_\theta + Q_{25}\frac{l}{2}\omega_\theta^2$$
$$-(I_{x2}\omega_2 + I_{x3}\omega_3)\omega_\theta - (I_{x1}+I_{SAx1})(\omega_\theta+\omega_\delta)\omega_1\cos\delta - (I_{y1}+I_{SAy1})\dot{\omega}_1\sin\delta \qquad \text{(A-39)}$$
$$+(Q_{24}-D)g\sin\theta\sin\beta + \frac{l}{2}(m_2-m_3)g\cos\beta$$

the equation (3-75), with equations (A-4), (A-5), (A-13), (A-15), (A-19), (A-21), and (A-25), becomes,

$$0 = -(b-c)G_{FSAz1} + c(G_{z2}+G_{z3}) - h(G_{x1}\cos\delta - G_{y1}\sin\delta + G_{x2}+G_{x3}) + r_{w2}G_{x2} + r_{w3}G_{x3}$$
$$+(D-Q_{24})A_x - [D(b-c)+Q_{24}c]\omega_\theta^2 + \frac{l}{2}Q_{25}\dot{\omega}_\theta + (I_{x1}+I_{SAx1})(\omega_\theta+\omega_\delta)\omega_1\sin\delta \qquad \text{(A-40)}$$
$$-(I_{y1}+I_{SAy1})\dot{\omega}_1\cos\delta + (D-Q_{24})g\cos\theta\sin\beta - c(m_2+m_3)g\cos\beta$$

From equation (A-5),

$$\dot{\omega}_1 = \frac{\tau_d}{I_{y1}} - \frac{r_{w1}}{I_{y1}}G_{x1} \qquad \text{(A-41)}$$

from equation (A-34),

$$\dot{\omega}_\theta + \dot{\omega}_\delta = \frac{1}{J_1 + J_{SA}}\tau_s \qquad \text{(A-42)}$$

from equation (A-17),

$$\dot{\omega}_2 = -\frac{r_{w2}}{I_{y2}} G_{x2} \tag{A-43}$$

from equation (A-23),

$$\dot{\omega}_3 = -\frac{r_{w3}}{I_{y3}} G_{x3} \tag{A-44}$$

The equations of motion (A-35) ~ (A-44) are written as equations (3-94) ~ (3-103) in chapter 3.

A system of 16 first order differential equations can be obtained from the 10 second order equations of motion (equations (A-35) ~ (A-44)) and five differential constraints for accelerations (equations (3-(52~56)). After introducing the notations (3-104), this system of 16 first order equations contains six derivatives ($\dot{\delta}$, $\dot{\omega}_\theta$, $\dot{\omega}_1$, $\dot{\omega}_2$, $\dot{\omega}_3$ and $\dot{\omega}_\delta$) and can be transformed in a system of six differential and ten algebraic equations which is the suitable form for solving the equations of motion for a constrained multi-body mechanical system (Haug, E.J., 1992). The six differential equations are,

$$\dot{\delta} = \omega_\delta \tag{A-45}$$

$$\dot{\omega}_1 = \frac{1}{I_{yl}}\tau_d - \frac{r_{wl}}{I_{yl}}G_{x1} \tag{A-46}$$

$$\dot{\omega}_2 = -\frac{r_{w2}}{I_{y2}}G_{x2} \tag{A-47}$$

$$\dot{\omega}_3 = -\frac{r_{w3}}{I_{y3}}G_{x3} \tag{A-48}$$

$$\dot{\omega}_\delta = \frac{1}{J_1 + J_{SA}}\tau_s - \dot{\omega}_\theta \tag{A-49}$$

$$\dot{\omega}_\theta = \frac{1}{c}(-r_{w2}\omega_\theta\omega_2 + A_y - \frac{l}{2}\omega_\theta^2) \tag{A-50}$$

The 10 algebraic equations are:

$$0 = G_{xl}\cos\delta - G_{yl}\sin\delta + G_{x2} + G_{x3} - MA_x - Q_3\omega_\theta^2 + \frac{l}{2c}(m_2 - m_3)(-r_{w2}\omega_\theta\omega_2 + A_y - \frac{l}{2}\omega_\theta^2) - Mg\cos\theta\sin\beta \tag{A-51}$$

$$0 = G_{xl}\sin\delta + G_{yl}\cos\delta + G_{y23} - MA_y + \frac{l}{2}(m_2 - m_3)\omega_\theta^2 + \frac{Q_3}{c}(-r_{w2}\omega_\theta\omega_2 + A_y - \frac{l}{2}\omega_\theta^2) + Mg\sin\theta\sin\beta \tag{A-52}$$

$$0 = -\frac{1}{c}Q_4(-r_{w2}\omega_\theta\omega_2 + A_y - \frac{l}{2}\omega_\theta^2) + \frac{l}{2}(m_2 - m_3)A_x + Q_3A_y + (b-c)(G_{xl}\sin\delta + G_{yl}\cos\delta) - \frac{l}{2}(G_{x2} - G_{x3}) - cG_{y23} - Q_3g\sin\theta\sin\beta + \frac{l}{2}(m_2 - m_3)g\cos\theta\sin\beta \quad \text{(A-53)}$$

$$0 = -(\frac{1}{I_{yl}}\tau_1 - \frac{r_{w1}}{I_{yl}}G_{x1})r_{w1}\cos\delta + r_{w1}\omega_1(\omega_\delta + \omega_\theta)\sin\delta + A_x - (b-c)\omega_\theta^2 \quad \text{(A-54)}$$

$$0 = -(\frac{1}{I_{yl}}\tau_1 - \frac{r_{w1}}{I_{yl}}G_{x1})r_{w1}\sin\delta + \frac{b-c}{c}(-r_{w2}\omega_\theta\omega_2 + A_y - \frac{l}{2}\omega_\theta^2) - r_{wl}\omega_1(\omega_\delta + \omega_\theta)\cos\delta + A_y \quad \text{(A-55)}$$

$$\frac{r_{w2}^2}{I_{y2}}G_{x2} - \frac{l}{2c}(-r_{w2}\omega_\theta\omega_2 + A_y - \frac{l}{2}\omega_\theta^2) + A_x + c\omega_\theta^2 = 0 \quad \text{(A-56)}$$

$$\frac{r_{w3}^2}{I_{y3}}G_{x3} + \frac{l}{2c}(-r_{w2}\omega_\theta\omega_2 + A_y - \frac{l}{2}\omega_\theta^2) + A_x + c\omega_\theta^2 = 0 \quad \text{(A-57)}$$

$$0 = G_{z1} + G_{z2} + G_{z3} - m_t g\cos(\beta) \quad \text{(A-58)}$$

$$0 = -\frac{l}{2}G_{z2} + \frac{l}{2}G_{z3} - \frac{b}{c}(d_1 + d_{sa})Ay + (r_1 - h)\sin(\delta)G_{xl} - h\cos(\delta)G_{yl} - hG_{y23} - \omega_\theta^2[-l\frac{(b-c)}{2c}(d_1 + d_{sa}) + ld_3] - \omega_\theta\omega_2[-r_2\frac{(b-c)}{c}(d_1 + d_{sa}) + r_2(d_2 + d_3)] - \tau_1\sin(\delta) + d_t g\sin(\beta)\sin(\theta) + (m_2 - m_3)\frac{l}{2}g\cos(\beta) \quad \text{(A-59)}$$

$$0=(b-c)G_{z1}-cG_{z2}-cG_{z3}+d_tAx+\frac{l}{2c}(d_3-d_2)Ay-(r_1-h)\cos(\delta)G_1x_1-h\sin(\delta)G_1y_1$$
$$-(r_2-h)G_{z2}-(r_3-h)G_{z3}+\omega_\theta\omega_2\frac{r_2l}{2c}(d_2-d_3)+\tau_1\cos(\delta)+\omega_\theta^2[-(d_1+d_{sa})(b-c) \qquad \text{(A-60)}$$
$$+d_2(c+\frac{l^2}{4c})+d_3(c-\frac{l^2}{4c})]+gd_t\sin(\beta)\cos(\theta)+g[-(b-c)m_{t1}+c(m_2+m_3)]\cos(\beta)$$

To be able to derive the control equation of motion, eqn. (4-17), we first need to find G_{x1} in terms of the state variables (δ, θ, ω_1, ω_δ, β) and inputs (τ_d, τ_s).

Multiplying eq.(A-51) by c and adding to (A-53), G_{x1} can be expressed in terms of other forces as:

$$G_{x1}=\frac{\frac{l}{2}(G_{x2}-G_{x3})\sin\delta-b(G_{x2}+G_{x3})\cos\delta-k_1b\cos\delta-k_2c\sin\delta-k_3\sin\delta}{b} \qquad \text{(A-61)}$$

where,

$$k_1=-MA_x-Q_3\omega_\theta^2+\frac{l}{2}(m_2-m_3)\dot{\omega}_\theta-Mg\sin\beta\cos\theta$$
$$k_2=-MA_y-Q_3\dot{\omega}_\theta+\frac{l}{2}(m_2-m_3)\omega_\theta^2+Mg\sin\beta\sin\theta$$
$$k_3=-Q_4\dot{\omega}_\theta+\frac{l}{2}(m_2-m_3)A_x+Q_3A_y-Q_3g\sin\beta\sin\theta+\frac{l}{2}(m_2-m_3)g\sin\beta\cos\theta$$

using equation (A-47), (A-48), and (A-50),

$$G_{x2}+G_{x3}=\frac{l}{2c}Q_2A_y-Q_1A_x-\frac{l}{2c}Q_2r_{w2}\omega_2\omega_\theta-(\frac{l^2}{4c}Q_2+cQ_1)\omega_\theta^2 \qquad \text{(A-62)}$$

$$G_{x2}-G_{x3} = \frac{l}{2c}Q_1A_y-Q_2A_x-\frac{l}{2c}Q_1r_{w2}\omega_2\omega_\theta-(\frac{l^2}{4c}Q_1+cQ_2)\omega_\theta^2 \quad \text{(A-63)}$$

Eventually, after a lengthy manipulation, G_{x1}can be expressed as follows;

$$\begin{aligned} G_{x1} = {} & [Q_6\cos^2\delta+\frac{c}{b^2}Q_8\sin^2\delta-\frac{l}{b}Q_7\sin\delta\cos\delta]r_{w1}\dot{\omega}_1 \\ & +[\frac{l}{2b}Q_7(\sin^2\delta-\cos^2\delta)+Q_{12}\sin\delta\cos\delta]r_{w1}\omega_1\omega_\delta \\ & +\frac{\tau_s}{b}\sin\delta+Mg\sin\beta\cos\theta\cos\delta-\frac{cM-Q_3}{b}g\sin\beta\sin\theta\sin\delta \\ & -\frac{l}{2b}(m_2-m_3)g\sin\beta\cos\theta\sin\delta \end{aligned} \quad \text{(A-64)}$$

Substituting equation (A-64) to equation (A-46),

$$\dot{\omega}_1 = \frac{\tau_d-Num(\delta)r_{w1}^2\omega_1\omega_\delta-r_{w1}grav(\delta)-\frac{r_{w1}}{b}\tau_s\sin\delta}{Den(\delta)} \quad \text{(A-65)}$$

where,

$$Num(\delta) = \frac{l}{2b}Q_7(\sin^2\delta-\cos^2\delta)+(\frac{c}{b^2}Q_8-Q_6)\sin\delta\cos\delta$$

$$Den(\delta) = I_{y1}+r_{w1}^2(Q_6\cos^2\delta+\frac{c}{b^2}Q_8\sin^2\delta-\frac{l}{b}Q_7\sin\delta\cos\delta)$$

$$Grav(\delta) = Mg\sin\beta\cos\theta\cos\delta-\frac{cM-Q_3}{b}g\sin\beta\sin\theta\sin\delta-\frac{l}{2b}(m_2-m_3)g\sin\beta\cos\theta\sin\delta$$

Substituting equation (A-50) to equation (A-49),

$$\begin{aligned} \dot{\omega}_\delta = {} & (\frac{Num(\delta)r_{w1}^2\sin\delta}{Den(\delta)}-\cos\delta)\frac{r_{w1}}{b}\omega_1\omega_\delta+\frac{r_{w1}^2\sin\delta}{bDen(\delta)}Grav(\delta) \\ & +(\frac{1}{J_1+J_{SA}}+\frac{r_{w1}^2\sin^2\delta}{b^2Den(\delta)})\tau_s-\frac{r_{w1}\sin\delta}{bDen(\delta)}\tau_d \end{aligned} \quad \text{(A-66)}$$

The equations (A-65) and (A-66) are simplified as the equation (A-67) which is the equation (4-17) in chapter 4.

$$\begin{bmatrix}\dot{\omega}_\delta \\ \dot{\omega}_1\end{bmatrix}=\begin{bmatrix}f(\omega_1,\omega_\delta,\delta,\theta,\beta) \\ F(\omega_1,\omega_\delta,\delta,\theta,\beta)\end{bmatrix}+Ad\begin{bmatrix}\tau_d \\ \tau_s\end{bmatrix} \tag{A-67}$$

where, τ_d, τ_s are the driving and steering torques, respectively. $\dot{\omega}_1$, $\dot{\omega}_\delta$ are the driving and steering angular accelerations, respectively, and

$$f(\omega_1,\omega_\delta,\delta,\theta,\beta)=[r_l^2\{\frac{l}{2b}Q_1(\sin^2(\delta)-\cos^2(\delta))+(Q_2-Q_3)\sin(\delta)\cos(\delta)\}\sin(\delta)-D\cos(\delta)]\frac{r_1}{bD}\omega_1\omega_\delta$$
$$+[bm_1\cos(\delta)\cos(\theta)-cQ_1\sin(\delta)\cos(\theta)-(cm_t+bm_1)\sin(\delta)\sin(\theta)]\frac{r_1 g\sin(\beta)\sin(\delta)}{b^2D}$$

$$F(\omega_1,\omega_\delta,\delta,\theta,\beta)=-[\frac{l}{2b}Q_1(\sin^2(\delta)-\cos^2(\delta))+(Q_2-Q_3)\sin(\delta)\cos(\delta)]\frac{r_1^2}{D}\omega_1\omega_\delta$$
$$-[bm_1\cos(\delta)\cos(\theta)-cQ_1\sin(\delta)\cos(\theta)-(cm_t+bm_1)\sin(\delta)\sin(\theta)]\frac{g\sin(\beta)}{bD}$$

$$Ad=\begin{bmatrix}-\frac{r_1}{bD}\sin(\delta) & \frac{1}{J_1}+\frac{r_1^2}{b^2D}\sin^2(\delta) \\ \frac{1}{D} & -\frac{r_1}{bD}\sin(\delta)\end{bmatrix}$$

where

$$D=I_1+r_1^2\left[Q_3\cos^2(\delta)+Q_2\sin^2(\delta)-\frac{1}{b}Q_1\cos(\delta)\sin(\delta)\right]$$

where, m_t is the total mass of the autonomous vehicle and m_i (i=1,2,3) are the masses of or each of the three wheels, and m_{1t} is the combined mass of front wheel and the streering assembly, respectively

J_i is the moments of inertia about the vertical axis Z_i, and I_i (i=1,2,3) are the moments of inertia about Y_i axis, respectively

r_1 is the radius of front wheel, b is the vehicle length from the origin of front wheel to the center of rear axle, and c is the distance from the center of mass to the center of rear axle, and l is the length of the rear axle, respectively

The other ground contact forces, also, can be derived by quite a lengthy manipulation of equations (A-45) ~ (A-60).

$$G_{x2} = Q_{13} r_{wl}[\frac{\frac{l}{4b}\sin\delta - \frac{1}{2}\cos\delta}{Den(\delta)}\tau_d - \frac{(\frac{l}{4b}\sin\delta - \frac{1}{2}\cos\delta) r_{wl}\sin\delta}{bDen(\delta)}\tau_s - \frac{Num(\delta)}{Den(\delta)}(\frac{l}{4b}\sin\delta - \frac{1}{2}\cos\delta \quad \text{(A-68)}$$
$$r_{wl}^2\omega_1\omega_\delta + (\frac{l}{4b}\cos\delta + \frac{1}{2}\sin\delta)\omega_1\omega_\delta - (\frac{l}{4b}\sin\delta - \frac{1}{2}\cos\delta)\frac{r_{wl}}{Den(\delta)}Grav(\delta)]$$

$$G_{x3} = Q_{14} r_{wl}[\frac{\frac{l}{4b}\sin\delta + \frac{1}{2}\cos\delta}{Den(\delta)}\tau_d - \frac{(\frac{l}{4b}\sin\delta + \frac{1}{2}\cos\delta) r_{wl}\sin\delta}{bDen(\delta)}\tau_s - \frac{Num(\delta)}{Den(\delta)}(\frac{l}{4b}\sin\delta + \frac{1}{2}\cos\delta \quad \text{(A-69)}$$
$$r_{wl}^2\omega_1\omega_\delta + (\frac{l}{4b}\cos\delta - \frac{1}{2}\sin\delta)\omega_1\omega_\delta - (\frac{l}{4b}\sin\delta + \frac{1}{2}\cos\delta)\frac{r_{wl}}{Den(\delta)}Grav(\delta)]$$

$$
\begin{aligned}
G_{y1} = & \frac{r_{w1}[\frac{l}{2b}Q_7(\sin^2\delta-\cos^2\delta)+Q_{12}\sin\delta\cos\delta]}{Den(\delta)}\tau_d \\
& -\frac{r_{w1}^2[\frac{l}{2b}Q_7(\sin^2\delta-\cos^2\delta)+Q_{12}\sin\delta\cos\delta]\sin\delta - Den(\delta)\cos\delta}{bDen(\delta)}\tau_s \\
& +[Num(\delta)[r_{w1}^2\frac{l}{2b}Q_7(\sin^2\delta-\cos^2\delta)+r_{w1}^2Q_{12}\sin\delta\cos\delta] \\
& -Den(\delta)[\frac{l}{b}Q_7\sin\delta\cos\delta+\frac{c}{b^2}Q_8\cos^2\delta+Q_6\sin^2\delta]]\frac{r_{w1}\omega_1\omega_\delta}{Den(\delta)} \\
& +[\frac{cM-Q_3}{b^2}(\cos^2\delta\sin\delta-\sin^3\delta)]r_{w1}^2\omega_1^2 \\
& -\frac{r_{w1}^2[\frac{l}{2b}Q_7(\sin^2\delta-\cos^2\delta)+Q_{12}\sin\delta\cos\delta]}{Den(\delta)}Grav(\delta)-Mg\sin\beta\cos\theta\sin\delta \\
& -(\frac{cM-Q_3}{b})g\sin\beta\sin\theta\cos\delta-\frac{l}{2b}(m_2-m_3)g\sin\beta\cos\theta\cos\delta
\end{aligned}
\tag{A-70}
$$

$$
\begin{aligned}
G_{y23} = & [\frac{r_{w1}(Q_{16}\sin\delta+\frac{l}{2}Q_7\cos\delta)}{bDen(\delta)}]\tau_d-[\frac{r_{w1}^2(Q_{16}\sin^2\delta+\frac{l}{2}Q_7\sin\delta\cos\delta)+bDen(\delta)}{b^2Den(\delta)}]\tau_s \\
& -[\frac{r_{w1}^2Num(\delta)(Q_{16}\sin\delta+\frac{l}{2}Q_7\cos\delta)+Den(\delta)(Q_{16}\cos\delta-\frac{l}{2}Q_7\sin\delta)}{bDen(\delta)}]r_{w1}\omega_1\omega_\delta \\
& +\frac{1}{b}(Q_{17}\sin\delta\cos\delta-\frac{l}{2}Q_{18}\sin^2\delta+lober2b^3Q_{19}\sin^2\delta)r_{w1}^2\omega_1^2 \\
& -\frac{r_{w1}^2(Q_{16}\sin\delta+\frac{l}{2}Q_7\cos\delta)}{bDen(\delta)}Grav(\delta)-Mg\sin\beta\sin\theta+\frac{cM-Q_3}{b}\sin\beta\sin\theta+\frac{l}{2b}(m_2-m_3)g\sin\beta\cos\theta
\end{aligned}
\tag{A-71}
$$

$$G_{z1} = [\frac{l}{2b^2}Q_{28}\sin\delta - \frac{1}{b}(Q_{29}+Q_{20}+Q_{23})\cos\delta]r_{w1}\dot{\omega}_1$$
$$+[\frac{1}{b}(Q_{29}+Q_{20}+Q_{22})\sin\delta + \frac{l}{2b^2}Q_{28}\cos\delta]r_{w1}\omega_1\omega_\delta \quad \text{(A-72)}$$
$$+[\frac{c}{b}hM - D + Q_{22} - \frac{h}{b}Q_3]\frac{r_{w1}^2}{b^2}\omega_1^2\sin^2\delta - \frac{1}{b}Q_{29}g\sin\beta\cos\theta + \frac{c}{b}(m_f+m_{1t})g\cos\beta$$

$$G_{z2} = [[\frac{h}{bl}(Q_3 - cM) - \frac{1}{4b^2}Q_{28} + \frac{1}{l}(D - Q_{23})]\sin\delta + \frac{1}{2b}(Q_{29}+Q_{20}+Q_{23})\cos\delta]r_{w1}\dot{\omega}_1$$
$$+[-\frac{1}{2b}(Q_{29}+Q_{20}+Q_{22})\sin\delta + [\frac{h}{bl}(Q_3 - cM) - \frac{1}{4b^2}Q_{28} + \frac{1}{l}(D - Q_{23})]\cos\delta]r_{w1}\omega_1\omega_\delta$$
$$[-\frac{1}{bl}(Q_{29}+Q_{22}+Q_{26})\cos\delta + \frac{1}{2b}(D - \frac{c}{b}hM + Q_{24} - Q_{22} + h(m_2 - m_3) - 2m_3(r_{w3} - h) + Q_{27} + \frac{h}{b}Q_3)\sin\delta \quad \text{(A-73)}$$
$$r_{w1}^2\omega_1^2\sin\delta + \frac{1}{l}Q_{29}g\sin\beta\sin\theta + \frac{1}{2b}Q_{29}g\sin\beta\cos\theta + \frac{bc(m_2+m_3)+bcM-c^2(m_f+m_{1t})}{2bc}g\cos\beta$$

And finally,

$$G_{z3} = Mg\cos\beta - (G_{z1}+G_{z2}) \quad \text{(A-74)}$$

The parameters used to simplify the derivation are listed in Appendix B.

Appendix B

The equations listed below are the parameters of the 16 differential algebraic equations of motion (eqn.(3-105) ~ eqn.(3-120)), the control dynamic equation (eqn.(4-17)), and equations for eight ground reaction forces G_{xi}, G_{yi}, and G_{zi} (i= 1,2,3) (eqn.(A-46), (A-68) ~ (A-74)).

$$Q_1 = \frac{I_{y2}}{r_{w2}^2} + \frac{I_{y3}}{r_{w3}^2} \tag{B-1}$$

$$Q_2 = \frac{I_{y2}}{r_{w2}^2} - \frac{I_{y3}}{r_{w3}^2} \tag{B-2}$$

$$Q_3 = c(m_{1r} + m_2 + m_3) - bm_{1r} \tag{B-3}$$

$$Q_4 = J_f + J_2 + J_3 + (b-c)^2 m_{1r} + (c^2 + \frac{l^2}{4})(m_2 + m_3) \tag{B-4}$$

$$Q_5 = -Q_3 + \frac{Q_4}{c} \tag{B-5}$$

$$Q_6 = Q_1 + M \tag{B-6}$$

$$Q_7 = Q_2 + (m_2 - m_3) \tag{B-7}$$

$$Q_8 = \frac{l^2}{4c} Q_1 + cM - Q_3 + Q_5 \tag{B-8}$$

$$Q_9 = \frac{l^2}{4c} Q_1 + Q_5 + cQ_7 \tag{B-9}$$

$$Q_{10} = cQ_1 + Q_3 + \frac{l^2}{4c} Q_7 \tag{B-10}$$

$$Q_{11} = \frac{l^2}{4c} Q_1 + Q_5 \tag{B-11}$$

$$Q_{12} = \frac{c}{b^2} Q_8 - Q_6 \tag{B-12}$$

$$Q_{13} = Q_1 + Q_2 \tag{B-13}$$

$$Q_{14} = Q_2 - Q_1 \tag{B-14}$$

$$Q_{15} = c(Q_6 - Q_1) - Q_3 \tag{B-15}$$

$$Q_{16} = -\frac{l^2}{4c} Q_1 + \frac{c(b-c)}{b} M - Q_3 - Q_4 \tag{B-16}$$

$$Q_{17} = \frac{b-c}{b} M - \frac{1}{b} Q_3 + \frac{1-b}{bc} Q_4 \tag{B-17}$$

$$Q_{18} = Q_7 - \frac{1}{b} Q_2 \tag{B-18}$$

$$Q_{19} = (bc - b^2c - bc^2 - c^2)M \tag{B-19}$$

$$Q_{20} = \frac{I_{y2}}{r_{w2}} + \frac{I_{y3}}{r_{w3}} \tag{B-20}$$

$$Q_{21} = \frac{I_{y2}}{r_{w2}} - \frac{I_{y3}}{r_{w3}} \tag{B-21}$$

$$Q_{22} = \frac{I_{x1} + I_{SAx1}}{r_{w1}} \tag{B-22}$$

$$Q_{23} = \frac{I_{y1} + I_{SAy1}}{r_{w1}} \tag{B-23}$$

$$Q_{24} = m_2(r_{w2} - h) + m_3(r_{w3} - h) \tag{B-24}$$

$$Q_{25} = m_2(r_{w2} - h) - m_3(r_{w3} - h) \tag{B-25}$$

$$Q_{26} = \frac{I_{x2}}{r_{w2}} + \frac{I_{x3}}{r_{w3}} \tag{B-26}$$

$$Q_{27} = \frac{I_{x2}}{r_{w2}} - \frac{I_{x3}}{r_{w3}} \tag{B-27}$$

$$Q_{28} = h(m_2 - m_3) + Q_{21} + Q_{25} \tag{B-28}$$

$$Q_{29} = hM - D + Q_{24} \tag{B-29}$$

$$S_m = S_b m_{1t} + S_a m_1 \tag{B-30}$$

$$D = S_m - m_{1t}(r_{w1} - h + S_{a+b}) \tag{B-31}$$

$$Num(\delta) = \frac{l}{2b} Q_7(\sin^2\delta - \cos^2\delta) + Q_{12}\sin\delta\cos\delta \tag{B-32}$$

$$Den(\delta) = I_{y1} + r_{w1}^2\left(Q_6\cos^2\delta + \frac{c}{b^2}Q_8\sin^2\delta - \frac{l}{b}Q_7\sin\delta\cos\delta\right) \tag{B-33}$$

$$Grav(\delta) = Mg\sin\beta\cos\theta\cos\delta - \frac{cM - Q_3}{b}g\sin\beta\sin\theta\sin\delta - \frac{l}{2b}(m_2 - m_3)g\sin\beta\cos\theta\sin\delta \tag{B-34}$$

where,

m_i (i=1,2,3), m_{SA}, m_f : the masses of each wheels, steering assembly, and the vehicle frame, respectively

$m_{1t} = m_1 + m_{SA}$: the combined mass of the front wheel and the steering assembly

$M = m_f + m_{1t} + m_2 + m_3$: the total mass of the vehicle

S_a : the distance between the center of mass of the steering assembly and the center point of the front wheel

S_b : the distance between the center of mass of the steering assembly and the linkage point of the steering assembly with the vehicle frame

S_{a+b} : the distance between the center point of the front wheel and linkage point of the steering assembly with the vehicle frame ($S_{a+b} = S_a + S_b$)

h	:	the height of the center of mass of the structure from the surface of the inclined plane (equation (3-5))